Dynamic Finite Element Modeling and Analysis

of a Hermetic Reciprocating Compressor

by

Allan D. Kelly

Thesis submitted to the Faculty of the

Virginia Polytechnic Institute and State University

in partial fulfillment of the requirements for the degree of

Master of Science

in

Mechanical Engineering

APPROVED:

Prof. Charles E. Knight, Chairman

Prof. Charles J. Hurst

Prof. Larry D. Mitchell

January 30, 1992

Blacksburg, Virginia

Dynamic Finite Element Modeling and Analysis

of a Hermetic Reciprocating Compressor

by

Allan D. Kelly

Prof. Charles E. Knight, Chairman

Mechanical Engineering

(ABSTRACT)

Dynamic finite element modeling and analysis of a refrigeration compressor was investigated as part of a noise emission study. Natural frequencies and normal mode shapes were calculated for the major structural components of the compressor. The components were later combined to form a model of the compressor assembly which was subsequently solved for its dynamic properties. Model development included coordination with test data for verification and revision to improve model prediction accuracy.

Considerable efforts were made to accurately represent the hermetic shell which presents several inherent modeling difficulties due to its geometry and other characteristics which result from a deep drawn manufacturing process. The importance of physical simplifications such as geometry representation, thickness variation, attachments, the welded seam, and residual stresses were established. In addition, theoretical limitations of the finite element method were addressed as a cause for analysis-test discrepancies. Housing models developed were found to agree within 12% of experimental natural frequencies up to 1100 Hz.

Compatibility of analytical normal modes with resonant dwell experimental deflection shapes was considered. Analytical forced vibration response showed situations when the deflected shapes can be a superposition of modes rather than the pure mode shape. Analytical simulation of the test setup improved the agreement of analysis and test data.

Additional components modeled include the internal compressor mechanism and its supports. Analysis showed that interactions with the internal components, particularly resonances within the suspension springs, are important for a valid representation of the compressor assembly. Resonances within the internal suspension components more than double or nearly triple the number of resonance frequencies in the compressor assembly.

Acknowledgements

I wish to thank Professor C. J. Hurst, Professor C. E. Knight, and Professor L. D. Mitchell for serving on my advisory committee. I am truly grateful for the guidance and technical support that each provided throughout this project. Thanks are also extended to Bristol Compressors, Inc. and to the Virginia Center for Innovative Technology for their sponsorship.

Additionally, I wish to recognize and thank my other colleagues who contributed to this research. Mr. Ken Wallace developed the initial housing models during the early stages of this project. Professor Knight directed the model development and frequently assisted with model refinement and analysis. Experimental measurements were performed by Professor Mitchell and Mr. Barry Agee. Next, Mr. Kevin Cardany and Mr. William Gardener were responsible for the solid modeling efforts. Finally, I thank Mr. David Gilliam of Bristol Compressors who provided countless drawings, components, specifications, and measurements throughout the project.

Table of Contents

List of Illustrations

List of Tables

Notation

a_k	real constant
$[B]$	strain-displacement matrix
$[C]$	structure damping matrix
$[c]$	modal viscous damping matrix
d.o.f.	degree of freedom
$\{d\}$	element nodal displacements
$\{D\}$	structure displacements, includes translations and rotations
$[E]$	material physical property matrix
$\{f\}$	element loads
$\{F\}$	applied loads, includes forces and moments
$\{F_r\}$	modal forces
$[\ I\ ]$	identity matrix
I_{aa}	area moment of inertia about the a-a axis
J_{aa}	mass moment of inertia about the a-a axis
j	identifies imaginary component of a complex number
$[K]$	structure stiffness matrix
$[k]$	diagonalized modal stiffness matrix
$[k_e]$	element stiffness matrix
$[k_{cms}]$	generalized stiffness matrix partitioned from substructures
$[M]$	structure mass matrix
$[m]$	diagonalized modal mass matrix
$[m_e]$	element mass matrix
$[m_k]$	generalized mass matrix of substructure k
$[m_{cms}]$	generalized mass matrix partitioned from substructures
$[N]$	shape function matrix
$\{p\}$	generalized coordinates

$[S]$	constraint matrix defining substructure interface compatibility
$[T]$	transformation relating dependent and independent d.o.f. of substructures
$\{u\}$	displacements within finite element
$[W]$	Ritz vector of component modes and assumed deflections
α, β	material damping coefficients
$\{\varepsilon\}$	element strains
$\{\gamma\}$	modal coordinates (mode participation factors)
λ	eigenvalue
$\{\phi_r\}$	eigenvector corresponding to the r^{th} mode
$[\Phi]$	matrix of mass normalized eigenvectors
θ	phase angle of forced response, rotational d.o.f.
ρ	mass density
ω	circular frequency
ω_r	natural frequency corresponding to the r^{th} mode
Ω	forcing frequency
ζ_r	modal viscous damping ratio corresponding to the r^{th} mode
{ }	column matrix
[ ]	square matrix
r	subscript, corresponds to r^{th} mode
j,k	integer subscripts
i	subscript indicating independent d.o.f.
d	subscript indicating dependent d.o.f.

1.0 Introduction

Noise emission from refrigeration compressors has been a growing concern over the past two decades. Bristol Compressors, Inc. recently initiated a compressor noise study in response to the increasingly competitive market. The short-range project goal is to reduce noise radiated from the model H23A reciprocating compressor, which is shown in Figure 1. It is a 5 ton two-cylinder unit which provides service for industrial air conditioning systems. The long-range goal is to provide Bristol Compressor, Inc. with the technologies necessary for designing quieter compressors. The long-range effort is approached by coordinating the efforts of acoustics research, experimental dynamics analysis, and the finite element method into a noise prediction scheme as shown in Figure 2. The interconnected disciplines of the noise prediction scheme show three roles of a finite element method (FEM) model: (1) to predict the modal properties of compressor components; (2) to combine the components into a system representing the compressor assembly which is subsequently solved for the system modal properties; and (3) to calculate the forced vibration response of the compressor assembly to mechanical and acoustic forcing functions. Experimental dynamic analysis (EDA) verifies and guides development of the FEM model. EDA also provides weighting functions for the acoustic prediction algorithm. Ultimately, acoustic modeling will determine sound intensities from the predicted velocities of the housing surface. Thus, an accurate FEM model is fundamental to a design process which includes noise prediction capabilities.

The short-range goal seeks immediate noise reductions by initiating the noise prediction scheme partially. In the short-range effort, forcing function determination is excluded. However, the remaining areas of acoustic measurements, acoustic modeling, experimental dynamics analysis and finite element modeling are pursued.

Figure 1. Bristol Compressor Inc. Model H23A

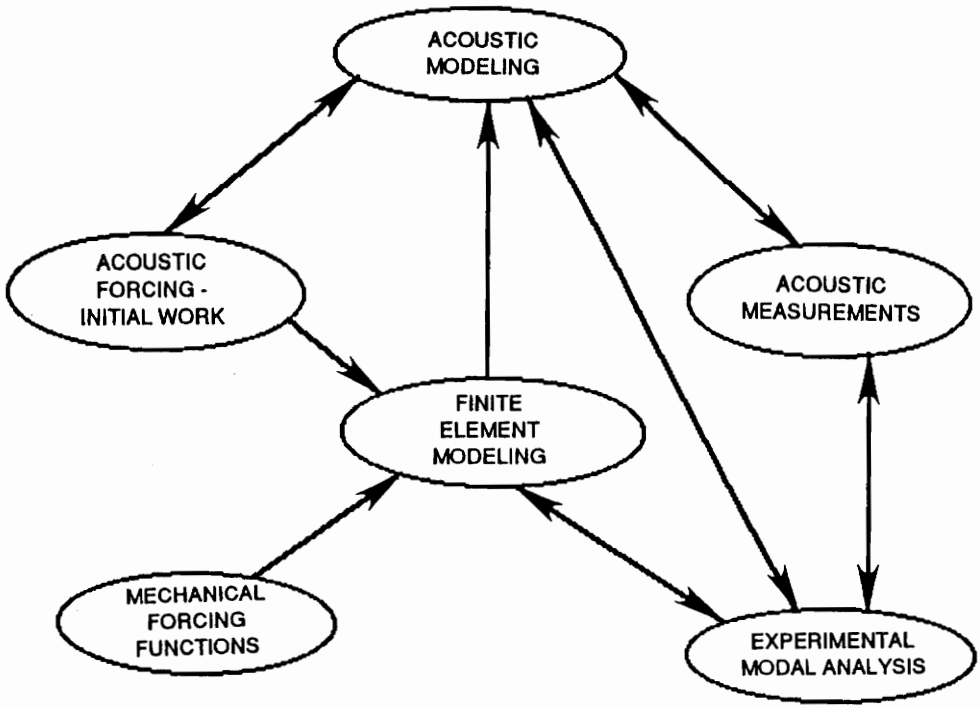

Figure 2. Coordination of Disciplines for Noise Prediction:
After Hurst et. al. [1]

This document discusses the development of a dynamic finite element model of the H23A compressor. The model is developed to calculate modal properties, or the natural frequencies and normal mode shapes of vibration. A big part of the model development includes interactions with experimental dynamic analysis to verify and update the models. Numerous model updates are made to improve agreement between the FEM calculations and test data. The history of accumulated updates will be summarized to serve as a set of modeling guidelines. In terms of the long-range goal, these guidelines should contribute to the development of future FEM models for use in noise prediction. While some suggestions made are simply a reminder to apply good FEM practices, others relate specifically to the compressor. Efforts are made to show what physical parameters can be simplified without introducing significant errors, and conversely, which parameters should not be simplified. Guidelines also provide insights to theoretical limitations that result in differences between analytical and experimental results. In terms of the short-range goal, the models can calculate the effect of design changes on modal properties. This will enable the analyst to evaluate modifications considered for noise reduction prior to constructing prototypes and testing. Areas beyond the scope of this study include mechanical and acoustic forcing functions for simulating compressor operation, acoustic interactions with the structure, and acoustic measurements. Acoustic modeling to predict sound levels will be considered only as a possible application of the FEM model for evaluation.

The remainder of this chapter provides a brief historical background of compressor modeling and then a discussion of dynamic model updating issues. Chapter 2 will introduce some theoretical background of the finite element method. Three specific areas are presented. Eigensolutions for natural frequencies and mode shapes, mode superposition techniques to predict the response to harmonic loads, and the component mode synthesis (CMS) method of assembling substructures for dynamic analysis. Chapter 3 describes the experimental database which guides the FEM model development. Experimentally determined modal properties of the housing and the compressor assembly are presented. The experimental procedures will not be presented at length. However, sufficient description is provided to show the need for later analytical simulation of the experimental

method. Development of the compressor models is discussed in Chapter 4 and Chapter 5. The compressor housing model is developed first, updated and verified before adding models of internal components. Correlation of the housing model is essential before developing the compressor assembly model because numerous revisions are necessary to obtain adequate performance. In addition, the housing plays an important role in noise radiation so there is a good deal of interest here. For both the housing and assembly models, solutions for natural frequencies and mode shapes in the 0 to 1500 Hz frequency range will be presented and compared with the experimental results. Simulation of the experimental tests are performed using forced vibration analysis, for both the housing and the compressor assembly. Finally, evaluation of the models is addressed in Chapter 6.

1.1 Brief History of Compressor Modeling

Modeling of hermetic compressors has been discussed somewhat in recent literature. The best source for compressor technology was found to be the Ray W. Herrick Laboratories of Purdue University's School of Mechanical Engineering. The Herrick Labs contribute significantly to compressor research and publication, and in addition, sponsor the International Compressor Engineering Conference.

Early efforts to model compressor housings employ classical shell theory with simple boundary conditions. Complicated geometries limit the accuracy of this approach but several generalizations could be found, such as the effects of internal pressure, as shown by Ingles [2] in 1972[1]. In 1980, Soedel [3] described the "often observed" mode splitting phenomenon with simple math models. Both of these topics are referred to later in this document.

---

[1] Values in brackets refer to sources listed at the end of document

Several efforts to model hermetic compressors with finite element methods were also found. In 1980, Maeda [4] and other engineers with the Matsushita Electric Industrial Co. determined normal modes of a compressor housing using NASTRAN®. Detailed modeling procedures were not presented, and large natural frequency differences between analytical and experimental results were not a concern. Three-dimensional analytical mode shapes were shown primarily to supplement experimental modal analysis results having limited spatial coordinates. A team from the Matsushita Refrigeration Co. followed up this work in 1988 [5]. Experimental modal analysis and finite element methods were employed to investigate housing resonances with regard to shape and material. No specific modeling details were given and the work presented was focused entirely on the housing top.

In 1988, Tavakoli and Singh [6] modeled compressor housing dynamics with an alternate procedure based on state space mathematics (which is better known as the transfer matrix approach). Modeling details included local attachments on the housing and a "ring" at the welded seam. A geometrically refined model was correlated to be within 6 to 12% of experimental modal analysis results.

In 1990 Laursen [7] investigated the tuning of housing natural frequencies, to avoid coincidence with vibration source frequencies, by varying housing stiffness through local shape changes. Eigenvectors were found experimentally and by an FEM model. Deviations of the model were not emphasized but were attributed to manufacturing variation and a coarse representation of housing thickness variations.

Another 1990 article by Johnson, et. al. [8] provided an overview of FEM analysis to reduce noise in air compressors. This paper, although favorable of FEM attributes, acknowledges limitations from experience with dynamic analysis. Visual correlation of shapes is described as effective for low modes only, and further recommendations are made to employ a mathematical comparison technique such as the modal assurance criterion (MAC). This leads to the next section, a general review of experimental-analytical comparison and updating.

1.2 *Analytical Model Updating*

Several avenues may be followed to coordinate analytical and experimental efforts. Due to the vibration and noise related issues of this investigation, modal parameters are considered for model verification. A large amount of information on this topic exists in modal analysis literature, where development and validation of theoretical models is of primary importance. Space permits only a brief summary here, so issues will be kept general unless thought to be specifically related to this investigation.

Model updating involves a (systematic or trial-and-error) process of comparing the analytical results with experimental data, then adjusting the model or refining measurements for better agreement. Correlation with experimental data is necessary to qualify the model prior to applications such as predicting response or evaluating redesigns. Approaches vary and are still being established, but the fundamental issues to consider are (1) selection of parameters to compare, (2) method of adjustments to improve correlation, and (3) specification of an agreement criteria [9].

Correlation parameters

Correlation parameters are the analytical results and experimental measurements selected to compare which must be available and compatible. Modal properties, response properties and spatial properties are three categories Ewins [10] presents for comparison.

Modal properties conventionally include natural frequencies and mode shapes. For corresponding modes, experimental frequencies may be compared directly to analytical predictions. Ewins recommends plotting the values on linear, analytical versus experimental axes to emphasize differences which occur in a systematic or random fashion. In addition, it may be beneficial to compliment the comparison with other parameters. Chen, Garba and Wada [11, 12, 13] recom-

mend including effective mass, kinetic energy and strain energy distributions for comparison and additional descriptive mode information. Their concern is that refinements which correlate a single parameter may not improve the agreement of other parameters or as in some reported cases, result in divergence of other parameters.

In conjunction with natural frequency correlation, one needs assurance that the analytical modes correspond to experimental modes. Methods available include visual and numerical comparison of mode shapes. The *visual* approach involves graphical comparison of mode shape plots. Visual comparison provides physical assurance to the analyst but becomes difficult as mode complexity increases. Additionally, visual methods do not quantify the degree of correlation and require interaction with the analysts. Alternately, *numerical* methods compare analytical and experimental eigenvectors by direct or statistical comparison of individual values at the measurement points. It is necessary to obtain compatible coordinates and normalize the modes to a common base. Ewins presents two statistical parameters, the Modal Scale Factor (MSF) and the Modal Assurance Criterion (MAC) which are both scalar quantities. Together, these parameters can indicate systematic and random deviations between the analytical and experimental modes or quantify the degree of correlation, respectively. Various other scalar mode shape correlation parameters may be defined, for example Chen and Garba [11] present a root sum square error between analytical and experimental displacements. Eigenvectors which match may be further scrutinized through orthogonality relations. For example, one may reduce the analytical mass matrix to agree with the experimental database, then examine the orthogonality conditions such as

cross-orthogonality :

$$[\Phi_{FEM}]^T[M_{FEM}][\Phi_{EXP}] = [I] \tag{1}$$

or experimental orthogonality:

$$[\Phi_{EXP}]^T[M_{FEM}][\Phi_{EXP}] = [I] \tag{2}$$

Diagonal terms found by Eq. (1) whose values approach 1 indicate matched modes. The degree of accuracy is evaluated from the magnitude of the off-diagonal terms. Any off-diagonal terms found with Eq. (2) indicate errors existing in the experimental modes and/or the analytic mass matrix. Numerical procedures such as this lead to automated correlation schemes. For example, if the test modes are presumed to be more accurate, this orthogonality relationship may lead to a criteria for updating the analytical mass matrix.

Response properties include analytically predicted response which may be compared to directly measured test parameters. Examples include frequency response functions (FRFs), modal forces and acoustic intensity predictions. Only local response FRFs and global displacement response of the model will be compared in this investigation. The properties selected for comparison are specific to the individual problem.

Spatial properties are the mass and stiffness elements of the system equation of motion. Although fundamental to the analytical model, experimental methods must extract these parameters from a (conventionally) limited amount of data, using methods described as system identification. The methods are beyond the scope here but Ewins and Sidhu [14] have successfully determined experimentally derived elements for comparison to reduced analytical mass and stiffness matrices. Information obtained by comparison of spatial properties directed the analysts to error locations on the structure.

Methods of Adjustment

Comparison of experimental data and analytical predictions by the methods mentioned above will show some degree of difference. Refinements must assess whether analysis or test data is most correct. Modeling errors may be the most obvious but several factors such as non-linearities, noise and human error can affect the test data. Approaches to refinement often coordinate both data sets in a complimentary fashion to develop reliable test and updating procedures.

A conventional approach to updating the model involves trial-and-error revisions. However, several authors agree that simply guessing at the required changes is rarely an effective method to adequately revise the model in a timely fashion. Feedback from the test data in the form of isolated local differences is essential to guide modeling revisions performed manually.

Alternate methods have been explored to improve the updating procedures of test and analysis data. Following from the spatial comparison procedures, Ewins [10] describes a method to directly refine the analytical stiffness matrix. Other methods involve systematic, automated iteration schemes for model tuning. Analytical parameters to be modified, such as material property or element thickness, are selected based on output parameter sensitivities (modes, frequencies, etc.). Dascotte [15] described a recent software package which interfaces with existing finite element codes and experimental modal systems to integrate test and analysis data bases for correlation and tuning.

One concern with model refinements is to maintain physical integrity of the model. Arbitrary modifications, for example changing stiffness matrix coefficients, are difficult to physically interpret. In addition, automated procedures require physical bounds to avoid unrealistic modification of properties. An important link between these approaches is pointed out by Blakely and Dobbs [16]. That is, *"efficient model revision techniques which force correlation are no substitute for good model development"* .

Agreement Criteria

Very little work has been directed towards determining acceptable levels of difference between analytical results and test data. Most agree that requirements depend on the unique applications of the model. For forced response calculations, Chen [17] considered model accuracy requirements in regard to the accuracy of forcing functions. The criteria is based on maintaining the model to produce errors no larger than inaccuracies of the forcing functions. Wada [12] recommends predefining the accuracy of a specific response prediction to a specified forcing function. The necessary correlation between the analytical results and the test data can then be determined. As an example,

if accelerations are needed within 10 % given an impulsive force, the math model is adjusted to a level of correlation which provides the appropriate accuracy of acceleration predictions. Hasselman [9] addresses issues of model verification and evaluation through statistical estimation and confidence bounds.

In this investigation, the correlation parameters include natural frequencies and mode shapes. As the work progresses, frequency response functions (FRFs) at a single point and resonance deflection shapes will also be compared. The method of adjustment follows a philosophy emphasizing physical insight. Visual comparison of analytical mode shapes with experimental laser-based deflection shapes localizes regions of model differences. This comparison provides the physical insight needed to guide model updating. For example, a visual comparison may indicate a portion of the housing that is too stiff. Rather than arbitrarily reduce the elastic modulus in the stiff region, a physical cause such as excessive geometric curvature, local mass loading, or a coarse mesh is investigated. Each change made to the model is physically justified and results are accepted. When physical integrity of the model is preserved, the updates can be generally applied to other compressor models.

Finally, an agreement criteria is not formally defined. For now, the models are expected to calculate mode shapes which visually correlate to the experimental deflection shapes. Corresponding frequencies should agree. Agreement is addressed more rigorously in Chapter 6. Models will be evaluated for subjective quality and for potential uses in the intended applications specified in the short- and long-range goals.

2.0 Analytical Techniques

The finite element method (FEM) is a systematic procedure developed to produce and solve a set of equations governing a physical system. FEM has been applied to many areas but this study focuses on the method's structural dynamic analysis capabilities. FEM has developed into a highly accessible analytical tool due to the advancing state of digital computers and the availability of commercial and private industry FEM software. This project primarily employs the I-DEAS™ software package, version 4.1, by the Structural Dynamics Research Corporation (SDRC). The analysis system is a Digital Equipment Corporation MicroVAX™ sited in the Department of Mechanical Engineering. Analysts working with existing codes such as this must take responsibilty to follow appropriate modeling procedures and become familiar with the code's theoretical techniques. This chapter presents an overview of FEM theory applicable to this study.

First, the FEM principals necessary to represent the structural characteristics of the compressor are discussed. This will include discretization of the structure into finite elements, determining properties of the elements, and assembling the elements into an approximate mathematical representation of the structure. Next eigensolutions to calculate natural frequencies and normal mode shapes are presented. Then the mode superposition method of calculating structural response to harmonic loads will be discussed. Finally, the component mode synthesis (CMS) method to assemble new structures from the modal representation of components is summarized.

2.1 Finite Element Method Principals

2.1.1 Discretization

To begin the FEM procedure, a structure is divided into smaller parts known as finite elements. The elements are connected at points called nodes. Elements have a simpler geometry and are easier to analyze than the full structure. By combining the analytical characteristics of the elements, the characteristics of the full structure are approximated. In general, accuracy of the approximation improves as more elements are used. In this investigation the compressor housing is developed from shell elements, as shown in Figure 3. In addition, beam elements and lumped-mass elements are used to represent other components.

2.1.2 Element Properties

Each element is characterized by a stiffness matrix $[k_e]$, a mass matrix $[m_e]$, and potentially a damping matrix, $[c_e]$. To determine element properties, displacement degrees of freedom (d.o.f.) are first assigned to element nodes. The six motions possible in 3-dimensional problems are x-y-z translations and $\theta_x - \theta_y - \theta_z$ rotations. Throughout the analysis, nodal displacements are the unknown quantities to be solved for.

Element stiffness matrices describe the equilibrium relationship between nodal forces and nodal displacements. For linear elastic material behavior, element stiffness matrices are $n \times n$ square matrices having the form

$$[k_e]\{d\} = \{f\} \tag{2.1}$$

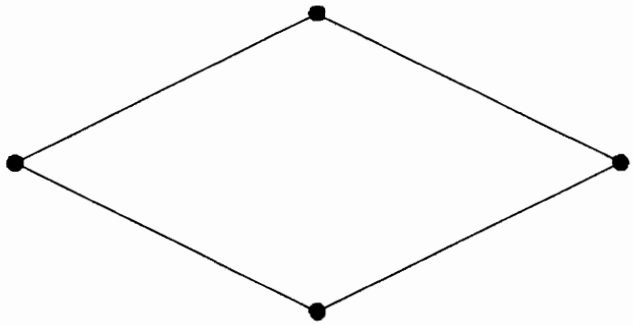

Linear Quadrilateral Shell Element

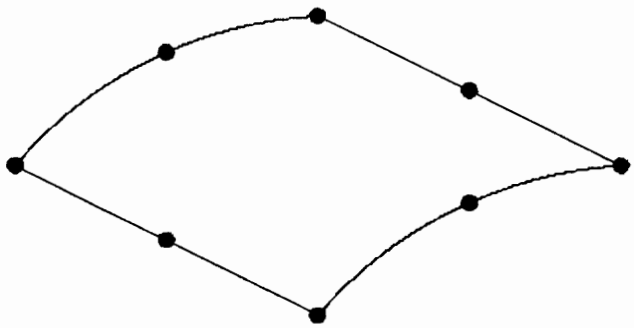

Parabolic Quadrilateral Shell Element

Figure 3. Shell Elements Used to Model the Compressor Housing

where n is the total d.o.f. of the element found by multiplying the number of nodes by the d.o.f. assigned to each node. For example, the linear shell element of Figure 3 having four nodes with 6 d.o.f. per node, requires a 24 x 24 stiffness matrix. Cook [20] presents three methods available to formulate stiffness matrices, (1) directly using physical reasoning, (2) variational or energy methods, and (3) weighted residual methods. One common basis for matrix formulation methods is the use of an assumed interpolation function to find physical quantities within the element from nodal values. Consider the function ϕ, which may be displacements or any physical quantity known at the nodes. Within the element, ϕ is a smooth function represented by a simple polynomial. For example, within the x-y plane of the 4-node linear shell element, ϕ may be interpolated with the first-order polynomial

$$\phi(x,y) = a_1 + a_2 x + a_3 y + a_4 xy \tag{2.2}$$

where the coefficients a_k are found in terms of nodal coordinates and nodal values of ϕ. Within the x-y plane of the 8-node parabolic shell element, ϕ can be interpolated with the second-order polynomial

$$\phi(x,y) = a_1 + a_2 x + a_3 y + a_4 xy + a_5 x^2 + a_6 x^2 y + a_7 xy^2 + a_8 y^2 \tag{2.3}$$

Elements formulated with the higher order polynomial provide a better fit to the actual values of ϕ within the element, so fewer elements are needed to achieve the same degree of accuracy [20]. Converting elements to the higher order interpolation scheme will be used later to refine the models developed. The coefficients a_k are related to nodal d.o.f. and the interpolation function is rearranged in a shape function matrix, [N]. Then, displacements within the element may be interpolated from nodal d.o.f. using the expression

$$\{u\} = [N]\{d\} \tag{2.4}$$

The shape function matrix and the nodal d.o.f. define the admissible displacement field of each element which is fundamental to formulation of element properties.

Stiffness matrices for beam elements have been well established by direct methods. For example, Craig [21] presents the full 12 x 12 stiffness matrix for the 3-dimensional beam element, developed from Bernoulli-Euler beam theory. Formulations for the shell element stiffness matrix vary however. Shell element formulations address several properties including shell geometry, which is formed on a curved surface and thin in comparison to planar dimensions. Simultaneous bending loads and in plane (membrane) loads are also considered. If the shell is thick, transverse shear deformation and thickness-direction normal stress become a factor. Three translational d.o.f. and two rotational d.o.f. are typically assigned to the nodes. The out-of-plane, or "drilling" rotational d.o.f. has no stiffness associated with it. Thus, shell elements typically have an artificial stiffness assigned to this d.o.f. for compatibility with other elements.

The principal of stationary potential energy [20] provides a general element stiffness matrix formulation based on the shape functions assumed.

$$[k_e] = \int_{Ve} [B]^T [E][B] dV \tag{2.5}$$

In eq. (2.5), $[E]$ is the material property matrix which relates the stress and strain components in the material. $[B]$ relates the element strain components to nodal displacements in a matrix of the form $\{\varepsilon\} = [B]\{d\}$. To obtain $[B]$, strain-displacement relations [20] are used to differentiate the element shape functions, $[N]$. Finally, numerical integration over the element volume, V_e, is necessary to evaluate the expression for $[k_e]$. Four different thin shell elements are employed in this investigation, each having potentially different formulations. The energy method described above is only one approach. Alternate approaches and further details of element formulation will not be presented.

Varied approaches to element mass matrix formulation also exist. One method, known as the "consistent" formulation derives the mass matrix similar to the stiffness matrix, using the integral expression

$$[m_e] = \int_{Ve} \rho [N]^T [N] dV \tag{2.6}$$

where ρ is the element mass density and $[N]$ are the shape functions used to interpolate over the element. The consistent-mass matrix uses the same shape functions as used to find $[k_e]$ and is consequently symmetric and full.

An alternate approach, known as the "lumped-mass" matrix formulation lumps point masses at the element nodes. The particular distribution of mass at each node is found by various methods. One approach simply divides the mass evenly among the nodes, while another uses diagonal terms from the consistent-mass matrix which are scaled to preserve the appropriate total element mass. Lumped-mass matrices typically have only diagonal coefficients which correspond to translational motion unless diagonal rotary terms and off-diagonal coupling terms are assigned. The diagonal mass matrix provides advantages during calculations and storage.

For comparison, Knight [23] reports that the lumped-mass matrices work well with refined meshes by reducing numerical difficulties associated with the off-diagonal terms. The consistent formulation generally performs better with coarse meshes because rotary inertia terms at the nodes are included.

2.1.3 Assembly of Structure Matrices

Connecting the elements results in mass and stiffness matrices for the full structure. The structure stiffness matrix, $[K]$, is built by summing the element stiffness matrix coeficients, $[k_e]$. Similarly, the structure mass matrix is built from the element mass matrices. Note that lumped-mass elements refer to additional mass matrices which are assembled into the structure mass matrix to represent point masses on the structure. No stiffness is associated with the lumped-mass elements.

Damping may be conceptually defined at the element level for finite element analysis with existing structural damping models. However, the introduction of complex numbers increases the computational requirements substantially. The conventional approach is to adopt the "proportional" damping scheme instead. This approach is also required later to diagonalize $[C]$. In the proportional damping scheme, the structure's damping matrix is defined as a linear proportion of the structure mass and stiffness matrices as follows.

$$[C] = \alpha[K] + \beta[M] \tag{2.7}$$

Finally, the assembly process produces the structural equation of motion,

$$[M]\{\ddot{D}\} + [C]\{\dot{D}\} + [K]\{D\} = \{F\} \tag{2.8}$$

which equilibrates the external load, $\{F\}$, with a combination of inertial, damping, and elastic forces. The external load is generally a function of time, and the matrix expression represents n equations where n is the total d.o.f. of the assembled structure.

2.2 *Eigensolution for Normal Modes of Vibration*

The next step is to solve for the structure's modal characteristics. An eigenvalue problem [20, 23] is set up by assuming

- Free vibration, no external loads are applied to free d.o.f.
- No damping, coefficients of $[C]$ are zeroed
- Harmonic motion; each d.o.f. has sinusoidal motion of the same frequency, in phase or exactly out of phase with all other d.o.f., in response to initial conditions

In terms of the differential equation of motion (2.8), peak amplitudes of nodal oscillation are defined in the vector $\{A\}$ so that

$$\{D\} = \{A\}\sin(\omega t) \tag{2.9a}$$

$$\{\ddot{D}\} = -\omega^2\{A\}\sin(\omega t) \tag{2.9b}$$

where ω is the circular frequency. Substitution of eqs.(2.9) into eq.(2.8) leads to the generalized eigenproblem,

$$([K] - \lambda[M])\{A\} = \{0\} \tag{2.10}$$

which may be solved for the eigenvalues, $\lambda_r \equiv \omega_r^2$. There is one independent eigenvalue for each d.o.f. in the structural equations. For each λ_r there is an associated eigenvector, $\{A\}_r$, which is a set of relative nodal displacements also obtained from eq. (2.10). To simplify further operations here, the eigenvectors will be "mass normalized" such that each modal mass is unity. That is,

$$m_r \equiv \{\phi\}_r^T[M]\{\phi\}_r = 1 \tag{2.11}$$

where $\{\phi\}_r$ is the mass-normalized mode shape corresponding to ω_r, and m_r is the r^{th} coefficient of the modal mass matrix. It may be shown with eq.(2.10) that modal stiffness is also simplified by mass normalization,

$$k_r \equiv \{\phi\}_r^T[K]\{\phi\}_r = \omega_r^2 \tag{2.12}$$

The eigenvectors possess unique properties and among the most important is orthoganality with respect to the symmetric mass and stiffness matrices:

$$\{\phi\}_j^T[M]\{\phi\}_k = \{\phi\}_j^T[K]\{\phi\}_k = 0 \qquad (j \neq k) \tag{2.13}$$

In the next section, the mode superposition technique is described which takes advantage of these properties to decouple the system dynamic equation of motion.

2.3 *Mode Superposition Method*

Modal superposition procedures transform the coupled structural differential equation of motion, eq. (2.8) with physical coordinates into a set of uncoupled equations with modal coordinates that may be solved independently [21]. The key step is to introduce the coordinate transformation

$$\{D\} = [\Phi]\{\gamma\} \tag{2.14}$$

where $\{D\}$ is the displacement vector in physical coordinates, $[\ \Phi\ ]$ is the modal matrix[2] whose columns are the mass-normalized mode shapes, and $\{\ \gamma\ \}$ is a vector of modal coordinates or mode participation factors. Premultiplying the system dynamic equation by $[\Phi]^T$ and introducing the coordinate transform of eq. (2.14) results in the structural equation of motion in modal coordinates

$$\begin{aligned}
&[m]\{\ddot{\gamma}\} + [c]\{\dot{\gamma}\} + [k]\{\gamma\} = \{F_\gamma\} \\
&\text{where} \\
&[m] \equiv [\Phi]^T[M][\Phi] = [\ I\ ] \\
&[c] \equiv [\Phi]^T[C][\Phi] \\
&[k] \equiv [\Phi]^T[K][\Phi] = [\omega^2] \\
&\{F_\gamma\} \equiv [\Phi]^T\{F\}
\end{aligned} \tag{2.15}$$

Proportional damping, as defined in eq. (2.7), is required to diagonalize $[C]$ and to obtain the modal viscous damping matrix, $[c]$. The diagonal coefficients of the modal damping matrix, c_r, are defined as

$$c_r = 2\zeta_r\omega_r \tag{2.16}$$

---

[2] Note this discussion presumes that in theory all modes are included in $[\ \Phi\ ]$. In practice, using the lower modes is sufficient to accurately describe the motion and make the computation tractable.

where ζ_r is the modal damping ratio. Now, with all of the structure matrices diagonalized and with the modal mass coefficients equal to unity, the uncoupled structural equations are re-written as r independent second-order differential equations of the form

$$\ddot{\gamma}_r + 2\zeta_r\omega_r\dot{\gamma}_r + \omega_r^2\gamma_r = F_{\gamma r} \qquad r = 1,2,...,n \text{ modes} \tag{2.17}$$

For each mode, eq. (2.17) is treated as a single d.o.f. system having solutions that are well documented [21, 24]. For instance, the solution to eq. (2.17) consists of a complimentary and a particular solution. First, the complimentary solution is found from the free-vibration response of the damped single d.o.f. system, one general form being

$$\gamma_r(t) = e^{(-\zeta_r\omega_r t)}\left(a_1\cos\omega_r\sqrt{1-\zeta_r^2}\ t + a_2\sin\omega_r\sqrt{1-\zeta_r^2}\ t\right) \tag{2.18}$$

The unknown coefficients, a_k, are solved for in terms of initial conditions. The complimentary solution is not considered, however, because the transient response is damped out as shown by the first term of eq. (2.18). Only the steady-state modal response will be considered. Steady-state response is described by the particular solution, which depends on the the dynamic forcing term, $F_{\gamma r}(t)$. The harmonic forces of this study are defined by the expression

$$\{F_\gamma\} = [\Phi]^T\{F\}e^{j\Omega t} \tag{2.19}$$

Therefore, the particular solution to eq. (2.17) becomes

$$\gamma_r(t) = |\gamma_r|\, e^{j(\Omega t - \theta)} \tag{2.20}$$

where $|\gamma_r|$ is the steady-state modal response amplitude and θ is the phase angle of steady-state response relative to the excitation. The modal response amplitude can be found with the complex frequency response function of eq. (2.22a).

$$\gamma_r = \frac{\frac{F_{\gamma r}}{k_r}}{1 - \left(\frac{\Omega}{\omega_r}\right)^2 + 2j\zeta\left(\frac{\Omega}{\omega_r}\right)} \tag{2.21a}$$

where the phase angle is obtained from

$$\tan\theta = \frac{2\zeta\left(\frac{\Omega}{\omega_r}\right)}{1 - \left(\frac{\Omega}{\omega_r}\right)^2} \tag{2.21b}$$

The final step of the mode superposition procedure is transformation of the structure's response back to physical coordinates using eq. (2.14). Each modal d.o.f. response, γ_r, is the scale factor or modal participation factor for the r^{th} mode. Response calculations considered in this study include plotting the velocity response, $\{\dot{d}_i\}$ at single physical d.o.f. over a range of forcing frequencies to obtain analytical frequency response functions. Also considered is the full structural response, $\{D\}$, at a specific forcing frequency.

2.4 *Component Mode Synthesis*

Component mode synthesis (CMS) refers to a modeling technique in which a large structure is composed of smaller substructures. The substructures are analyzed independently for natural frequencies and mode shapes. The substructure modes, or component modes, are later used to develop an approximate mathematical model of the full structural system which will be referred to as the CMS model. The CMS model may be solved to determine the large structure's modal properties and subsequently, response to dynamic excitation.

Much of the CMS technology evolved in the aerospace industry, where the components are often complex and many are designed and produced by different organizations. Thus, one advantage of the CMS procedures is the independence provided for design and analysis of substructures. Another advantage of the CMS method is a reduction of the d.o.f. required for large structural models, particularly systems having several natural components. In this study, the reciprocating compressor will be divided into a housing component and several internal components for CMS analysis.

The following section presents an overview of a CMS procedure known as the Craig-Bampton method [21]. Several other variations of the CMS method exist and are reviewed in reference [22]. The various CMS methods differ in the approach taken to enforce compatibility at the substructure interfaces, and in the type of mode set used to describe physical displacements of the substructures. For example, the mode set may include component normal modes found with fixed, free or loaded boundary conditions at the interface points. In addition, the mode sets are often supplemented by static deflection shapes. I-DEAS™ employs the Craig-Bampton approach among some of the other variations [19].

Consider an undamped structure that is divided into two components, *1* and *2*, which have a common redundant interface point. The components are represented by the substructure matrices $[m_1]$, $[k_1]$, $[m_2]$ and $[k_2]$. The first step is to calculate the normal modes of each substructure, k. Then a set of Ritz vectors, $[W_k]$ is established. $[W_k]$ is a matrix whose columns are mass-normalized component modes and constraint modes of the substructures. Constraint modes of a substructure are static deflections found by imposing a unit displacement at a single physical interface coordinate while zeroing displacement at the remaining interface coordinates. A constraint mode is found for each physical d.o.f. in the substructure interface. Once obtained, the Ritz vectors define a transformation between component physical, $\{D_k\}$, and generalized coordinates, $\{p_k\}$

$$\{D_k\} = [W_k]\{p_k\} \tag{2.22}$$

The next step is to calculate the generalized mass matrix, $[m_k]$ and the generalized stiffness matrix, $[k_k]$. For each substructure,

$$[m_k] = [W_k]^T[m_k][W_k] \qquad (k = 1,2) \tag{2.23a}$$

$$[k_k] = [W_k]^T[k_k][W_k] \qquad (k = 1,2) \tag{2.23b}$$

Depending on the number of component modes retained in $[W_k]$, the size of the component matrices may be reduced significantly. Next the component generalized coordinate, mass, and stiffness matrices become elements of partitioned matrices for derivation of the system equation of motion.

$$\{p\} = \begin{Bmatrix} p_1 \\ p_2 \end{Bmatrix} \tag{2.24a}$$

$$[m_{cms}] = \begin{bmatrix} m_1 & 0 \\ 0 & m_2 \end{bmatrix} \tag{2.24b}$$

$$[k_{cms}] = \begin{bmatrix} k_1 & 0 \\ 0 & k_2 \end{bmatrix} \tag{2.24c}$$

Since all of the generalized coordinates are not independent, constraints must be applied to the interface coordinates to assure force and displacement compatibility at the interface. Dependent coordinates, $\{p_d\}$, are selected from the redundant d.o.f. The remaining coordinates form the independent coordinates, $\{p_i\}$. A constraint equation may be written in the form of

$$[S]\{p\} = \{0\} \tag{2.25a}$$

which is further partitioned into dependent, d, and independent, i, components such that

$$[S_d \; S_i]\begin{Bmatrix} p_d \\ p_i \end{Bmatrix} = \{0\} \tag{2.25b}$$

The system dynamic equation of motion is obtained from eqs. (2.24) and (2.25) using a Lagrangian derivation [21, 22]. Then, the constraint eq. (2.25) is used to write the linear transformation, $\{p\} = [T]\{p_i\}$. The transformation matrix, $[T]$, relates the full set of generalized coordinates, $\{p\}$ to the independent coordinates, $\{p_i\}$ so the system equation may be rearranged in terms of the independent generalized d.o.f. Finally, the desired CMS system equation of motion becomes

$$\begin{aligned} &[M]\{\ddot{p}_i\} + [K]\{p_i\} = \{0\} \\ &\text{where} \\ &[M] = [T]^T[m_{cms}][T] \\ &[K] = [T]^T[k_{cms}][T] \end{aligned} \tag{2.26}$$

Equation 2.26 is then solved for the system natural frequencies and normal mode shapes in terms of the generalized coordinates, $\{p_i\}$. Solution in the generalized coordinates substantially reduces the computational requirements. Once the system modal properties are solved for, an adaption of the mode superposition procedure is used to calculate forced vibration response. Unlike section 2.3 which proceeds from physical coordinates, the mode superposition would be formulated in the CMS method generalized coordinates.

3.0 Experimental Database

Experimental measurements were made to determine the dynamic characteristics of a compressor housing and for a pressurized compressor assembly. The experimental procedure involved conventional modal analysis and laser-based experimental dynamic analysis to find frequency response functions (FRFs), natural frequencies, and mobility maps. In this section, the experimental procedure is briefly described and results are summarized to exemplify the data which guides analytical model development, based on references [1] and [25]. A detailed discussion will not be included because the experimental techniques belong to a separate phase of the project

First, an ensemble of transfer FRFs were found by impact and random excitations. These provided a range of resonance frequency estimates and the optimal forcing location necessary to excite all structural modes. Figure 4 and Figure 5 show typical FRFs of the housing and the compressor assembly, respectively. Comparison of the two FRFs shows an approximate doubling of the externally observable *modal density*, or the number of modes occurring in the same frequency range, upon compressor loading. The additional frequencies result from a number of mechanical and acoustic interactions between the housing and the internal components which are further examined when the model is discussed in Chapter 5. The labeled peaks indicate resonances at which the mode shapes were also documented.

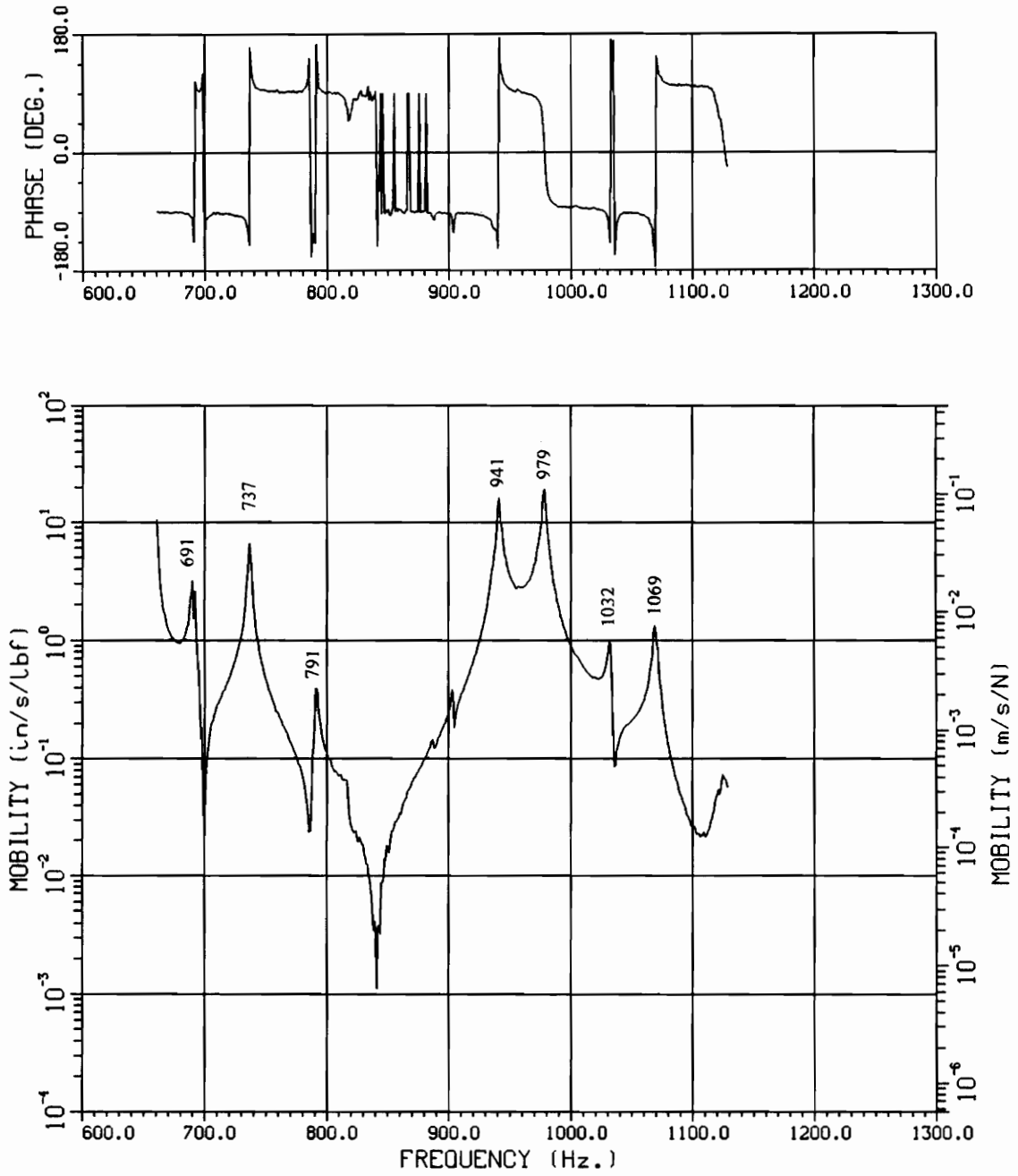

Figure 4. Experimental Housing Transfer FRF:

Force at girth; response at top

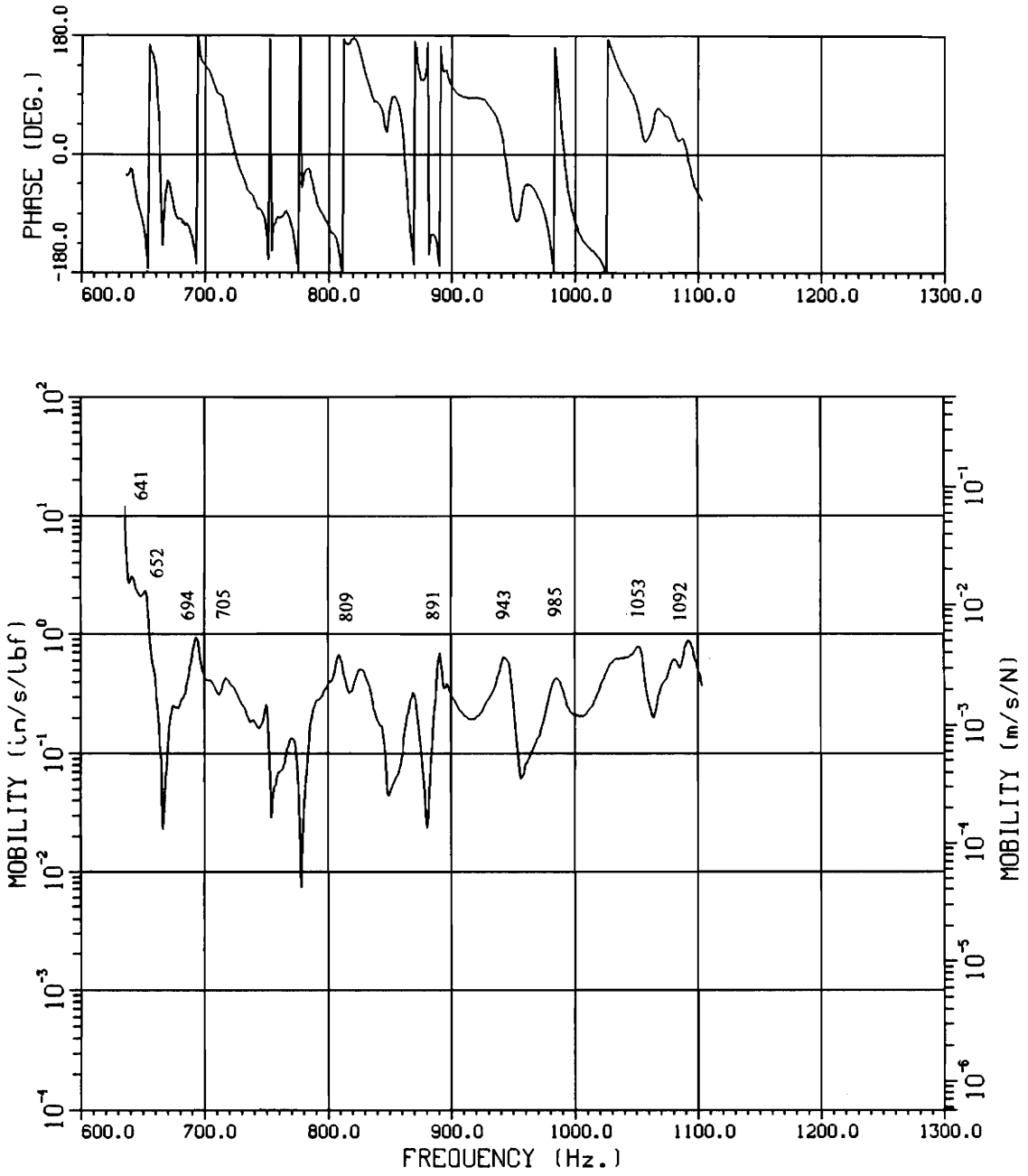

Figure 5. Experimental Loaded Compressor Assembly Transfer FRF:

Force at girth; response at top

Next, to document the shapes, mobility (velocity/applied force) response was recorded with a scanning laser Doppler velocimeter while shaking the housing at a single resonance frequency. The exact natural frequencies were found at this point within 1 milliHertz by comparing the phase angle between the velocity and force signals. Figure 6 and Figure 7 show typical mobility maps of the compressor housing and the compressor assembly, respectively. The mobility maps indicate the resonance deflection shape which is thought to be dominated by the mode shape corresponding to the shaking frequency. To read the maps, notice that negative mobilities are shown in blue through yellow colors, red indicates positive mobilities, and nodal lines are shown in black. The smooth face opposite the electrical box side is referred to as the front. By comparing scans taken at each side of the compressor, the housing deflection is determined. The two mobility maps shown here exemplify several traits of the compressor that are of significant interest for model development. One notable area is the coupling, or simultaneous motion of the housing's side and top, shown in the 944 Hz scan of the housing. Also notice the restraining effect of the girth joint. In the compressor assembly scan, the localized bottom motion is due to interaction of the internal compressor mechanism at its connection point to the housing.

The complete experimental database of natural frequencies and mode shapes, compiled from numerous mobility scans, is summarized in Table 1. A total of eight housing shapes and fourteen assembly shapes were found for the Bristol Compressor Model H23A. The shapes are described by a plus-minus notation which identifies the direction of housing motion observed in sequential views around the compressor. The "complex" modes involve too many nodal lines to effectively describe with this notation. As shown by the summary, several of the housing mode shapes were found in the compressor assembly, with some modification. In general, the modified housing modes showed a decrease in natural frequency as one may suspect from the additional mass. Some modified housing modes showed local interactions with the internal components at their region of connection to the housing. In the high-frequency complex modes, the lower portion of the housing showed consistently more motion in the region where the internal compressor is suspended. In addition, several new modes were found that are unique to the loaded assembly.

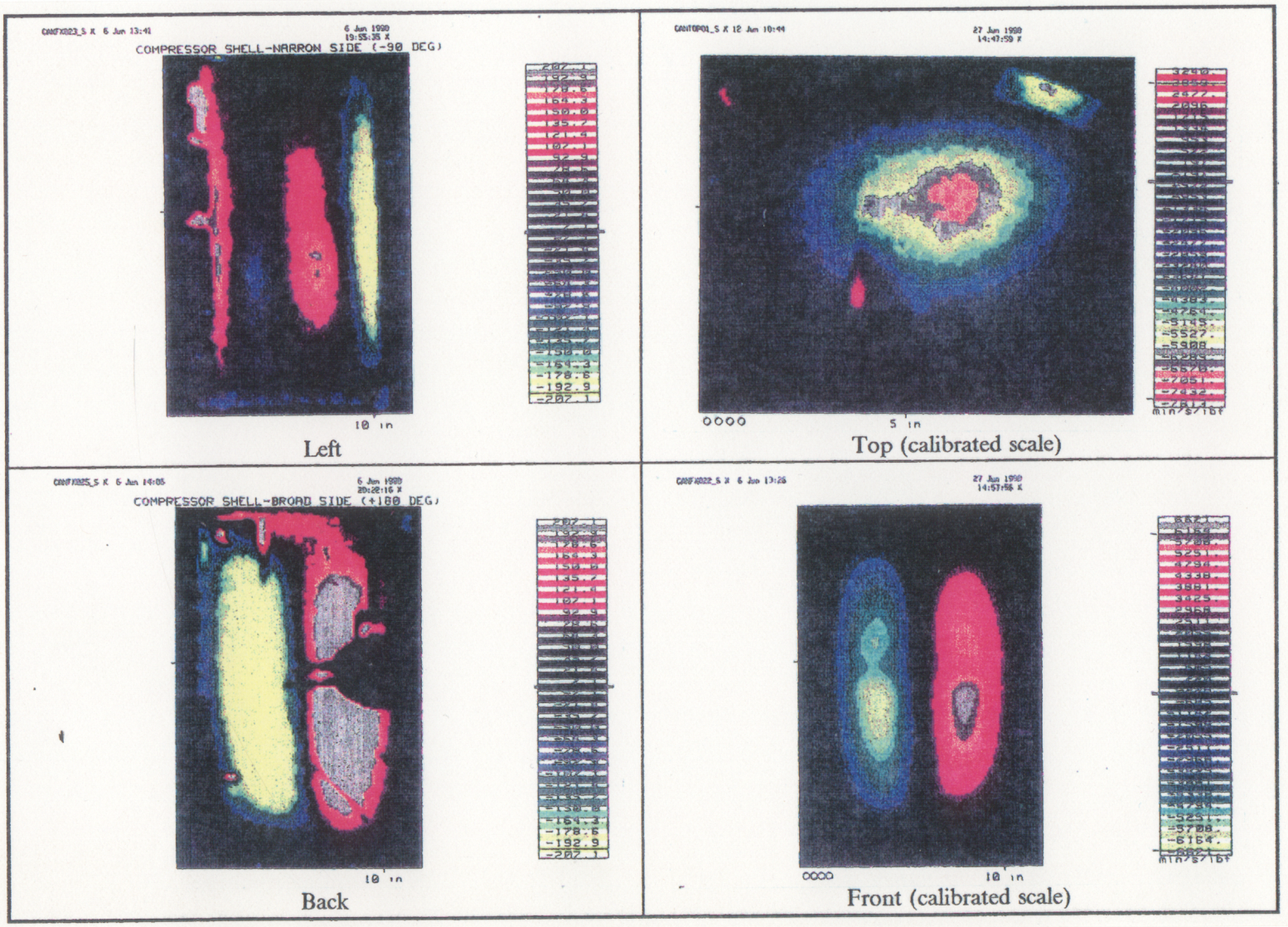

Figure 6. Experimental Mobility Map of Compressor Housing Excited at 944 Hz

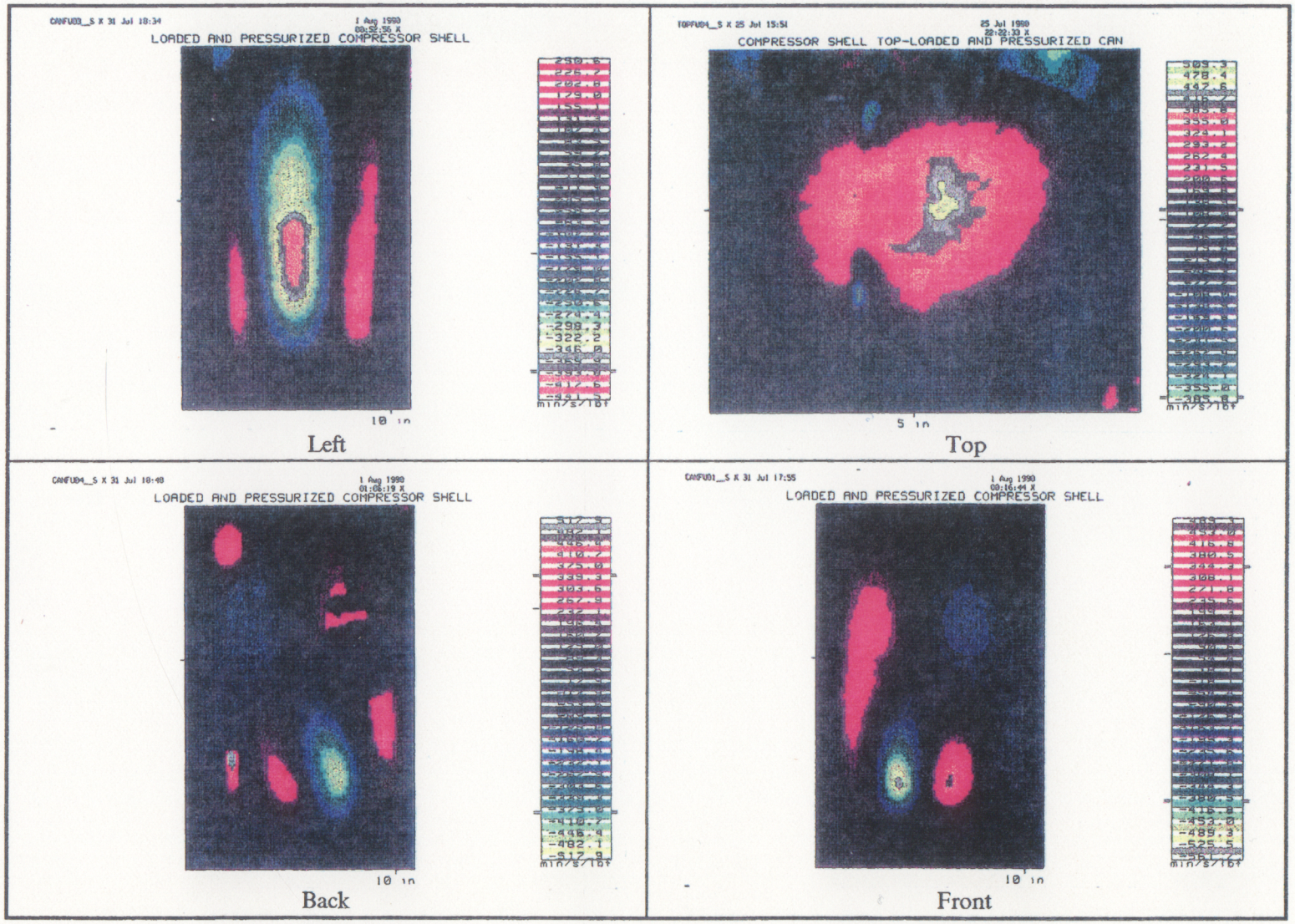

Figure 7. Experimental Mobility Map of Loaded Compressor Assembly Excited at 1054 Hz.

Table 1. Experimental Dynamic Characteristics of the Bristol Compressor model H23A

Housing Mode Shape						Pressurized Compressor Assembly Mode Shape							
Freq.,Hz	Front	Right	Back	Left	Top	Freq.,Hz	Front	Right	Back	Left	Top	Δ %	Comments
689.37	- + -					640.65	- + -	- +		+ -	+	-7.1	Same
736.39	+ -	- + -	- +	+ - +		652.37	- +	+ - +		- + -	-/+	-11.4	Opp. phase
						691.42	- +	+ - +		- + -	+	-----	New
791.14	- + -		+			702.11	- + -	- +		+ -	+	-11.3	Same
						807.23	- +	+ - +	+ -		+(?)	-----	New
						893.58	+ -	- + - +	+ - + -	+ - +		-----	New
944.06	- +	+ - + -	- +	+ - + -	-							-----	No Match
1032.25	+ - +	+ - +	+ - +	+ - +	-/+	950.80	+ - +	+ - +	+ - +	+ - +	+	-7.8	Top differs
1069.05	+ - + -	- +		- +	-	988.79	- + - +	+ -	- + - +	n - +	+	-7.5	Opp. phase
						1054.28	+ - + - + -	- + -	- + - + - +	+ - +	+	-----	New
984.15	- +	+ - + -	- +	+ - + -	+	1091.82	+ - + - + -	- +	+ - + - + -	+ - + - + - +	+	+10.9	Rough match
						4849.0						-----	Complex
						4893.0						-----	Complex
						5483.0						-----	Complex
						6070.0						Complex Top	Complex

Legend: + = positive going velocity; - = negative going velocity; n = node

Extracted and updated from Hurst, et. al. [1].

4.0 Compressor Housing Finite Element Models

Development of compressor housing models using shell-type finite elements is discussed in this chapter. Initial modeling simplifications are described and potential modeling errors are presented. Eigenvalue modeling updates are documented and efforts are made to show the significance of each refinement on model performance. Initial model and refined model normal mode solutions are presented and compared to the experimental dynamic analysis database. Forced response analysis emulating the experimental dynamic analysis is presented in section 4.2, and is found to enhance the model development procedure.

4.1 Housing Eigenvalue Model Development

4.1.1 Compressor Description

Figure 1 on page 2 shows some of the compressor features which complicate analytical model development. The compressor housing is drawn in two sections from initially flat steel blanks. Using a retaining ring and dies, the blanks are deformed into the appropriate shapes. Then, the top and bottom sections are welded together from the outside with a single lap-joint at the compressor midsection, referred to as the girth. Interaction of the housing sections at the girth joint is difficult to represent analytically. Service connections present other modeling difficulties. One factor is mass loading by accessories, another factor is the geometry modifications made to incorporate ac-

cessories. Several difficulties inherent to the manufacturing process are not as apparent. The housing potentially has regions with local yielding, thickness changes, and geometric variations different from the design specifications and from unit to unit. All may lead to modeling inaccuracies.

4.1.2 Initial Housing Model

Consider the initial[3] housing model, "SVIFF", shown in Figure 8. This model serves as the starting point for repeated updates made to improve accuracy. The initial housing geometry was developed from the manufacturer's production drawings. Efforts were made to represent the geometry accurately but some simplifications exist. The surfaces are smooth and symmetric to ease geometry definition. The bottom mesh conforms to the surface recesses which incorporate the mounting feet. Nodes in the bottom are located at points corresponding to the spot welds used to attach the feet. Average thickness in the model is less than the stock material, however, it is uniform and does not include the regional variation of the housing thickness. A band of thick elements is used to represent the girth. No other accessories or geometric attributes were included.

4.1.3 Initial Housing Eigensolution

Results of the initial, free-free housing model eigensolution do not agree with the experimental dynamics analysis (EDA) data as well as one would like. Five of the initial analytical modes were correlated to experimental modes but significant differences exist, particularly in the top. Table 2 compares the initial analytical natural frequencies to the test data.

---

[3] Initial after several solutions to check the solution procedure and boundary conditions performed by Mr. Ken Wallace on the housing models "SOLN1", "SOLN2", "SVIR" and "SVIFF" during the early stages of this project.

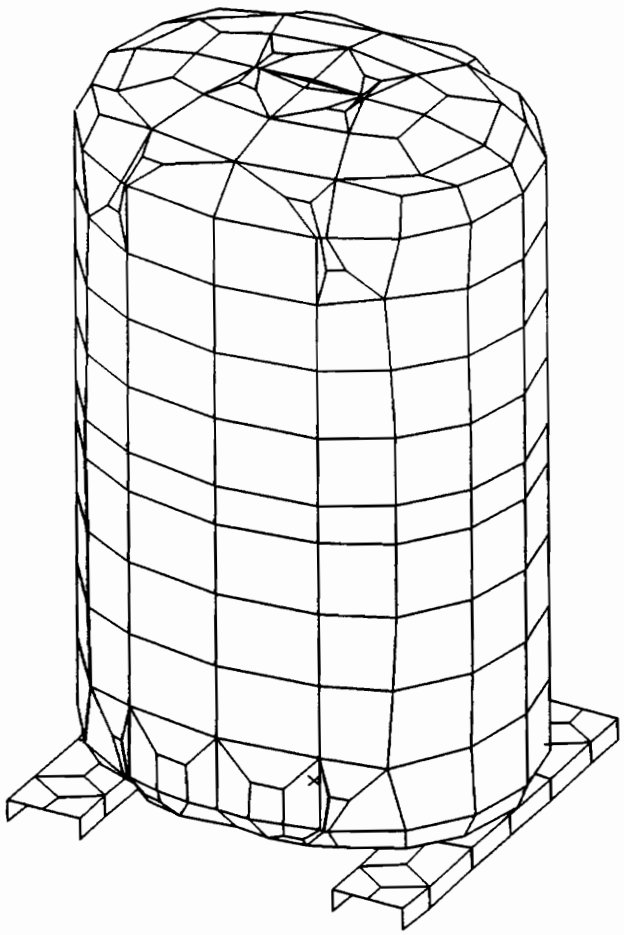

Model Specifications

- Model Filename: "SVIFF"
- 388 Nodes
- 372 linear quadrilateral shell elements
- 2328 total d.o.f.
- free-free boundary conditions
- $T_{avg} = 0.108$ in.
- $T_{girth} = 2T_{avg}$
- Isotropic material properties

Figure 8. Initial Compressor Housing Finite Element Model

Table 2. Initial Housing Model Correlation

Analytical Mode Descriptor [1]	Analytical Frequency [Hz]	Experimental Frequency [Hz]	Difference
M8(3,1)	737	689	7.0 %
M9(3,1)	802	736	9.0 %
M10(2,1)	843	791	6.6 %
M11(4,1)	1029	944,984 [3]	9.0, 4.6 %
M12(0,0,T1)	1476 [2]	944,984	56., 50. %
M13(4,1)	1119	1032	8.4 %
M14(2,1)	1135	1069	Shapes Differ

1 See Appendix A for a description of the mode descriptor scheme
2 Out of numerical order
3 No independent top motion was found experimentally. The 944 and 984 Hz experimental shapes have the same circumferential node line pattern. They are distinguished by the coupling of top motion having a 180 ° phase difference.

Figure 9 through Figure 15 show the initial analytical mode shapes corresponding to the natural frequencies of Table 2. A model representing only one-half or one-quarter of the housing geometry could find the mixture of symmetric and antisymmetric mode shapes as well, with a considerable reduction of model size. However, later models incorporated non-symmetric geometries and the forced response analysis models found nonsymmetric deflection shapes which required the full model.

Comparison of the initial results with the experimental data shows:

- Natural frequency differences range from 45 to 532 Hz (4.6 to 56 % of the experimental value)
- No coupling between top and side motion is found analytically to correspond with the test data
- The first independent top mode found analytically is at 1476 Hz, 532 Hz (56%) too high
- Experimental deflection scans reveal a constraining effect by the girth which is not as significant in the analytical shapes. This can be seen in the front view of Figure 6 on page 30.
- Mode M14(2,1) does not agree with the experimental shape

The following sections discuss model updating efforts to improve agreement between the analytical model and test data.

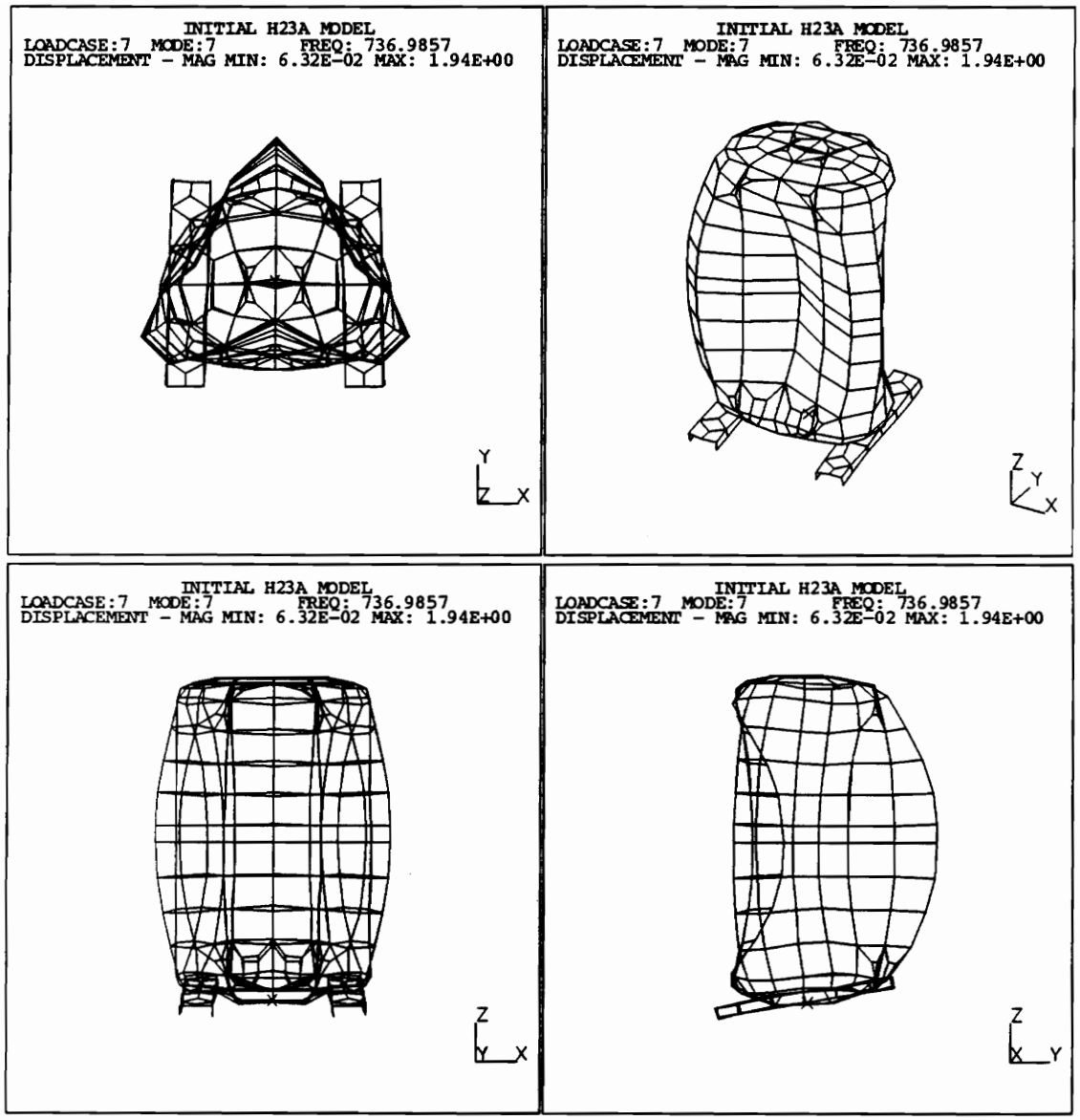

Figure 9. Initial mode shape M8(3,1) corresponding to 737 Hz

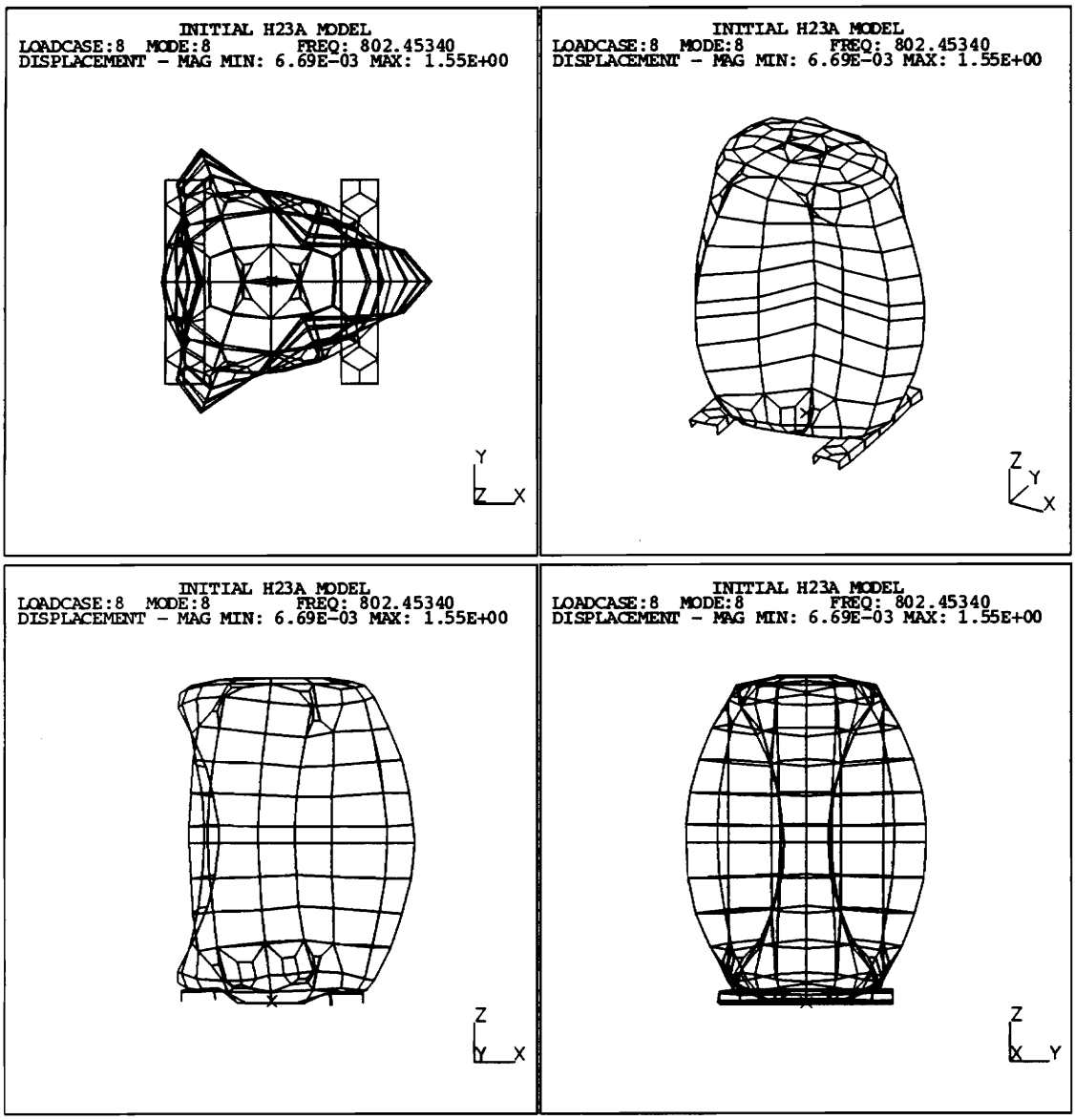

Figure 10. Initial mode shape M9(3,1) corresponding to 802 Hz

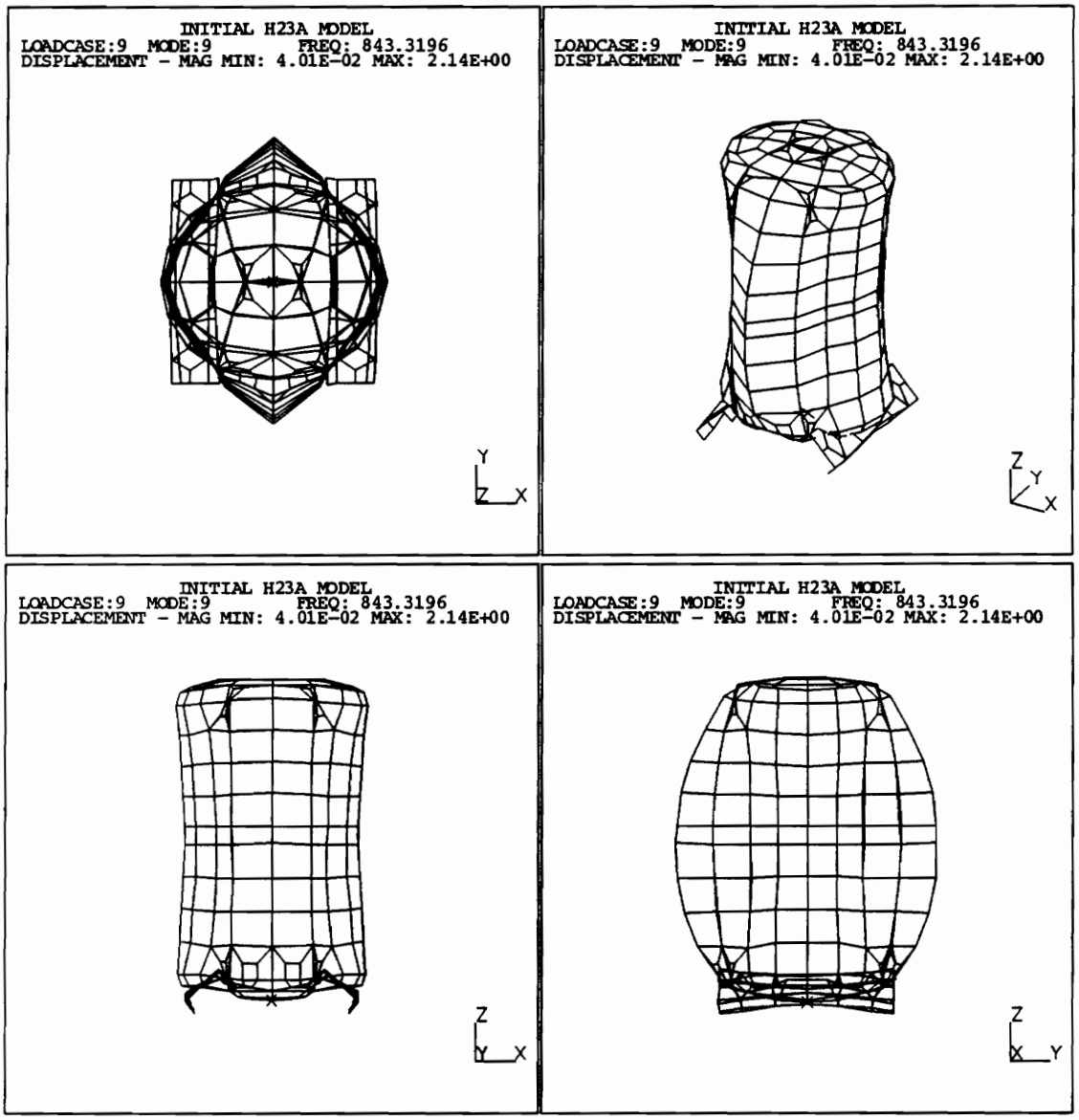

Figure 11. Initial mode shape M10(2,1) corresponding to 843 Hz

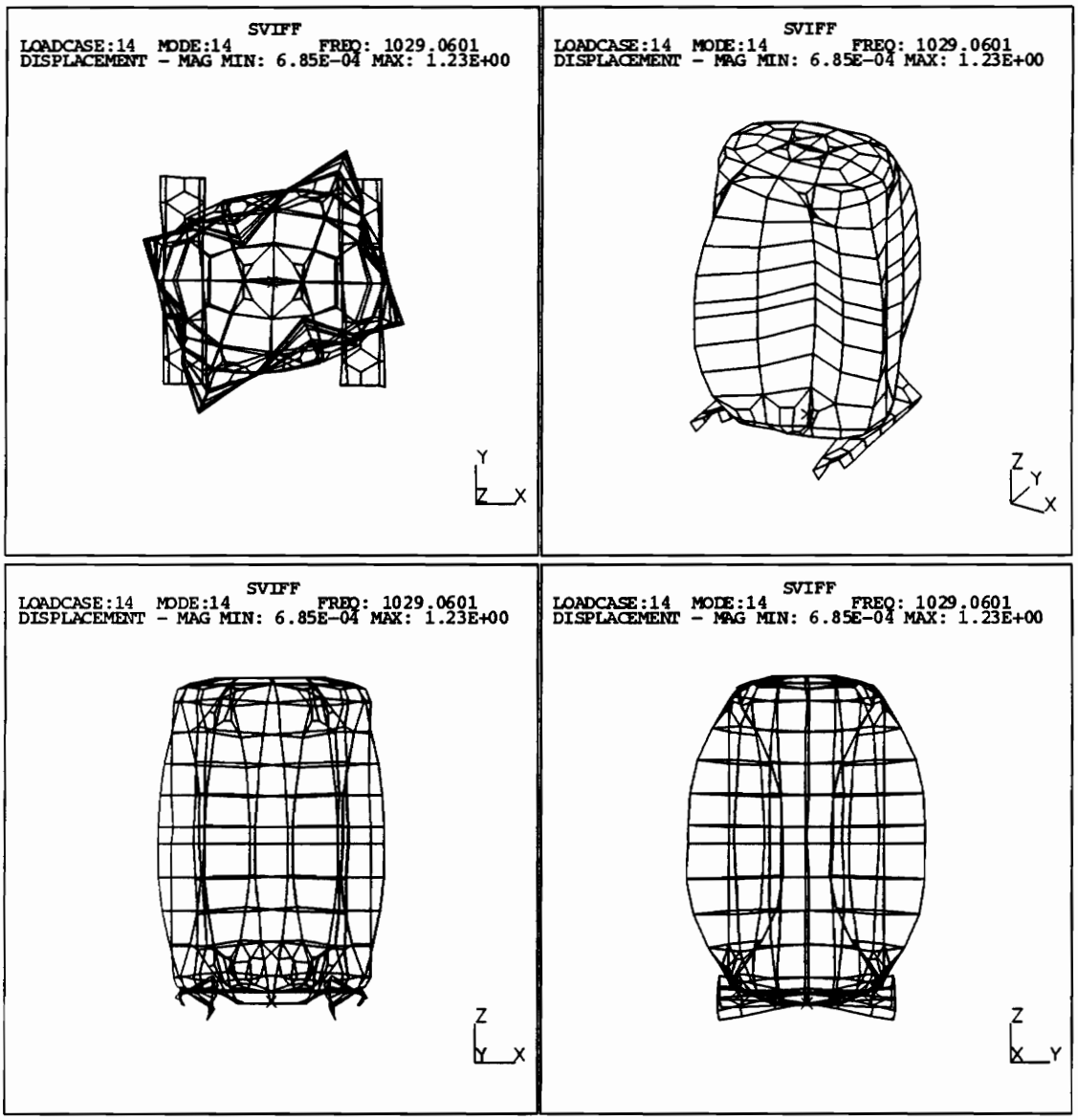

Figure 12. Initial mode shape M11(4,1) corresponding to 1029 Hz:

This shape is correlated to the experimental housing scan shown in Figure 6 on page 30.

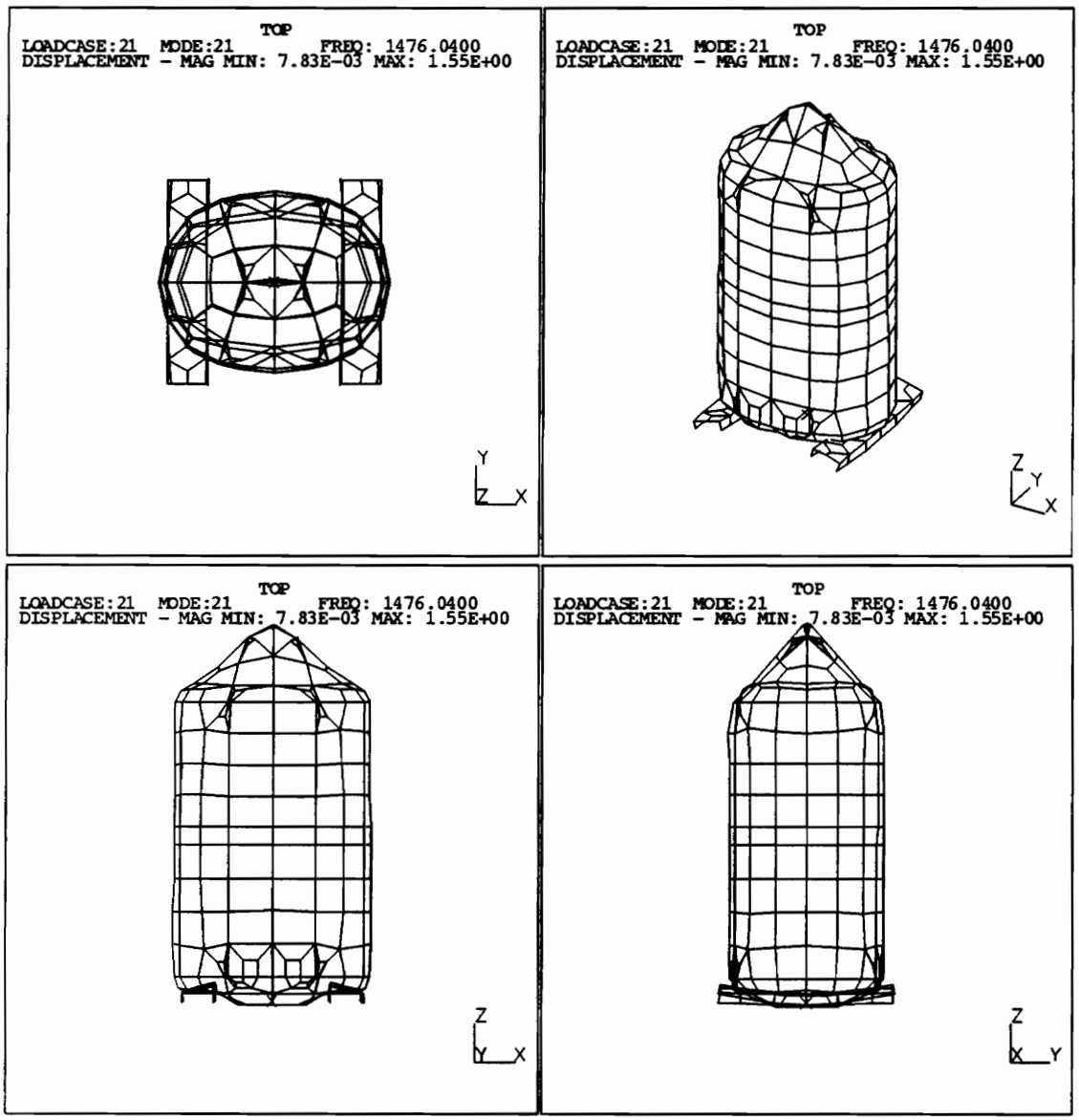

Figure 13. Initial mode shape M12(0,0,T1) corresponding to 1476 Hz

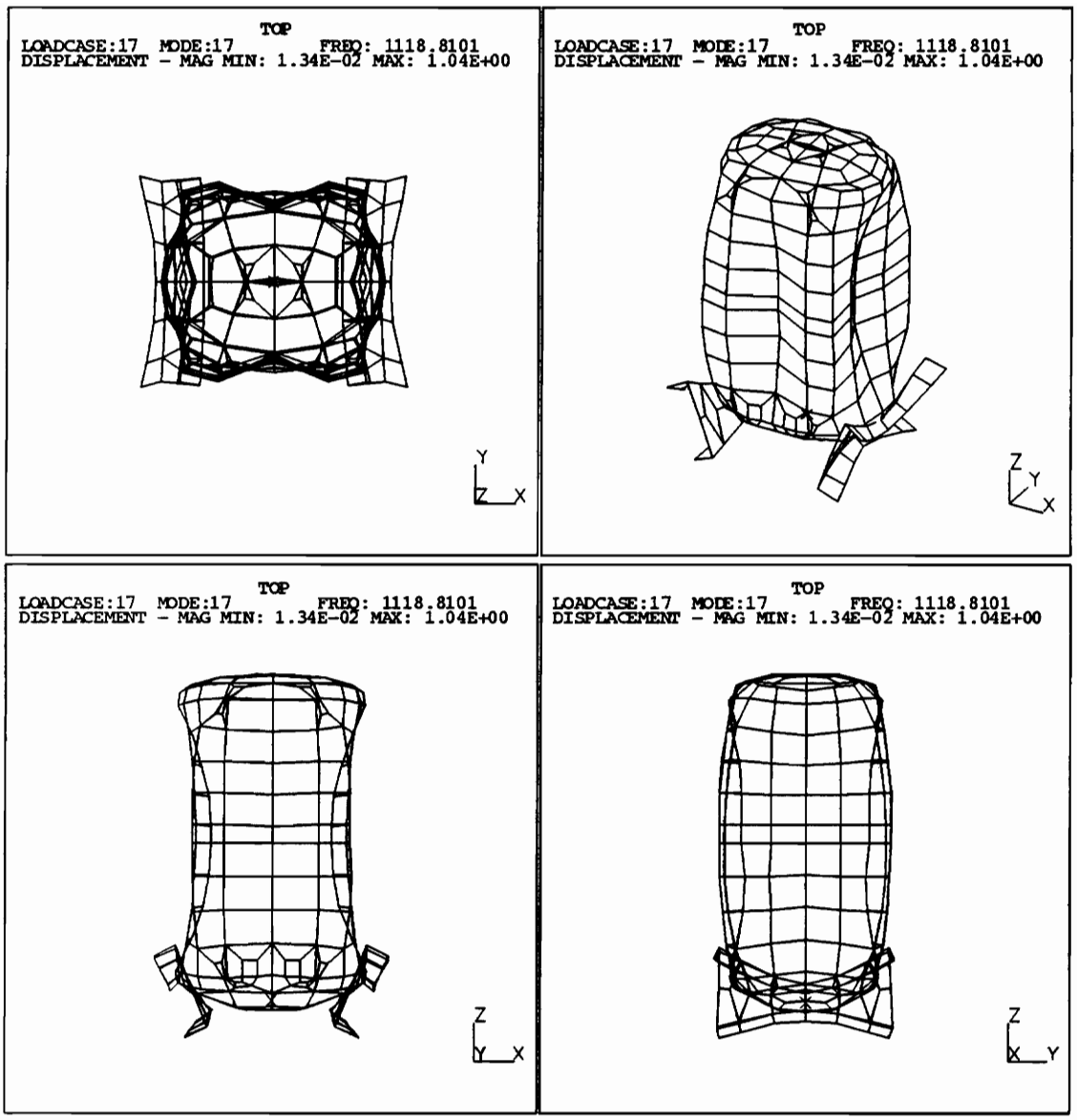

Figure 14. Initial mode shape M13(4,1) corresponding to 1119 Hz

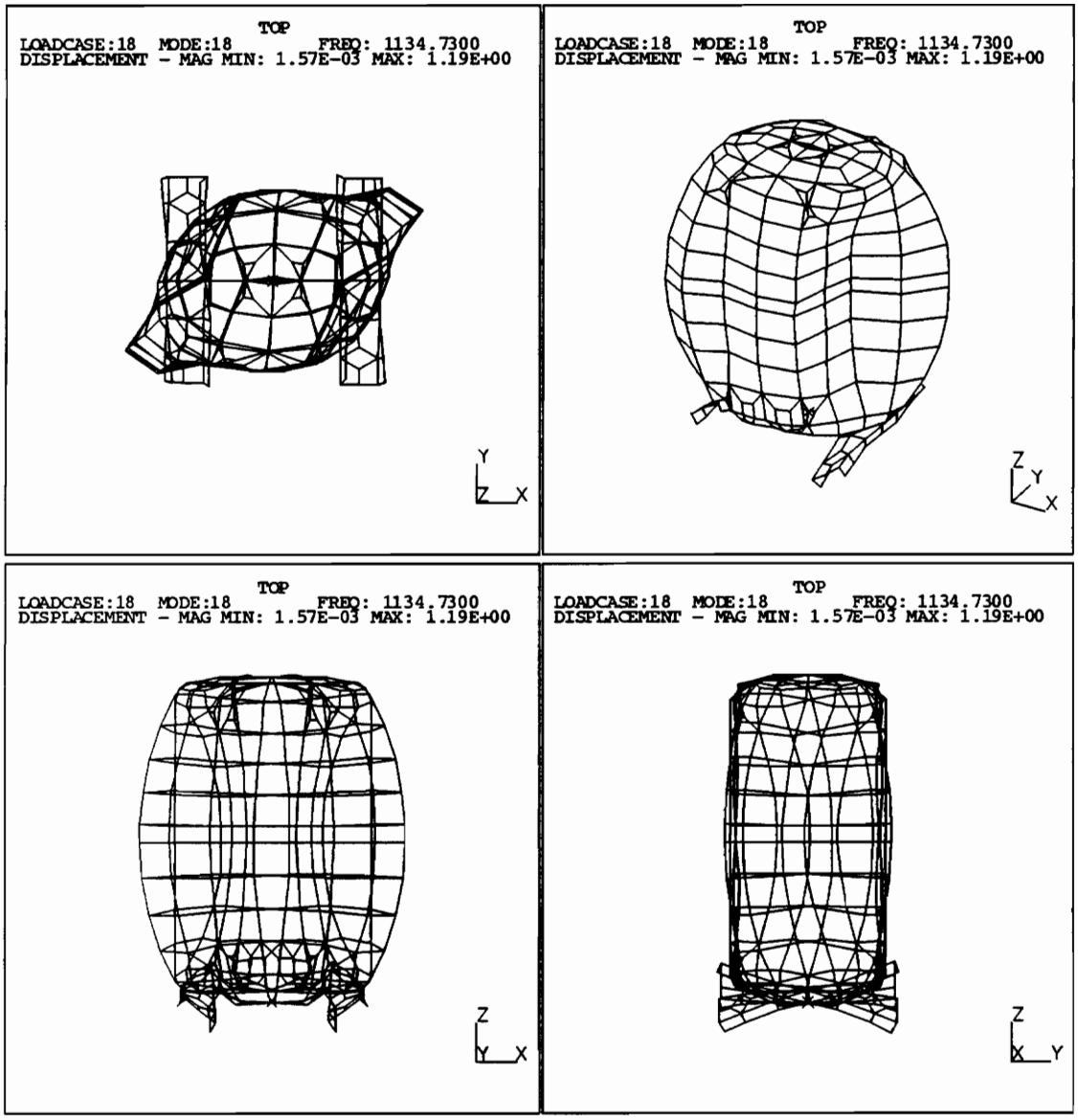

Figure 15. Initial mode shape M14(2,1) corresponding to 1135 Hz

4.1.4 Housing Model Updates

This section documents the revisions made to the initial model with perhaps an overwhelming amount of data. Although presented as concisely as possible, the data is felt necessary for completeness and to allow readers to personally evaluate conclusions derived from it. First, repeated updates made to the initial model are summarized chronologically in Table 3. The model updates target a range of potential causes for difference between the model predictions and test data. Next, complete eigensolution results of each revised model are presented in Table 4. Throughout the revisions, the models predict the same mode shapes. Frequencies listed for the earlier models are out of numerical order because the mode shapes are arranged with regard to the updated models. A more concise format is shown in Table 5 on page 47 which lists the range of natural frequency changes found for each update parameter considered, in order of significance. The factors which affect natural frequency prediction most are related to both theoretical factors and over-simplification by the analyst. Parameters which have a minimal affect on the frequency predictions are equally valuable to future modeling ventures. Each parameter will be discussed at length in the next section.

Table 3. Housing Model Descriptions

Model Name	Description	Comment
SOLN1	Guyan reduction solution, restraints on bottom, uniform 0.120 in. (3.04 mm) housing thickness	Preliminary model
SOLN2	Guyan reduction solution, restrained at mounting brackets, uniform 0.120 in. (3.04 mm) thickness	Preliminary model
SVIR	subspace iteration solution, restrained at mounting brackets, uniform 0.120 in. (3.04 mm) thickness	Preliminary model
SVIFF	Subspace iteration solution, free-free boundary conditions, uniform 0.108 in (2.74 mm) thickness	Preliminary model
SVILM	**SVIFF** with lumped-mass matrix formulation rather than a consistent mass matrix	[*M*] formulation (first revision)
SVITV	**SVIFF** with five regions having varied thickness, includes flat area on compressor top	Geometry variations
SVI#4	**SVITV** with coincident elements around girth	Joint stiffness
SVI#5	**SVI#4** with vertical mesh refinement near girth	Further discretization
SVI#6	**SVI#5** with extensive mesh refinement at top	Discretization
SVI6NAST	NASTRAN® solution to **SVI#6** using the Lanczos eigensolution algorithm	[*K*] varied(?) Solution method change
SVI#6*	**SVI#6** with top spring mount mass and inertia	Local mass loading
SVI6SPAR	**SVI#6*** with parabolic ordered elements	Element order
H23A1	**SVI#6*** with mesh refinement at shockloop and electrical connection regions	Discretization
H23TRLIN1	**SVI#6*** with top geometry refinements accounting for manufacturing variance	Geometry
H23TRPAR	**H23TRLIN1** with parabolic ordered elements	Element order
H23TRLIN2	**H23TRLIN1** with a lumped mass matrix	[*M*] formulation
H23TRLIN3	**H23TRLIN1** solved with SDRC CAEDS™ version 4 release 1 rather than I-DEAS™ version 4.1	[*M*],[*K*] formulation

Table 4. Housing Model Updating Summary

Analytical Mode Descriptor [1]	Model Name, Eigenfrequency [Hz.]																
	SOLN1	SOLN2	SVIR	SVIFF	SVILM	SVITV	SVI#4	SVI#5	SVI6 NAST	SVI#6	SVI6*	SVI6 SPAR	H23A1	H23 TR PAR	H23 TR LIN1	H23 TR LIN2	H23 TR LIN3
R1	197	68	68														
R2	351	83	83														
M1-6(RB'S)																	
M7 (ERROR)														254	123	123	293
M8 (3,1)	827	820	778	737	745	747	657	658	735	662	662	653	651	652	662	666	732
M9 (3,1)	943 [2]	938 [2]	843	802	796	808	720	721	796	724	724	713	717	713	724	715	781
M10(2,1)	908	897	880	843	851	841	770	771	868	772	772	772	761	773	772	768	827
M11(4,1)	DNF [4]			1029		DNF	864	865	1036	866	866	873	862	873	866	866	980
M12(0,0,T1)	DNF			1476 [2]		1025	1027 [2]		1414 [2]	1067 [2]	1021 [2]	1022 [2]	997 [2]	987 [2]	967	966 [2]	1039
M13(4,1)	1223			1119		DNF	968		1084	977	977	976	973	977	978	954	1162
M14(2,1,T1)	1299 [3]			1134 [3]			1124		1140	1233	1129	1117	1122	1102	1109	1110	1177
M15(5,1)				1550			1276		1605	1279				1323	1278	1161	
M16(5,1)				DNF					1794 [5]	1322				1345	1321	1347	
M17(4,2,T2)				1543 [3]					1808	1476					1475	1415	
M18(4,2,T2)				1572 [3]				(1908,	1932) [3]	(1513,	1887)				1513	1562 [2]	
M19(5,2,T2)										1551					1550	1433	
M20(5,2,T2)										1577					1576		
M21(0,0,T2)										1850					1614		
M22(0,0,T2)										DNF					1684		
M23(0,0,B1)										1737					1736		
M24(6,1)										1823					1824		
M25(5,2,T2)															1852 [6]		
M26(5,3,T3)										1916					1890 [6]		
M27(4,3,T3)															2022 [6]		
M28(0,0,T3)															2067 [6]		
M29(5,2,B2)															2090 [6]		
M30(5,3,B2)															2129 [6]		

1 see Appendix A for a description of the mode descriptor scheme
2 out of numerical order
3 sides match but no top motion
4 did not find in the frequency range solved for
5 NASTRAN ® found an M = 2 axial node line
6 additional side modification to incorporate side spring mounts

Table 5. Significance of Housing Model Updates

Parameter	$\Delta\omega_n$	Remark
Geometric variations	-24 to -36 % -1.9 to -5.4 %	• Local flattened spot on top • Less curvature of actual top due to manufacturing variance
Finite element method variance	+ 6.5 to + 23 % + 6.0 to + 19 %	• NASTRAN® formulation and solution with Lanczos algorithm • SDRC CAEDS™ solution
Coincident elements for girth stiffness reduction	-17 to -8.8 %	• Effective to correlate most modes involving side motion
Lumped mass matrix	-9 to + 3 %	
Local Masses	-4.0 to -8.9 %	• Mass loading most significant if located on an antinode
Element order [1]	-2.7 to + 3.5 %	• Increased from linear to parabolic; additional transverse shear effects
Mesh refinement [1]	-0.5 to -2.3 % + 0.1 to + 0.2 %	• Bottom and electrical area • Vertical on sides near girth
Thickness variations	-0.3 to + 1.4 %	• Dominated by girth region, effect on top not isolated
Residual Stress	0 %	• Not a factor, confirmed by stiffness comparison and experimental tests of an annealed housing

1. Model refinement issues become more important as higher modes are solved for and mode complexity increases

4.1.5 Reasons for Inaccuracy of FEM Housing Model Predictions

Accuracy loss in the analytical solutions may result from a number of sources. This section further discusses the update parameters of section 4.1.4 which are categorized as modeling errors or theoretical limitations of the finite element method. Modeling errors result from differences between the physical system and the analytical model. Even with the capabilities of FEM, certain simplifications to the structure must be made. The modeling errors section will address the question "what physical features affect the model significantly". The theoretical limitations section will point out occasions when results change due to element formulation or solution method variation. It is important for the analyst to recognize all potential causes for modeling inaccuracy to use the method effectively. It is hoped that these sections in particular will be beneficial to others involved with the analysis of compressor housings.

4.1.5.1 Modeling Errors

Loads and Restraints

Physical interactions such as loads and restraints are often difficult to realize in modeling situations. For the eigenvalue problem there are no applied loads. Restraints however, are a factor. The unrestrained or free-free condition was preferred for the eigensolutions since it became most versatile in later steps. For example, in the component mode synthesis step the free-free solution may be used to efficiently find additional eigensolutions to any number of restrained or support stiffness cases. In addition, the free-free modal properties may also serve as a substructured component in a larger system. When the choice is made to restrain the housing models, the mounting feet provide a more realistic support. Unfortunately, free-free solutions find a large number of modes involving only the feet (for example, nine mounting feet resonances occur below 1200 Hz.). A typical mounting foot resonance is shown in Figure 16. These modes increase the computational effort

necessary to find the housing modes of primary interest and account for the sparse data of the early models in Table 4. Later models deactivate mounting foot resonances by zeroing the foot material density.

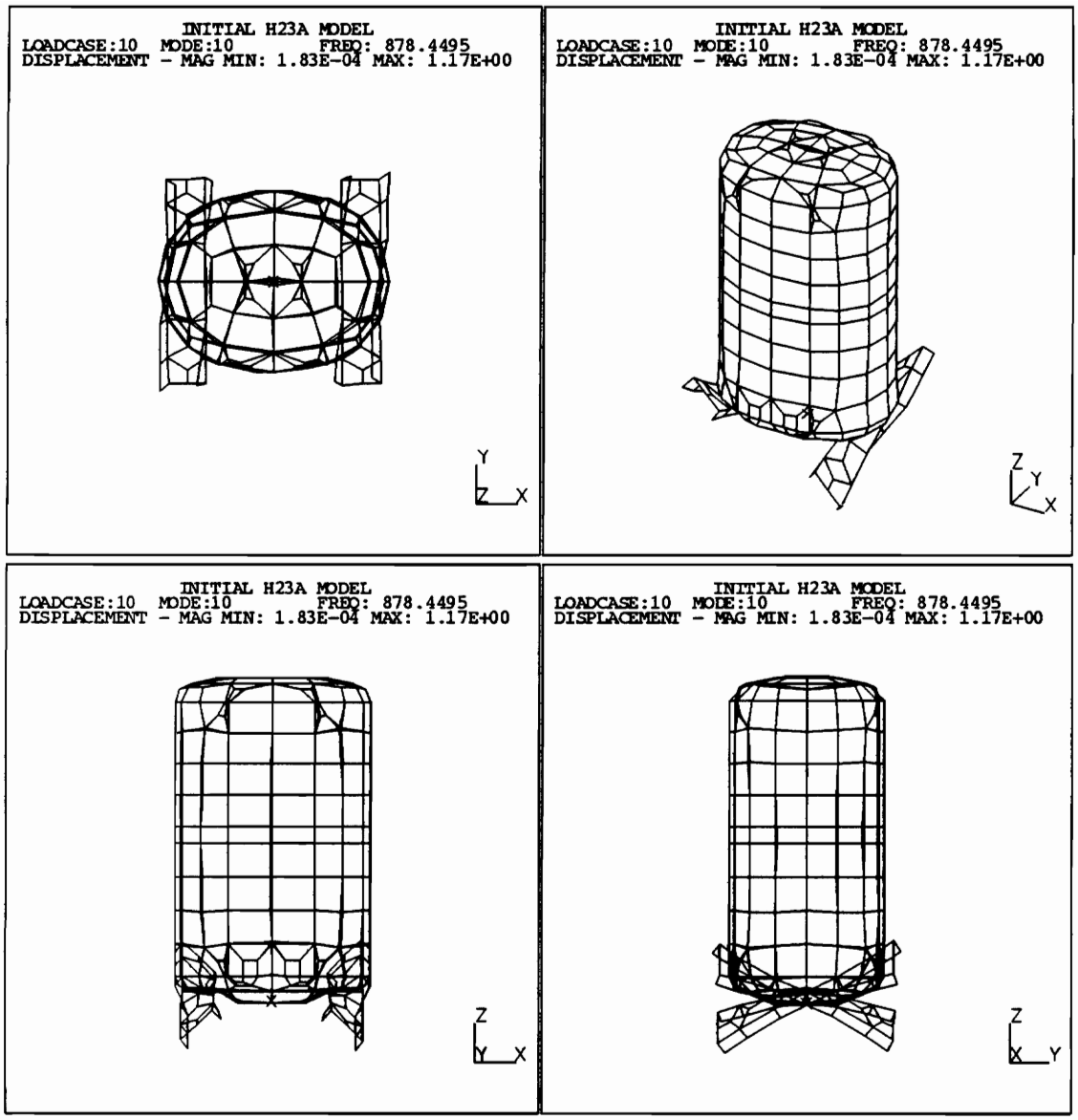

Figure 16. Typical mounting foot resonance at 878 Hz

Girth joint

The girth joint refers to the single-lap connection at the midsection of the housing which joins the upper and lower halves. A restraining effect by the girth was found in the experimental deflection scans involving side motion which was not found by the initial housing model. This effect is very clear [25] when viewing the scans in a three-dimensional mountain plot format (not shown). It is believed that the girth is stiffer than the sides, due to the additional curvature and the additional material. In addition, the weld bead could be responsible for the restrained motion found. This suggested a need to refine the analytical model's girth region, but the higher initial natural frequencies indicated that the sides were too stiff already. The overly stiff model could result from the single band of double thick elements representing the girth or from a coarse mesh.

One approach to improve the girth joint representation is with constraint equations which enforce the appropriate boundary conditions in the lapped region. This avenue was not followed to avoid anticipated difficulties during the eigensolution. A second option recommended by Cook [20] is to use an effective elastic modulus to better approximate the joint stiffness. The appropriate value would be established by experimental testing or additional detailed modeling of the joint. A third but similar approach, is to perform detailed modeling of the girth which is solved independently and then included by substructuring or "superelement" procedures. The approach selected was to model the girth with a band of coincident elements. Overlapping two elements reduces the girth stiffness in an effort to better represent the welded joint. The lapped elements use the appropriate thickness for the upper and lower halves of the housing. Employing the girth modification reduces (though not uniformly) the natural frequencies of modes involving side motion by as much as 17 %, to a range closer to the test frequencies. The girth is, therefore, thought to be an important factor to consider when representing the structural characteristics of the housing. The coincident elements were employed and found to improve the model's agreement with test data, however the modification does not result in the "waist line" found experimentally. The best girth representation

is yet to be determined. It is possible that the more flexible coincident elements improved correlation by compensating for a side mesh which is too stiff.

Local Masses

Local masses such as the internal spring mounts and service connections may significantly reduce natural frequencies if positioned at the antinode of a particular mode shape. For example, model updates showed a drop of 40 and 100 Hz (-4.0 and -8.9 %), respectively, in the first two top modes when a 1/10 lbm. (45 g) lumped-mass element representing the top-spring mass was added near the housing top's center.

Geometric Variations

Geometric variations describe the spatial differences between actual compressor housings and the FEM model. Thickness changes in the housing that result from the drawing process were one known geometry difference. The manufacturer provided measurements taken at the major and minor axes of a housing which had been sawed into quarters. To update the model, thickness changes were averaged into five regions. The broadside, narrowside, bottom, top, and girth regions were made 22%,15%,13%,10% and 1% thinner, respectively, to better represent the thickness changes which occur during production. Results showed that natural frequency predictions were not very sensitive to these regional thickness changes. Modeling experience with another compressor (Bristol Compressor, Inc. model H25) showed that uniformly increasing housing thickness 0.015 in. (0.381 mm) resulted in a 0.4 to 8.9 % natural frequency increase [1]. Thus, expecting a higher sensitivity to thickness variations is warranted. However, notice that material thickness at the girth remains essentially constant in the model revision. The girth was established to have a significant effect on stiffness of the housing sides. Therefore, during this update the girth joint is believed to overshadow frequency changes due to the thickness variations of other regions.

Another geometric concern is the flattened area which accommodates the electrical fusite block on the top surface. Employing the flat area correction to the FEM model reduced top stiffness and consequently, reduced the top mode natural frequencies as much as 451 Hz (-36%).

Manufacturing Variances

Manufacturing variances occur when the actual housing differs from the FEM model which was developed from engineering drawings. One such difference was found in the top surface by measuring the experimental housing with a vertical height gage. Less curvature on the actual top surface was found which could account for a lower stiffness and consequently the lower test frequencies. The FEM model's nodal coordinates were changed to better agree with the true surface of the test housing. The resulting frequency reductions were modest, the largest being 54 Hz (-5.4%). One note of caution: adjusting nodes may lead to erratic results. Arbitrarily moving nodes to compensate for variances on the top surface resulted in the "M7(error)" mode listed in Table 4. This mode is also plotted in Figure 17. This error is currently unresolved, but model history and the experimental database insist that the mode does not exist. Cook [20] cautions analysts that warping quadrilateral elements such that all nodes are not coplanar may lead to erratic results, however, sufficient evidence was not found to prove that warped elements led to this error. The following work developing mode superposition solutions ignore this eigenvector.

Material Property Differences

Material property differences were the last potential modeling error investigated. Property values were taken from a standard engineering reference [27]. Significant deviation from the actual values was not anticipated, unless the properties were modified during the manufacturing process. Specifically, yielding and residual stresses from the drawing process may create local regions which no longer display a linear elastic modulus but respond with a reduced, tangent-modulus stress-strain relation. A reduced modulus would lower stiffness in the actual housing and account for the higher frequencies found by the analytical model. This was investigated and did not prove to be the case.

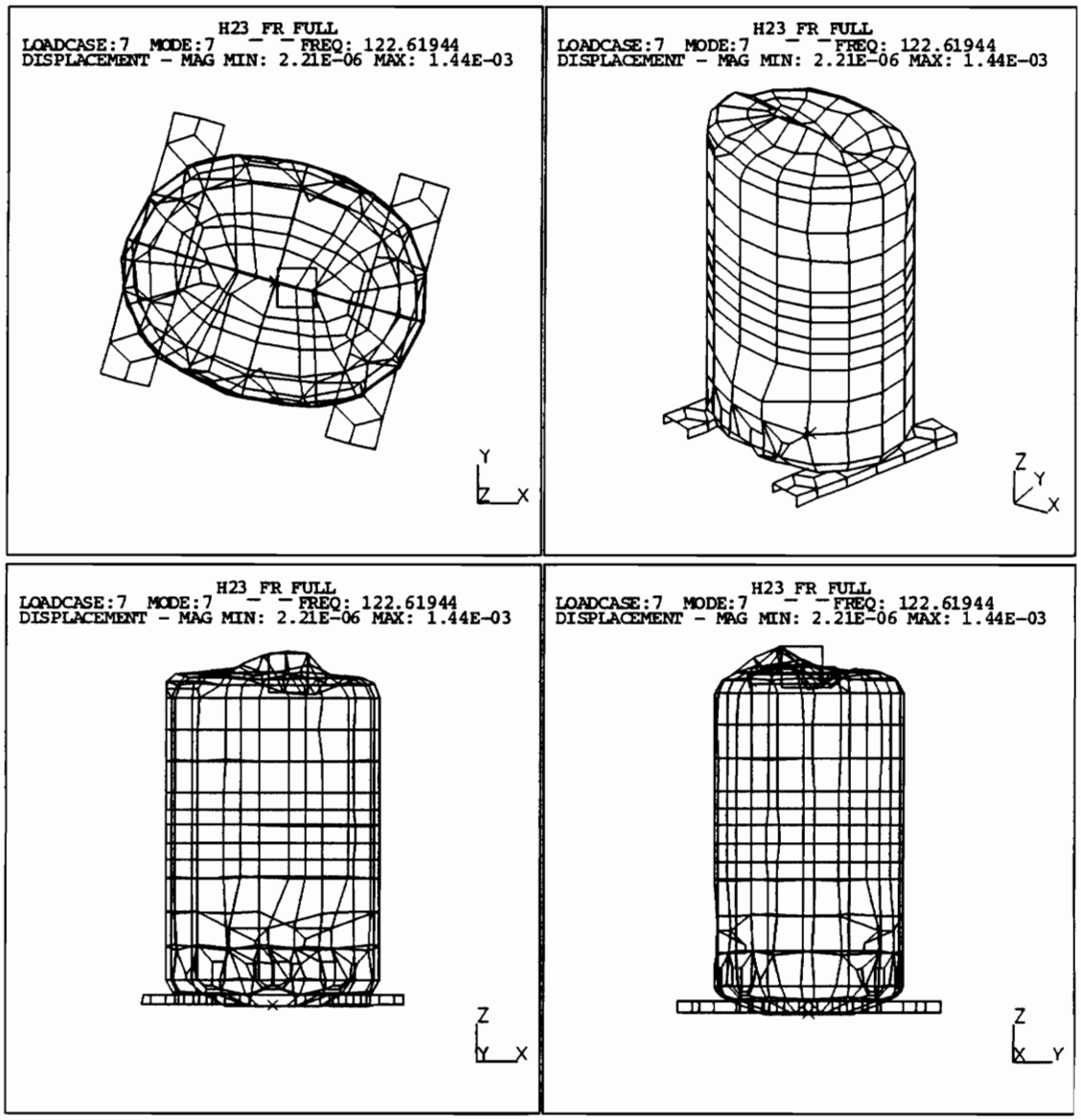

Figure 17. Erroneous mode M7(error):

Error occurred after the top nodes were arbitrarily moved to better represent true top surface.

First, the experimental stiffness of a point on the top surface was calculated from a driving point frequency response function (FRF) in a low frequency range. Static solution provided a comparable stiffness of the analytical model, which was 25 % higher than the experimental value. A much larger difference was expected for the tangent modulus effect. Further evidence came from impact tests of an annealed housing. Test FRFs of the annealed housing were equivalent to FRFs of a non-annealed production model.

4.1.5.2 Theoretical Limitations of the Finite Element Method

Numerical Difficulties

Numerical difficulties result from the truncation of numbers by the computer. The programmer has the most responsibility in avoiding problems of this nature. However, users of commercial code can introduce ill-conditioning problems when large stiffness variations are modeled. Significant numerical errors are thought to have been avoided in the models developed.

Discretization Errors

Discretization errors result from modeling a continuous system having infinite d.o.f. by a finite data set. Updates targeting discretization errors sought to improve the shape of distorted elements and to reduce the size of elements in regions having a coarse mesh. First of all, the eigenvalue models must have enough elements to assume the displacement configuration of each mode. Higher frequency modes become more complex and, thus, require further refinement. The need for mesh refinement is conventionally indicated by stress discontinuities at element boundaries. However, the dynamics problem called for different parameters such as natural frequency to evaluate the state of convergence. "If refinement does little to change [natural frequency] results, one has evidence (but not proof) that results are satisfactory" [20].

Mesh refinements were performed by dividing the existing elements (known as "h refinement") or by adding nodes to elements and/or increasing the interpolation polynomial (known as "p refinement"). Element subdivisions are difficult because of the housing model's complicated geometry, therefore h refinements are made sparingly. In one case, elements near the girth were subdivided vertically to improve resolution. This modification was made to improve resolution at the girth region in response to the constraining effect shown by test data. In another case, the mesh was refined over the full top section. P refinements require no re-meshing and are convenient to employ, but computational efforts become burdensome because the mesh is effectively refined over the full structure. As the update summary shows, elements were increased from linear to parabolic, which have additional midside nodes and a higher interpolation scheme. Natural frequencies decreased by only 3 %, indicating that the linear elements are adequately refined for the frequency range considered.

The element distortion apparent in the initial housing mesh of Figure 8 is another concern included with discretization errors. The distortion results from defining the nodes and elements automatically, with a mesh generating algorithm within the software package. Cook [20] reports several errors that may result from element distortion. First, distortion stiffens elements and reduces accuracy, although it may be contained to the neighborhood of the distorted element due to Saint-Venant's principle. Next, the stiffness variation of distorted elements also tends to produce ill-conditioned structure equations with the associated numerical difficulties. Finally, abrupt element size changes lead to a poor discrete representation of the continuous mass distribution, cause artificial wave reflections, and numerical noise in dynamics problems. Revisions were made to improve element geometry, however, the sensitivity of natural frequency predictions to element distortion was not investigated.

Many limitations of the finite element method are less obvious and put commercial code users at a disadvantage. Assumptions made during the software's theoretical formulation may be buried deeply in the code and without complete documentation. Throughout the project it was necessary

to run simplified test cases for clarification of topics that were not well documented for the code used. At other times source literature referenced by the software manuals was consulted.

In dynamic modeling, other theoretical limitations occur in the mass and stiffness matrices which define the eigenproblem,

$$([K] - \lambda[M])\{A\} = \{0\} \tag{4.1}$$

or in the algorithm chosen for eigenvalue extraction. The theoretical factors concerning the model revisions will be briefly described here. Rigorous derivations of element formulation and solution algorithms are well beyond the scope of this document but may be found in theoretical texts [20, 26] and the specific adaptions are available in software manuals [18, 28, 29].

Mass matrix formulation

Consistent-mass matrices were used almost exclusively in the housing models. However, two models were solved with the alternative lumped-mass matrix. The lumped-mass housing solutions found the same mode shapes with non-uniform shifts in natural frequency. I-DEAS™ [18] reports that the lumped-mass matrix will "soften" the model to improve natural frequency predictions. Contrary to the expected softening, some frequencies increased when the model was solved with a lumped-mass matrix formulation.

Stiffness Matrix Formulation

Model revisions potentially include four different shell element formulations. The I-DEAS™ parabolic shell element is formulated to approximate Mindlin plate theory rather than Kirchoff theory as in the I-DEAS™ linear formulation [18]. Therefore, the parabolic element includes transverse shear effects neglected in the linear element. Selection of an equivalent linear quadrilateral shell element was strived for in the NASTRAN® solution. However, significantly large natural frequency differences were found as shown in Table 5. The only known difference between the I-DEAS™ linear shell and the NASTRAN® linear shell are transverse shear effects.

Transverse shear adds flexibility and, therefore, one would expect lower natural frequencies. Since this was not the case, numerous possible variations of other formulation parameters presumably caused the frequency increase found by the NASTRAN® model. A similar formulation difference is believed to exist in the linear element of CAEDS™.

Solution Method

Once the structure mass and stiffness matrices are assembled to define the eigenvalue problem described by eq. 4.1, a number of techniques are available for eigenvalue extraction. The appropriate algorithm "depends on the order n of the matrices, their sparsity, the number of eigenvalues to be extracted, and where in the eigenspectrum the eigenvalues of interest are located" [20]. For the housing model problems, the selection depended on availability within the software package and attributes of the algorithm. Subspace iteration was used most frequently, to take advantage of free-free boundary conditions and an independence of master d.o.f. selection. In addition, the Guyan reduction and Lanczos methods were also used. The eigenvalues determined by different solution methods should not vary if $[K]$ and $[M]$ remain the same although solution efficiencies may differ a great deal.

Modeling errors can be controlled by the analyst and adhering to good FEM practices can avoid the problems associated with a poorly developed model. However, results showed a significant variance due to FEM theoretical factors which may not be controllable. Solutions to identical models differed by as much as 20 % between different software packages.

4.1.6 Updated Housing Model Eigensolution

Many of the revisions previously discussed are apparent in the updated empty housing model shown in Figure 18. The colored areas indicate five regions with thickness variations. The total d.o.f. was increased from mesh refinement on the top and at the midsection near the girth. The coincident girth elements are not apparent since the two elements are "stacked" on the same four nodes.

Modal properties predicted by the updated model were found to agree better with the test data. The updated natural frequencies are compared in Table 6. Modes involving side motion are improved primarily because of the girth modification. The top mode frequencies are much improved due to geometric refinements and addition of the top-spring guide mass. However, the natural frequency corresponding to the M11(4,1) mode is farther away from the corresponding test frequency after updating.

Table 6. Updated Housing Model Natural Frequency Correlation

Analytical Mode Descriptor [1]	Analytical Frequency [Hz]	Experimental Frequency [Hz]	Difference
M8(3,1)	662	689	-3.9 %
M9(3,1)	724	736	-1.7 %
M10(2,1)	772	791	-2.3 %
M11(4,1)	866	944,984 [2]	-8.2,-12 %
M12(0,0,T1)	967	944,984	-2.4,-1.7 %
M13(4,1)	978	1032	-5.3 %
M14(2,1,T1)	1109	1069	Shapes Differ

1 See Appendix A for a description of the mode descriptor scheme
2 No independent top motion was found experimentally. The 944 and 984 Hz experimental shapes have the same circumferential node line pattern. They are distinguished by the coupling of top motion having a 180 ° phase difference.

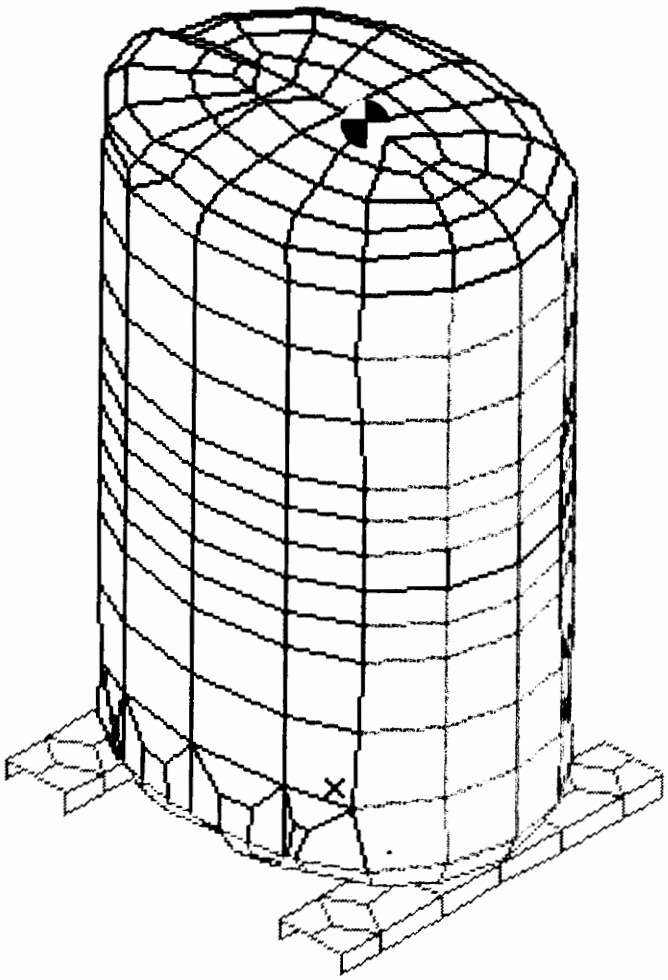

Model Specifications

- Model filename; "H23TRLIN1"
- 426 nodes
- 424 linear quadrilateral shell elements
- 1 lumped mass element for top spring guide
- 2556 total d.o.f.
- free-free boundary conditions
- Colors indicate thickness variations
- Coincident elements at girth
- Mesh refinements at top and near girth
- Geometric refinements at top

Figure 18. Updated Housing Finite Element Model

A top view summary of the first twelve updated mode shapes is shown in Figure 19. The first five side mode shapes still agree with the test results. However, comparison of the mode shapes with the test results show differences yet to be resolved. For example, the model predicts a unique, independent top and side eigenvector for the first top mode rather than the coupled shapes that are found experimentally. In addition, the experimental shape found at 1069 Hz is still not found by the analytical normal mode solutions.

The current level of agreement between analytical modes and the test data may be improved with continued model updating. However, as shown by the M7(error) mode, the possibility of corrupting the model in some fashion exists. In addition, lengthy revisions often lead to negligible changes in the model's predictions. Rather than considering further updates, the correlation process is expanded to include response parameters determined from analytical simulation of the test procedure.

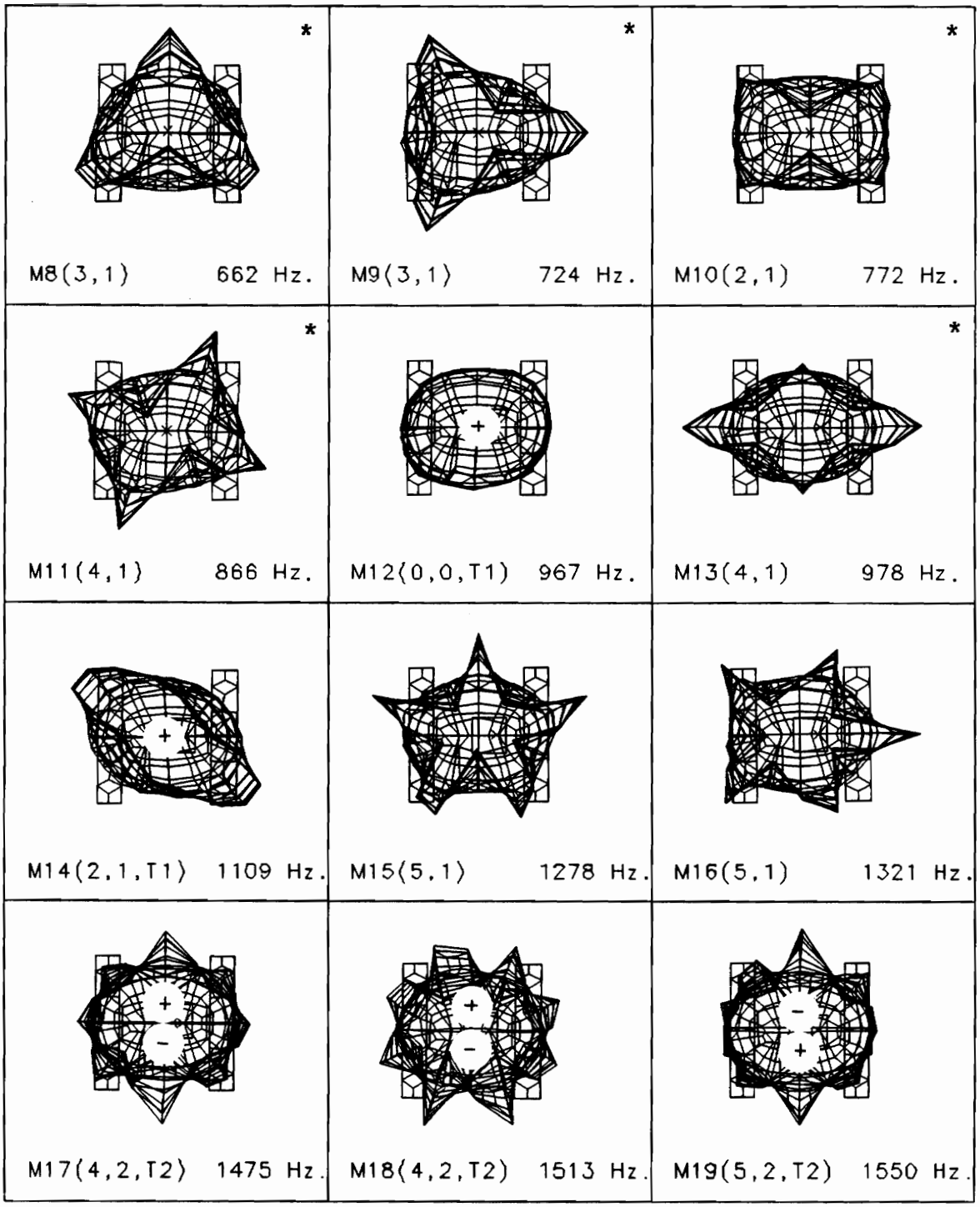

Figure 19. Updated Housing Analytical Mode Summary:

+ indicates displacement out of page;

- indicates displacement into page;

* indicates experimentally verified modes

4.2 *Compressor Housing Forced Response Analysis*

In this section the experimental dynamic analysis is simulated using the component mode synthesis (CMS) and mode superposition techniques of Chapter 2. First, the updated empty compressor housing model will be combined with a finite element adaption of the experimental shaking mechanism. Then, the normal modes of the combined system are found. Forced vibration response is calculated at a single point in the form of frequency response functions for comparison to test data. Displacement shapes of the housing which correspond to resonant and intermediate frequencies are also found. Correlation between analytical results and test data is reconsidered with insights gained from the forced response analysis.

4.2.1 Housing Component Mode Synthesis Model

Housing Component

The housing CMS model includes only two components: the empty housing and an exciter mechanism to transmit applied excitation forces. Modes 1-24 of the updated housing model, excluding the erroneous mode, represent the housing component in the CMS model. In addition, modal viscous damping ratios of $\zeta_r = 0.005$ are defined for each mode of the housing component. The damping ratios are chosen from past experience with steel structures [31] and are sufficient to develop the modeling procedures of interest here. Inappropriate damping estimates will limit the forced response model's ability to accurately predict response amplitudes, most significantly near resonance frequencies. For additional damping estimates, one may consult reference [30], or obtain damping ratios experimentally using experimental modal analysis techniques [10].

Stinger Component

Experimentally, the housing is driven with an electomagnetic shaker through a slender rod known as the stinger. Analytically, the shaker and stinger are represented by a harmonic force and a beam element, respectively. A schematic of the stinger assembly is shown in Figure 20 along with the finite element representation. Experimentally, the stinger serves two purposes: it avoids unintentional modification to the structure and assures uni-directional force application [10]. Both of these characteristics are available analytically, therefore modeling the stinger is not essential. However, including the stinger assembly introduces exciter-structure interactions which have been the focus of considerable attention in modal analysis [32, 33]. The specific concern are differences between the shaker generated force and the structurally applied force, which are not necessarily equal during resonance excitation. The applied force is needed to calculate modal parameters such as mobility,

$$Y_{ik} = \frac{\dot{X}_i}{F_k} \qquad (4.2)$$

where

$\dot{X}_i \equiv$ velocity response at point i

$F_k \equiv$ input force at point k

In modal analysis, any differences between the shaker force and the applied force are compensated for by direct measurement of the applied force near the structure's surface. Analytically, the connection forces were not readily available to calculate modal parameters. However, the ability to apply a constant, known force at any point allows calculation of comparable functions. To calculate analytical mobility response, a single force with unit amplitude will be applied directly to the structure at the exciter connection point. Then, all response calculations are per unit force.

Schematic of Stinger Assembly:

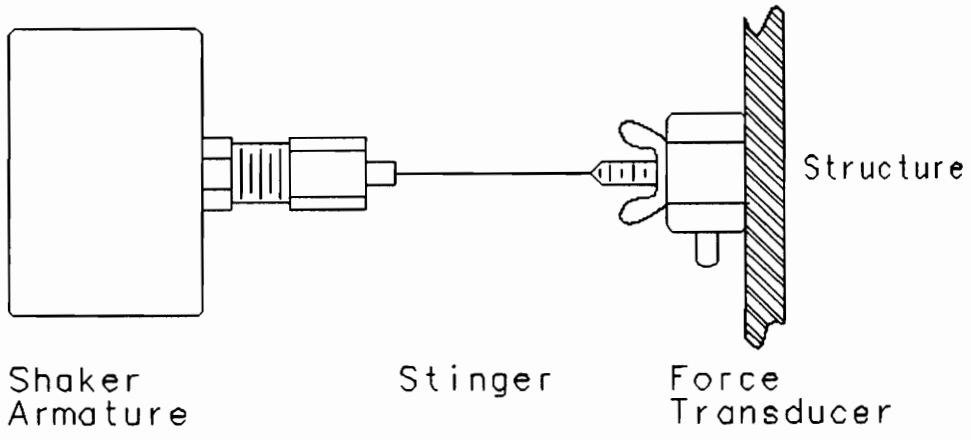

FEM Representation of Stinger Assembly:

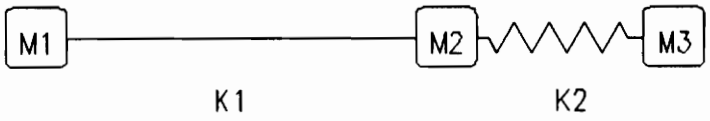

M1 = Shaker armature mass
M2 = 65 % of transducer mass plus connector mass
M3 = 35 % of transducer mass
K1 = Single FEM linear beam element
K2 = Transducer stiffness

Figure 20. Stinger Assembly for Forced Response Excitation

Housing CMS System

The stinger assembly and the housing components were combined as a new analytical system. The stinger was connected perpendicular to the housing at a point on the girth corresponding to the experimental connection point. This point was determined to be an optimal location to excite all modes by conducting an experimental modal survey [1]. Another eigensolution provides the unrestrained natural frequencies and mode shapes of the combined housing and stinger assembly system. Table 7 lists the resulting eigenfrequencies which are slightly (0.0 to 1.0%) lower than those found by the full model. It has been pointed out that the CMS solutions are approximate but the small differences here are most likely due to mass loading by the attached stinger assembly. These eigenvectors will be used in the modal superposition calculations to determine forced response.

Table 7. Compressor Housing CMS Eigensolution Summary

Analytical Mode Descriptor [1]	CMS Model Frequency [Hz]	
M8 (3,1)	661	(-0.2 %) [2]
M9 (3,1)	717	(-1.0 %)
M10(2,1)	771	(-0.1 %)
M11(4,1)	858	(-0.9 %)
M12(0,0,T1)	966	(-0.1 %)
M13(4,1)	973	(-0.5 %)
M14(2,1,T1)	1106	(-0.3 %)
M15(5,1)	1272	(-0.5 %)
M16(5,1)	1316	(-0.4 %)
M17(4,2,T2)	1475	(-0.0 %)
M18(4,2,T2)	1512	(-0.1 %)
M19(5,2,T2)	1550	(0.0 %)
M20(5,2,T2)	1576	(0.0 %)

1 See Appendix A for a description of the mode descriptor scheme
2 Values in parenthesis indicate difference between CMS model and Updated Housing Model

4.2.2 Analytical Forced Response of Compressor Housing

Frequency Response Functions

Analytical frequency response functions (FRFs) are found by calculating the displacement, velocity or acceleration response of a single point (d_i,$\dot{d}_i$,$\ddot{d}_i$) while a single force (F_k) is applied over a range of discrete frequencies. The experimental shaker force is represented by $F = 1 \cdot \cos(\Omega t)$, which is the real component of eq. 2.19. For future reference, the excitation is defined in the frequency domain. The Fourier transform equivalent, $F(\Omega)$, is a real-valued, unit amplitude "spike" at the forcing frequency Ω.

The force is applied directly to the housing in a normal direction, so the input force has a known constant amplitude of 1. Thus, the analytical velocity response per unit excitation ($\dot{d}_i/1$) should approximate the experimental mobility transfer function (v/F). Figure 21 shows an analytical transfer function from a point on the girth to a point on the top of the housing.

Comparison with the experimental FRF shown in Figure 4 on page 27 can be informative. Overall shapes of the two FRFs are similar although amplitudes differ. The most promising similarity is coupling between the top and side which was not observed in the eigensolutions. Notice that each of the side modes is visible in the top response. Notable differences include the comparative amplitudes and spacing of peaks which emphasize errors in the analytically predicted natural frequencies. The analytical peak at 856 Hz should occur closer to the 973 Hz. peak. In addition, M12(0,0,T1) at 967 Hz and M13(4,1) at 978 Hz. are blended into the single peak at 973 Hz with the current damping level. These differences show limitations of the model during response calculations.

Response errors result from the limited accuracy modal property estimates (natural frequencies, mode shapes, and damping ratios) used in the mode superposition calculations. Damping ratios

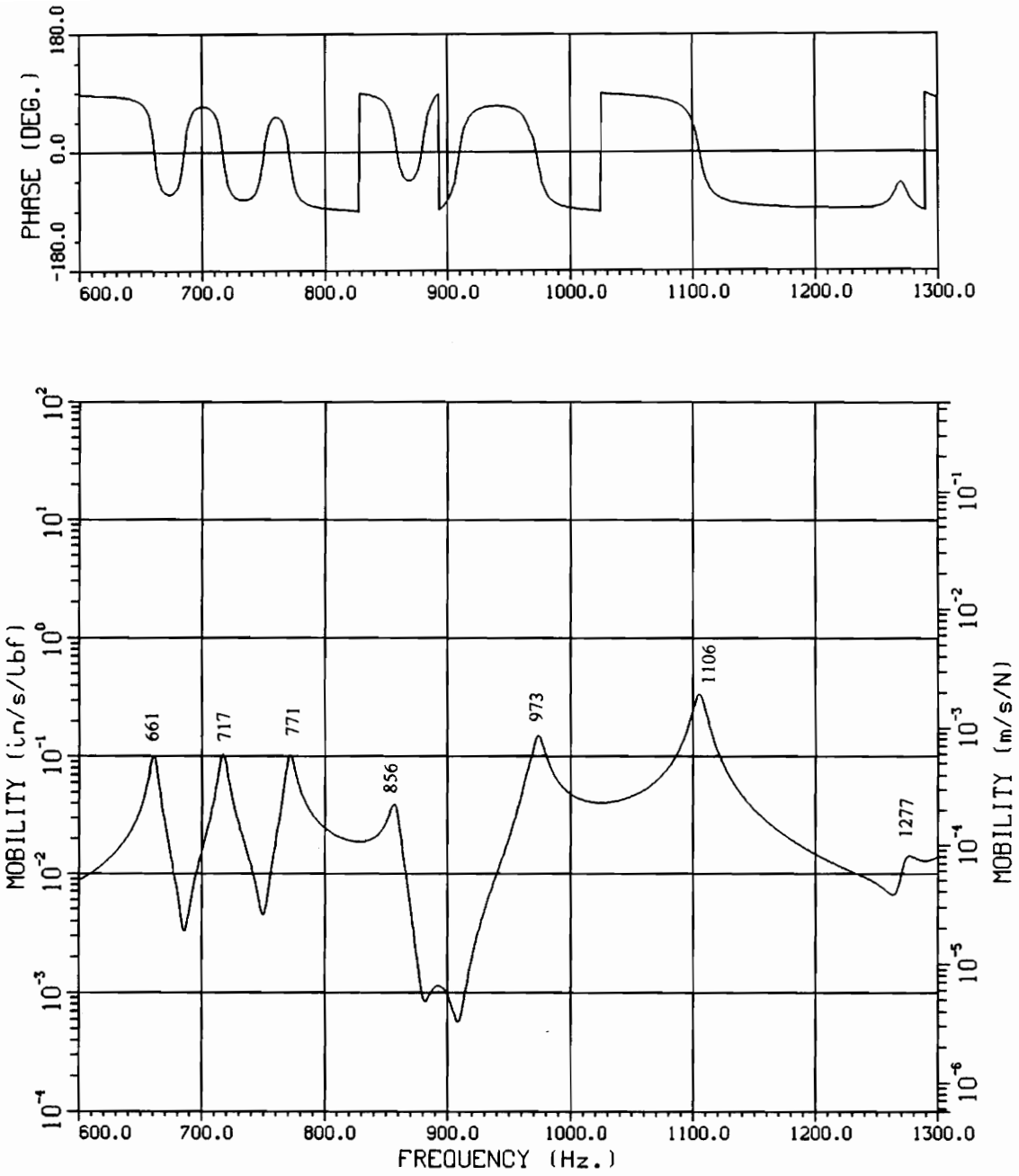

Figure 21. Analytical Housing Response:

Force at girth; response at top

are particularly important to predict the amplitude of response near resonance peaks, and this FRF may be improved considerably with better damping estimates. The correct mode shapes are fundamental to response calculations but natural frequencies also affect the response amplitudes, although it may be less obvious. The reasoning behind this lies in the mode superposition methodology. Response calculated at each discrete frequency is a weighted sum of all modes. Shifts in the natural frequency which correspond to each mode shape change the weighting factor. For example, consider two peaks in an FRF indicating "mode 1" at frequency ω_1 and "mode 2" at frequency ω_2 ($\omega_2 > \omega_1$). Presume that both modes are contributing to the response, that is, neither is being excited at a nodal location. If mode 2 is shifted away from mode 1, then mode 2 will have a lower weighting factor at ω_1. Consequently, mode 2 will contribute less to the response calculated at ω_1. The inverse also applies, if mode 2 is shifted closer to mode 1 then mode 2 contributes more to the response at ω_1. Additional problems occur if the natural frequency differences reverse the order of mode 1 and mode 2 ($\omega_2 < \omega_1$). Not only do the weighting factors potentially change, but mode 2 will be 180° out of phase when added. An acceptable level for modal property errors based on mode superposition requirements is desirable but was not investigated in this study.

Forced Response Deflection Shapes

Analytical forced response deflection shapes are found by calculating the steady-state vibration response over the full displacement field at a specific forcing frequency. Response deflections were determined for system natural frequencies (shown in Table 7) and intermediate frequencies. Figure 22 shows a top view summary of forced response deflection shapes. These shapes are in response to a unit amplitude harmonic force applied through the stinger assembly, rather than at the connection point as in the response calculations made for the FRF. The "phase" value corresponds to the response angle argument, $(\Omega t - \theta)$, of eq. 2.20. Thus, the phase indicates a particular time increment during the response cycle. Peak amplitudes occur at 0 ° and 180 ° because the response is harmonic. It should be emphasized that deflection shapes are not mode shapes. Damping

effects and excitation interactions are included, and modal influence by surrounding modes is possible.

As expected, forcing specifically at a natural frequency results in a deflected shape similar to the corresponding mode shape. The experimental technique depends on this characteristic to document mode shapes. However, occasions exist when the deflected shape may differ from the pure mode shape. One notable case is shown by the analytical response at 970 Hz, in which the first top mode M12(0,0,T1) is expected to be dominant. Analytical results showed that the first top mode could not be excited independently of the adjacent side modes.

Further examination of the analytical deflection shapes has lead to improved correlation of the model. Referring to the 960 and 970 Hz deflection shapes, one may observe the opposite phase top motion coupled to side motion. This phenomena is verified by the test data at 944 and 984 Hz., and was not found during the eigenvalue analysis. Another observation is the analytical shapes found in the 1040 to 1069 Hz range, which agree with the uncorrelated deflection shape previously described by "shapes differ". This finding increases confidence in the analytical models. One may argue that the analytical mode M14(2,1,T1) is correct, and the experimental shape at 1069 Hz is not at pure mode but a superposition of adjacent modes. On the contrary, one may speculate that the actual second top mode occurs at 984 Hz and is coupled to different side modes. In this scenario, the model indeed misses the 1069 Hz mode. At this point, speculation is necessary. Verification requires techniques beyond the scope of this project. Experimentally, a multi-shaker, phase related excitation scheme could insure experimental extraction of pure mode shapes. Alternatively, it may be possible to mathematically extract the pure mode shapes from conventional modal analysis data. Presently, further model refinements are desired to improve agreement with the existing experimental database.

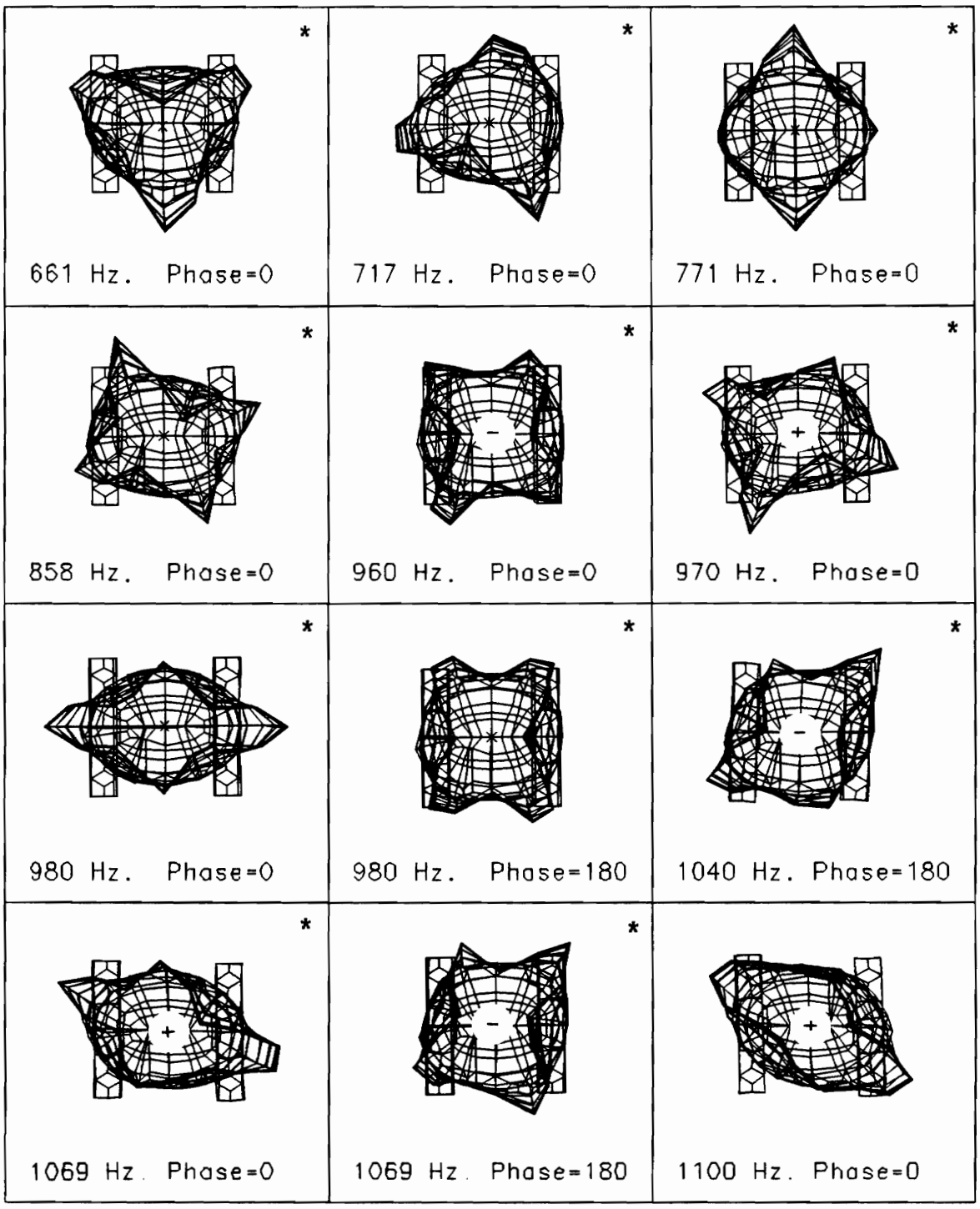

Figure 22. Housing Analytical Deflection Shapes:

+ indicates displacement out of the page;

- indicates displacement into the page;

* indicates an experimentally verified shape

Housing Mode Participation in Forced Response

To further emphasize the possibility of modal combination in resonance deflection shapes, consider the modal participation factor. For a specific input force at a given frequency, each mode has a scaling coefficient, known as the modal participation factor, (γ_r), from eq. 2.21*a*. The mode participation factor describes the contribution of a particular mode shape to the system response. Figure 23 shows the modal participation factors of the housing modes which correspond to the deflection shapes shown in Figure 22. The top figure shows a case when the pure mode is dominant and, therefore, isolated in the deflected shape. The middle figure shows the coupling of at least two side modes when the housing is forced specifically at the first top resonance. The final graph indicates that several side modes and a top mode contribute to the analytical deflection shape found at 1069 Hz.

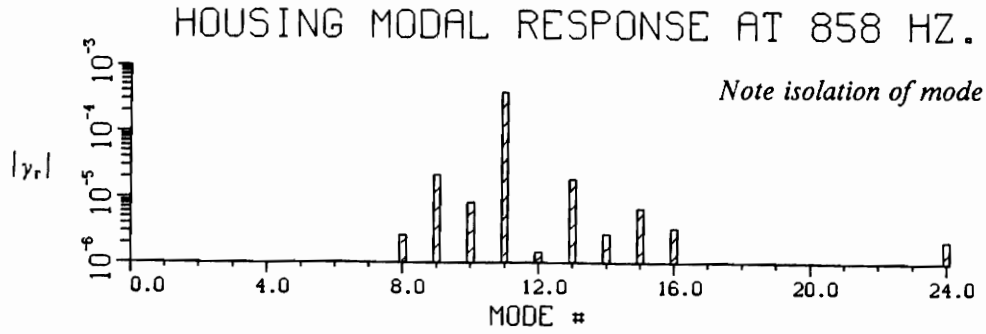

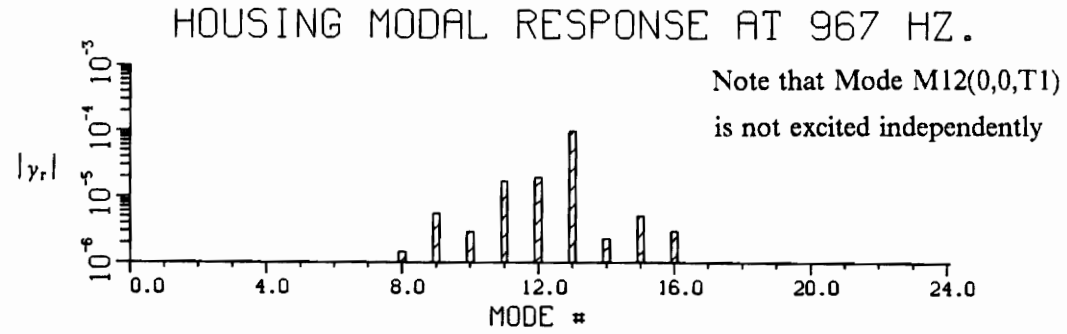

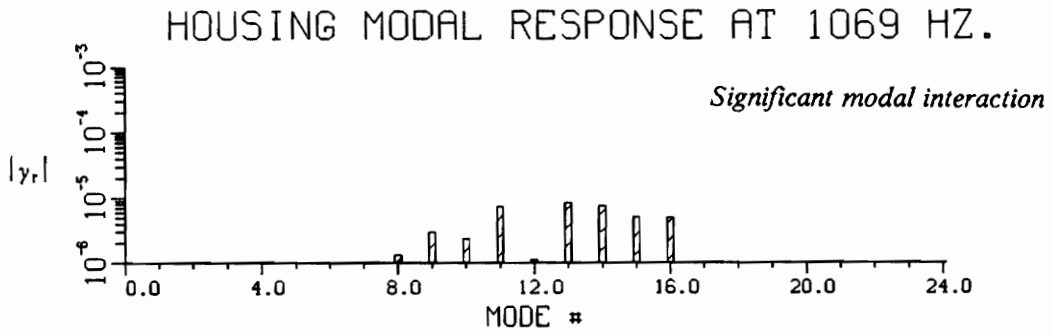

Figure 23. Modal Participation Factor Comparison

4.2.3 Comments on the Compressor Housing Forced Response Model

First of all, in proceeding to the modal superposition prior to a thorough validation of the eigensolution, there is a danger of summing forced response solutions with incorrect modes. However, in the model development of this project, forced response analysis revealed occasions when the analytically predicted modes should not agree with the experimental deflection shapes. Specifically, the experimental shapes may be significantly influenced by surrounding modes in modally dense frequency ranges such as the 900-1100 Hz region in the housings. A combination of analytical mode shapes and deflection shapes are beneficial to fully evaluate the model.

Proceeding to forced response analysis also enhances correlation efforts by providing more information to compare with test data. Additional parameters include transfer frequency response functions which are readily calculated between any two points to provide local evaluations of the model. The influence of damping, modal superpositioning and excitation force interactions can also be investigated. In addition, questions raised during the eigenvalue solution can now be answered. The top/side coupling was found to be a modal superposition of an independent top mode with one or more side modes. Similarly, the differing shape is possibly the modal combination of a top mode with adjacent side modes in the natural frequency spectrum.

This ends the empty housing model preparation. The additional correlation found by forced response analysis results is encouraging. All of the shapes documented experimentally were predicted by the model. Some differences between the analytical results and test remain but will not hinder further model development greatly. The next chapter discusses procedures to model the compressor assembly using the housing model as a component.

5.0 Compressor Assembly Models

In this chapter, models of the compressor assembly are developed using the refined housing model. Internal components are modeled independently and combined to obtain an assembly model, as shown in Figure 24 with additional elements highlighted. Since the internal compressor mechanism is comparatively more rigid than the housing, it is represented by a lumped mass. The compressor mechanism is supported by mounting springs, spring hangers, and a discharge tube known as the shockloop. Verification of the individual components is essential for any hope of modeling the system accurately; therefore, independent model development for the additional components will be discussed in detail.

Normal mode analysis is performed on a compressor assembly model reduced by component mode synthesis (CMS) and on a *full model* of the compressor assembly. In the CMS model, the components are developed and analyzed independently then combined to represent the compressor assembly as discussed in Chapter 2. The full model has all components of the compressor assembly defined in a single finite element model. Solutions by both approaches are summarized and sample mode shapes of the system are presented. Next, the experimental dynamic analysis is simulated through forced response analysis of the compressor assembly model. Finally, normal mode and forced response solutions are compared with experimental results to evaluate the loaded assembly models.

It should be pointed out that experimental tests were performed on a compressor assembly pressurized with freon. Fluid-structure interactions and internal pressurization were not included in the modeling efforts presented here. Codes are available with formulations to include these effects, but have a great deal more complexity. Intuitively, pressurization will increase the housing stiffness thus

increasing natural frequencies. To confirm this observation, Ingalls [2] employed the Berry-Reissner theory relating the natural frequencies of a cylindrical shell to internal pressure changes. The theory does not, however, guarantee a uniform frequency shift for the complex geometries found in compressor housings.

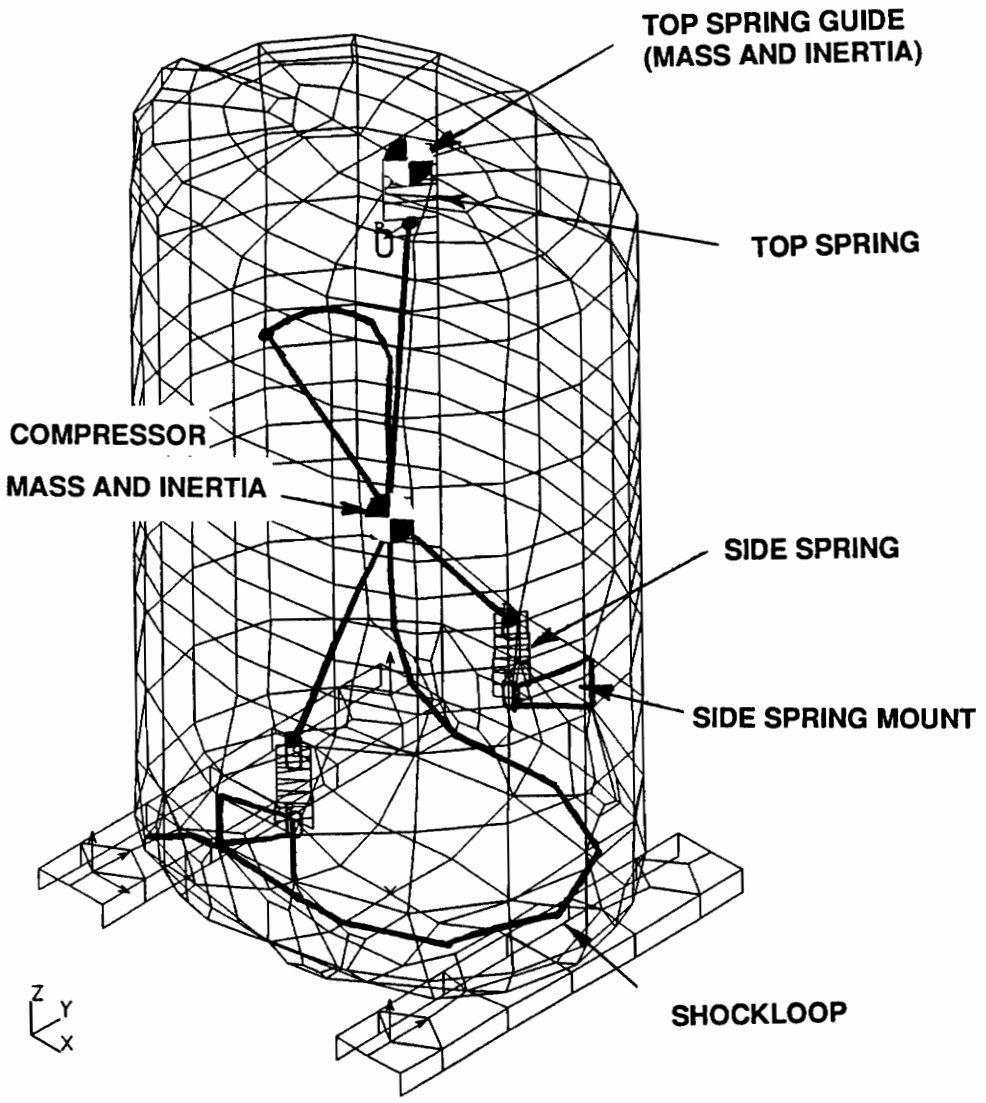

Figure 24. Compressor Assembly Finite Element Model

5.1 Compressor Assembly Model Development

5.1.1 Additional components

Rigid-Compressor Mass

The internal compressor mechanism was represented by a lumped mass connected with rigid elements to the mounting springs and shockloop. The term rigid element implies that the motion of all the nodes on the element are to be related to each other as if connected by infinitely rigid massless beams. Properties such as mass, mass moments of inertia, and center of gravity were determined from a geometric solid model of the compressor mechanism's major components. When possible, the lumped mass properties were verified with experimentally measured values. Assembled compressor mechanism properties are repeated[4] in Table 8.

Table 8. Compressor Mechanism Lumped-Mass Properties

Property	Analytical		Measured		Difference
Weight†	67.5	(300)	70.0	(311)	-3.6 %
J_{xx}††	2.72	(307)	2.72	(307)	0.0 %
J_{yy}	1.17	(132)	1.27	(143)	-7.9 %
J_{zz}	2.44	(276)	2.42	(273)	0.8 %
J_{xy}	0.0004	(0.05)			
J_{xz}	-0.0003	(-0.03)			
J_{yz}	-0.297	(-33.5)			

† Weight units are lbf (N)
†† Inertia properties about the mechanism's center of gravity
Inertia units are lbf•s^2•in (N•s^2•mm)

[4] Thanks are extended to Mr. Kevin Cardany and Mr. William Gardner who developed the solid models. Additional details may be found in [1].

Shockloop

The shockloop component was modeled with 35 linear beam elements having properties appropriate for stainless steel tubing. It is good modeling practice to conserve a structure's volume during discretization [20, 23, 34]. Specifically, Bernhard and Seidel [34] recommend adjusting curved sections of the shockloop geometry so that the combined length of the straight elements equals the total length of the curved section. This modification reduces the static stiffening associated with a coarse mesh and also improves the representative mass. Results from an independent, free-free eigensolution of the shockloop model showed ten resonances in the 132 to 1600 Hz frequency range.

Mounting Spring Components

First, the mounting springs were modeled with beam finite elements as shown in the refined model of Figure 25 (a). Static FEM calculations were made to determine spring constants. Then the complete stiffness matrix for 6 d.o.f. motion at each end of the spring was assembled. Strong coupling was found between the translational and rotational motions of these springs which result in off-diagonal stiffness matrix terms. The coupling terms should be included in the model, but simple spring elements allowed entry of only diagonal terms. Therefore, a single massless beam element was created to represent each mounting spring of the initial compressor assembly model. The *12 x 12* stiffness matrix of the three-dimensional beam element is defined by seven properties; cross-sectional area, a torsional constant, area moments of inertia, length, elastic modulus and shear modulus. These properties were selected so that the beam-stiffness matrices approximated the desired spring-stiffness matrices.

Eigensolutions of the initial compressor assembly model having the single-beam element mounting springs were of limited use. Table 9 compares the normal modes of the initial compressor assembly

model with the equivalent housing model. The housing modes were not affected by loading, as if completely isolated from the compressor mass. Housing mode frequencies differed from the empty housing modes by less than 1 % and no additional assembly modes were found due to interaction with the internal compressor mechanism.

Table 9. Initial Compressor Assembly Model Results

Mode Description	Housing Model Frequency, Hz.	Loaded Assembly [1] Frequency, Hz.	Difference
		9.0	
		13.8	
Compressor suspension modes		16.0	
		23.9	
		27.1	
		34.2	
M8(3,1)	662	662	0.0 %
M9(3,1)	724	725	0.1 %
M10(2,1)	772	771	-0.1 %
M11(4,1)	866	873	0.8 %
M12(0,0,T1)	1021	1025	0.4 %
M13(4,1)	977	969	-0.8 %
M14(2,1,T1)	1129	1128	-0.1 %

1. Internal mounting springs represented by single massless beam elements
Shockloop modes deactivated by zeroing mass density

Experimental results contradicted the initial assembly model's predicted modes. Test data showed an approximate doubling of the number of resonances upon loading the housing with the compressor mechanism and pressurizing with freon. The additional resonances were attributed to several potential causes, including.

- interaction between the internal compressor mechanism and the housing
- acoustic interactions within the freon environment
- housing interaction with natural frequencies within the springs, known as spring surge.

Correct operation of the rigid compressor element and appropriate entry of the lumped-mass properties were verified by a simplified test case. The test case solved for the modes of a rigid bar suspended by two springs with the FEM code. It is a simple example which is common to elementary vibration texts such as reference [24]. Acoustic interactions were beyond our analytical

computational resources; therefore, efforts concentrated on the other causes. Further investigation into the effects of spring surge, however, proved to be a critical factor. Hamilton [35] discusses the problems associated with spring surge in regard to the mechanical noise transmission path in the following quotation from his text.

> "Compressor suspension systems (support springs) and discharge lines are designed to take advantage of these [vibration isolation] phenomena by making the components 'soft' and the natural frequencies much lower than the driving frequencies. The compressor will then operate in the mass controlled region $[\Omega/\omega_n > 1]$, the compressor motion will be small, and the forces exerted on the shell by the springs or the refrigerant lines will be small. However, at frequencies much higher than the suspension natural frequency the springs and tubes will exhibit a number of local deformation modes. These modes will short circuit the expected suspension isolation and transmit significant forces to the shell at their local resonant frequencies. This effect will be particularly adverse if these local natural frequencies correspond with any of the shell's natural frequencies or compressor pumping harmonics".

Closed-form analytical solutions for spring stiffness and axial surge frequencies are shown in Appendix 2. Calculations such as these showed that both the top and side springs had surge frequencies within the range of shell modes. Therefore, the single-beam spring elements were replaced with series of beam elements to introduce spring surge effects into the FEM model. Considerable efforts were made to minimize the additional d.o.f. required for the mounting-spring sub-models in order to maintain reasonable d.o.f. in the compressor assembly model and to reduce the time and cost for solutions.

A few finite element modeling guidelines may be followed to insure reliable performance by the reduced d.o.f. spring models. First of all, spring models with extensive mesh refinement were created as a standard for comparison. Figure 25 compares a refined side spring model having 12 parabolic beam elements per coil to a reduced model having only four linear elements per coil. With this limited amount of discretization, it was imperative to conserve the reduced spring model's volume as with the shockloop. For the four node-per-coil spring models developed, the coil diameter was increased so that the combined length of four elements was equivalent to the circumference of a coil. This modification alone does not completely resolve over-stiffening by the coarse

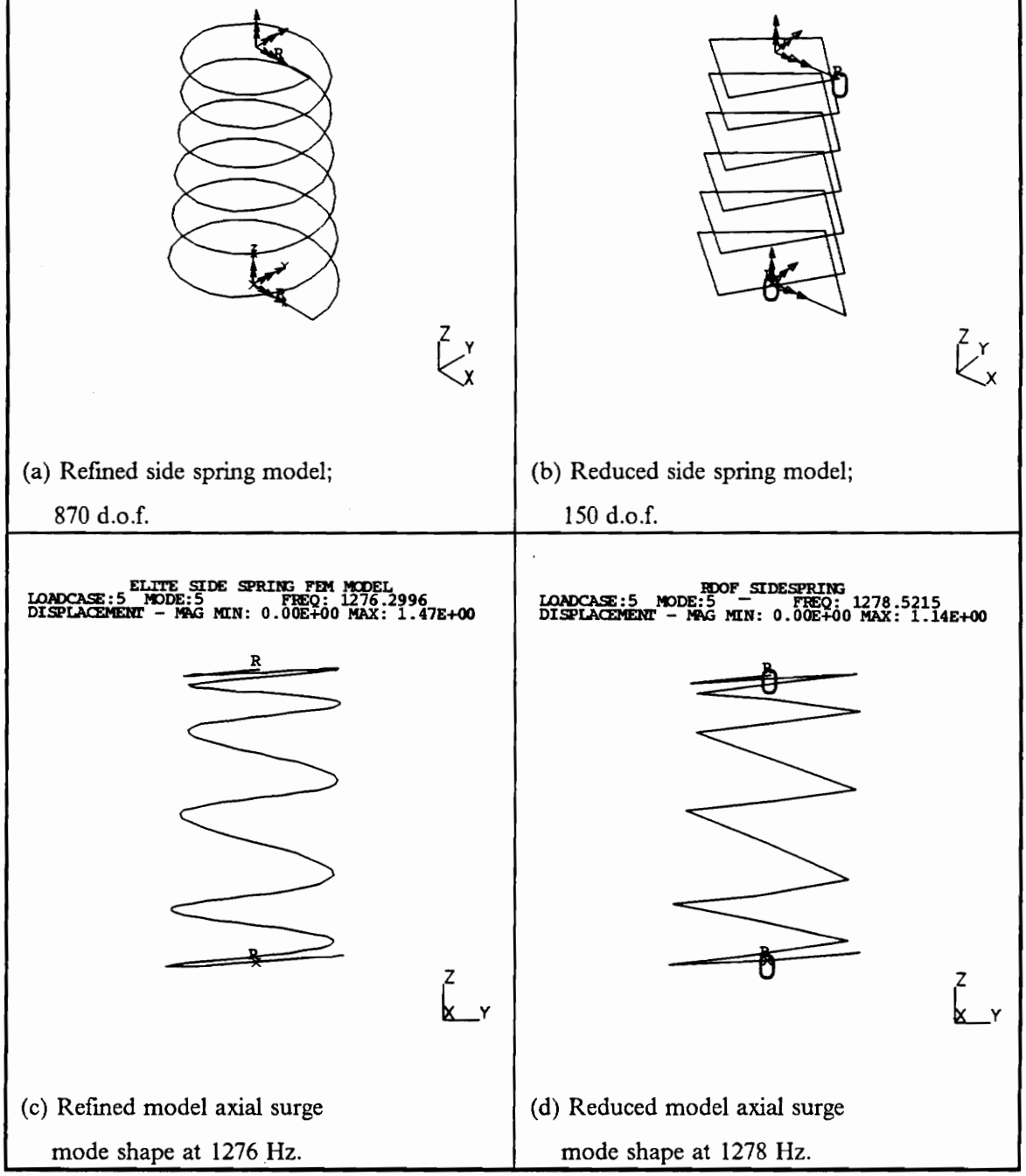

(a) Refined side spring model; 870 d.o.f.

(b) Reduced side spring model; 150 d.o.f.

(c) Refined model axial surge mode shape at 1276 Hz.

(d) Reduced model axial surge mode shape at 1278 Hz.

Figure 25. Spring Model Comparison

mesh. Consequently, natural frequency predictions will be elevated, for example, frequencies found with the reduced springs considered here ranged from 7 to 13 % high.

Although model tuning is against our modeling philosophy, non-physical modifications were employed to improve correlation with the refined models. However, the modification was made so that it can be generally applied to other models independent of this investigation. The best tuning parameter was found to be mass density which results in a more uniform shift of natural frequencies. In addition, the modified mass density, $\rho_{modified}$, necessary for correlation of the reduced d.o.f. spring models may be calculated directly from

$$\left(\frac{\rho_{modified}}{\rho_{reduced}}\right) = \left(\frac{f_{reduced}}{f_{refined}}\right)^2 \tag{5.1}$$

Mass density of the top and side mounting springs of this study was increased by a factor of about 1.3 to reach agreement with the refined models.

The natural frequencies are sensitive to other parameters but modification by other avenues were unsuccessful. At first the torsional constant, J, was changed in an effort to correlate natural frequencies. The effect proved to be localized, depending on the mode shape. For example, reducing J to match the first axial mode has no effect on a radially expansive mode and has inconsistent effects on the lateral modes. The localized effects result in a non uniform reduction of natural frequencies and consequently a change in the numerical order of mode extraction. The jumbled modes are difficult to correlate. Modifications to area moments of inertia, I_{xx} and I_{zz} cause local effects similar to those found with torsional constant modifications. In addition, relations between I_{xx}, I_{zz} or J and the natural frequency are not readily available, so iterations are necessary to arrive at the appropriate modified values. Elastic modulus is another potential parameter which may be used to tune the reduced d.o.f. spring models but was not considered in this investigation.

The most reliable reduced d.o.f. springs combined volume matching with the mass density modification. Figure 25 shows an axial mode shape found by the refined and reduced side spring models.

In addition, Table 10 compares the first ten modes found by the refined and reduced side spring modes. Similarly, Table 11 compares the top spring models. Correlation of the first ten modes were verified for both the top and side reduced d.o.f. spring models. Axial modes matched best but other modes were off by less than 5.3%.

Table 10. Side Spring Normal Modes

Mode shape Description	Refined Model 870 d.o.f. Frequency, Hz.	Reduced Model 150 d.o.f. Frequency, Hz.	Difference
Axial	653	653	-0.0 %
Radial	752	736	-2.1 %
X lateral	806	763	-5.3 %
Y lateral	822	778	-5.3 %
Axial	1276	1278	+0.1 %
X lateral	1414	1388	-1.8 %
Y lateral	1438	1413	-1.7 %
XY lateral	1490	1454	-2.4 %
Axial	1818	1821	-0.2 %
YX lateral	1995	1978	-0.8 %

(Fixed-fixed boundary conditions)

Table 11. Top Spring Normal Modes

Mode shape Description Frequency, Hz.	Refined Model 510 d.o.f. Frequency, Hz.	Reduced Model 90 d.o.f.	Difference
Axial	367	367	0.0 %
Radial	400	390	-2.5 %
Y lateral	520	496	-4.6 %
X lateral	530	509	-4.0 %
Y lateral	640	637	-0.5 %
X lateral	687	688	0.1 %
Axial	695	691	-0.5 %
X lateral	769	755	-1.8 %
X,Y lateral	818	807	-1.3 %
Y lateral	934	928	-0.6 %

(Fixed-fixed boundary conditions)

Closed-form solutions provided some degree of confidence in the FEM spring models developed. For example, the first axial surge frequencies were found to be 377 Hz. and 610 Hz. for the top spring and side spring, respectively. An average coil diameter was used for the tapered side spring calculation.

Static stiffening remains a concern in the reduced d.o.f. spring models. Table 12 compares spring constants for top mounting-spring determined by closed-form and static finite element calculations. The torsional stiffness, which corresponds to an axial-direction rotation, predicted by the reduced d.o.f. model agrees well with the refined model prediction. However, the axial and lateral spring constant predictions are significantly higher. This artificial stiffening is expected to affect only the low-frequency compressor-suspension modes of the assembly model.

Table 12. Top Spring Stiffness Comparison

Spring Constant	Closed Form Solution	Reduced d.o.f. FEM Model	Refined FEM Model	Diff.
Axial, $\frac{\text{lbf}}{\text{in}}$ ($\frac{\text{N}}{\text{mm}}$)	99.0 (17.3)	129 (22.6)	100 (17.5)	+ 29 %
Lateral, $\frac{\text{lbf}}{\text{in}}$ ($\frac{\text{N}}{\text{mm}}$)	-----	159 (27.8)	117 (20.5)	+ 36 %
Torsional, $\frac{\text{lbf}\cdot\text{in}}{\text{rad}}$ $\left(\frac{\text{N}\cdot\text{m}}{\text{rad}}\right)$	51.1 (5.77)	51.2 (5.78)	51.0 (5.76)	+ 0.4 %

5.1.2 Component Assembly

The components may now be assembled into a *full model* of the compressor assembly which is solved directly. Alternatively, the components may be solved independently, then combined into a CMS model of the compressor assembly. The CMS method is potentially less accurate but maintains several advantages over a full model. For example, the CMS method calculates system modes significantly faster than a full model. In addition, strain energy calculations are available from the CMS eigensolution for the full system and for each substructure. Strain energy distributions, which compare each substructure's contribution to the total strain energy are useful to classify mode shapes quickly. Under certain circumstances, it is possible to determine kinetic and dissipative energy, as well as modal energy distributions which indicate how each component mode contributes to the assembly's modal properties [19]. Strain energy distributions were considered in this study.

For the CMS results presented here, each modal component is represented by modes in the range of 0-1600 Hz. Higher modes were truncated and represented only by residual flexibility procedures in the CMS solution. The cut-off frequency selected limits the range of system modes which may be solved for, and the frequency range of forcing functions. As a rule-of-thumb, Cook [20] recommends cut-off frequencies up to three times the highest forcing frequency for use in mode superposition calculations. Computational requirements limited the number of modes available, forcing violation of this criteria. However, to insure that the effects of truncated modes were negligible, a limited number of forced response calculations were made using additional modes. No significant changes in forced response calculations were found due to the higher cut-off frequency.

5.2 *Compressor Assembly Model Eigensolution*

Next, normal modes are calculated for the compressor assembly. The addition of internal surge effects by the springs and shockloop results in a dramatic modal density increase. The compressor assembly natural frequencies and mode shapes may grouped into four categories:

- Rigid compressor suspension modes
- Modified Housing modes
- Internal resonances that are inconsequential
- Internal resonances which couple significantly to housing flexure

Rigid compressor suspension modes describe low-frequency oscillation of the lumped-mass compressor mechanism on the internal mounting springs. The motions are not necessarily independent X,Y,Z translation or rotation but rather a combination of translations or rotations. The natural frequencies corresponding to suspension modes occur in the range from 18 to 36 Hz. Recall that the reduced d.o.f. mounting springs artificially elevate the spring stiffness and, therefore, the suspension frequencies of this model. The frequency range of 9-34 Hz. determined with the assembly model having single-beam spring elements is thought to be more accurate.

The *modified housing modes* category describes housing deflections documented previously by the empty housing model. The loaded housing modes are typically found at lower frequencies, an expected trend which is also documented experimentally. In addition, interaction with the internal components can increase the local complexity of the shape, particularly in the mounting bracket regions.

Internal resonances describe the surge frequencies of the mounting springs or shockloop within the compressor assembly model. Examining mode shapes involving internal resonances generally show large relative amplitude motion of the mounting springs or shockloop components with little or no visible flexure of the housing. Actually, each internal resonance results in some amount of

housing motion which, analytically, may be exaggerated to show the resulting deflected housing shape. Analytically, three responses to internal resonances were observed.

- Internal resonances couple primarily to a single housing mode. Usually, but not necessarily, an adjacent mode in the frequency spectrum.
- Internal resonances couple to several housing modes which results in a unique housing deflection due to modal combination.
- Internal resonances may have a localized effect. For example, top spring surges tend to increase motion of the housing top surface. Side springs affect the broadside motion in the mounting bracket region.

Many of the internal resonances do not result in significant flexure of the housing, which is arbitrarily defined as the case when at least 15 % of the total system's strain energy is in the housing component. Therefore, the internal resonance category is further divided into the *inconsequential* and *significantly coupled* categories. Mode shape plots exemplifying these categories are shown in Figure 26 through Figure 31. Mode shapes determined with the CMS model include the corresponding strain energy distributions to show how system modes can be classified without graphic processing of the analysis results.

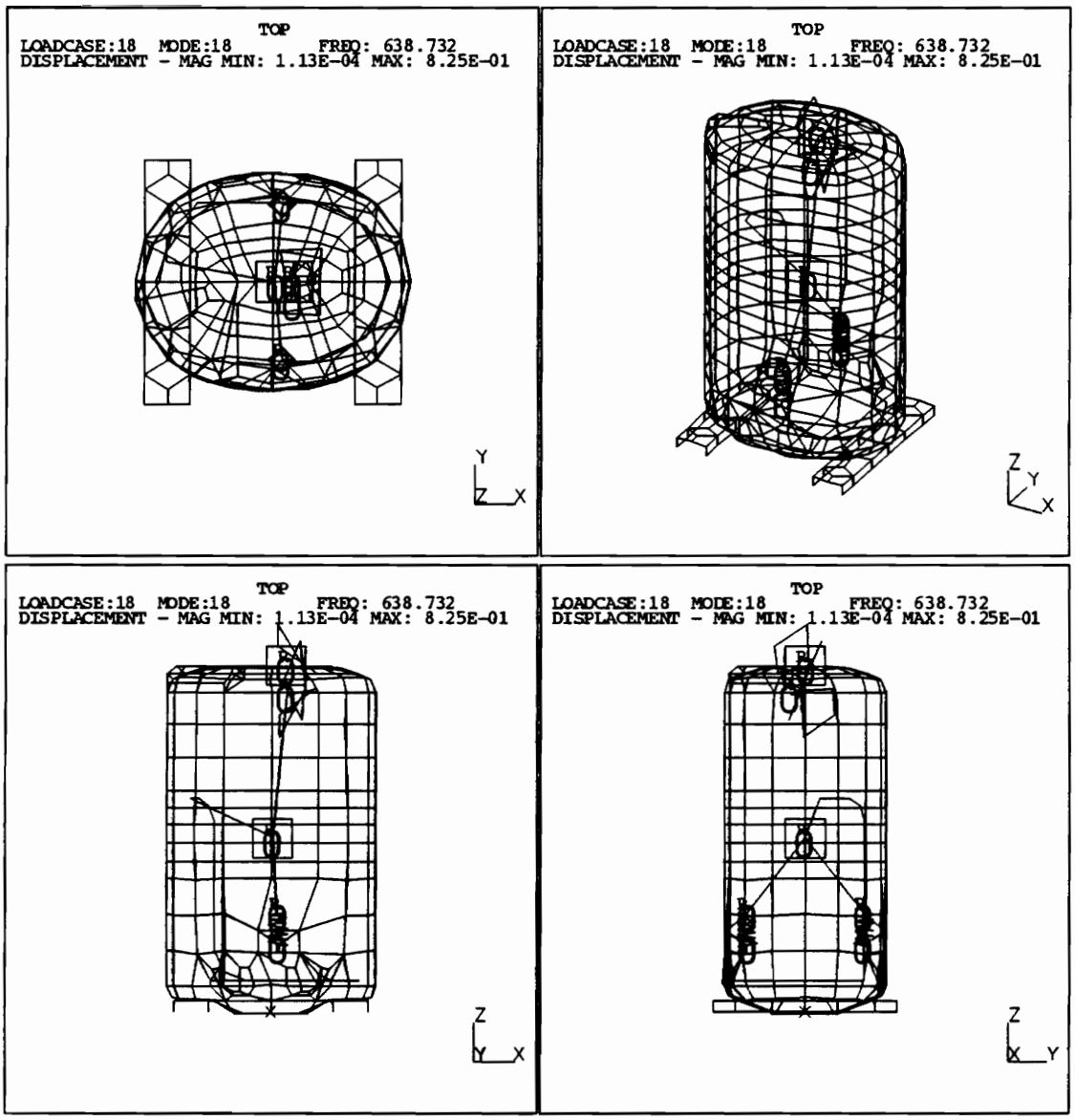

Figure 26. Compressor Assembly Mode Example (full model):

Top spring surge mode corresponding to 639 Hz

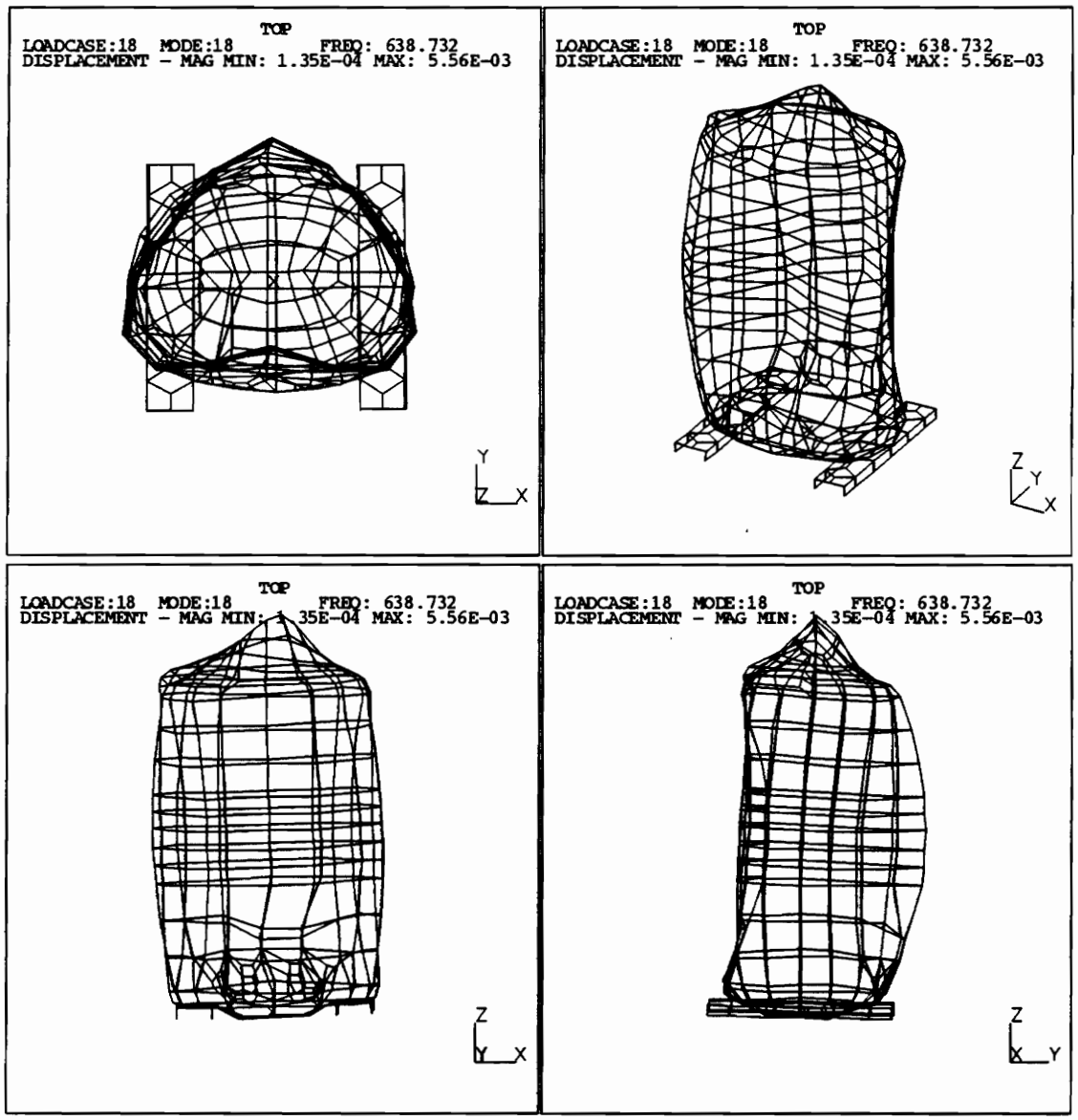

Figure 27. Compressor Assembly Mode Example (full model):

Exaggerated housing deflection due to top spring surge mode corresponding to 639 Hz. Surge is coupled primarily to the M8(3,1) housing mode with additional local top motion.

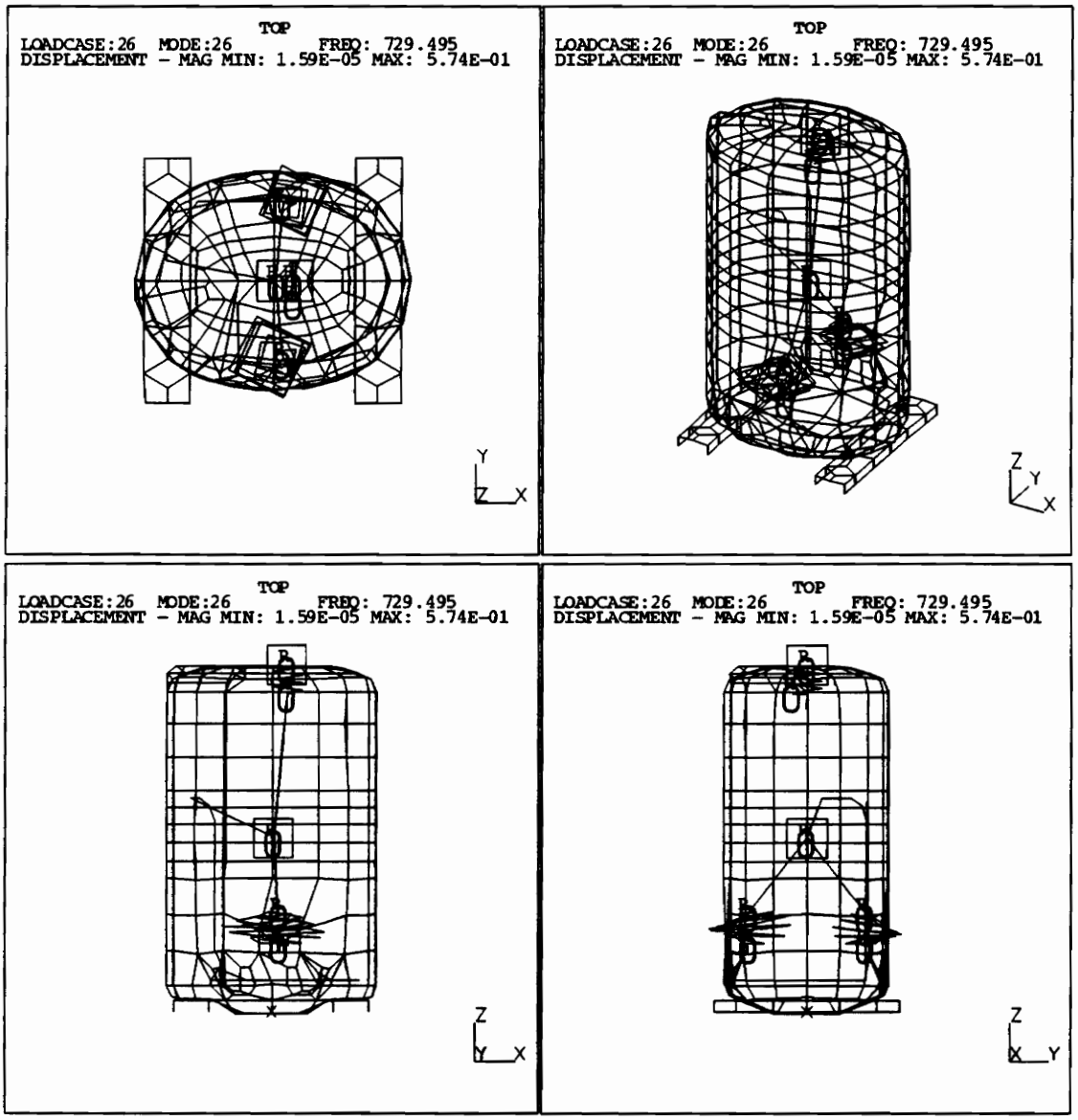

Figure 28. Compressor Assembly Mode Example (full model):

Radial side spring surge mode corresponding to 729 Hz

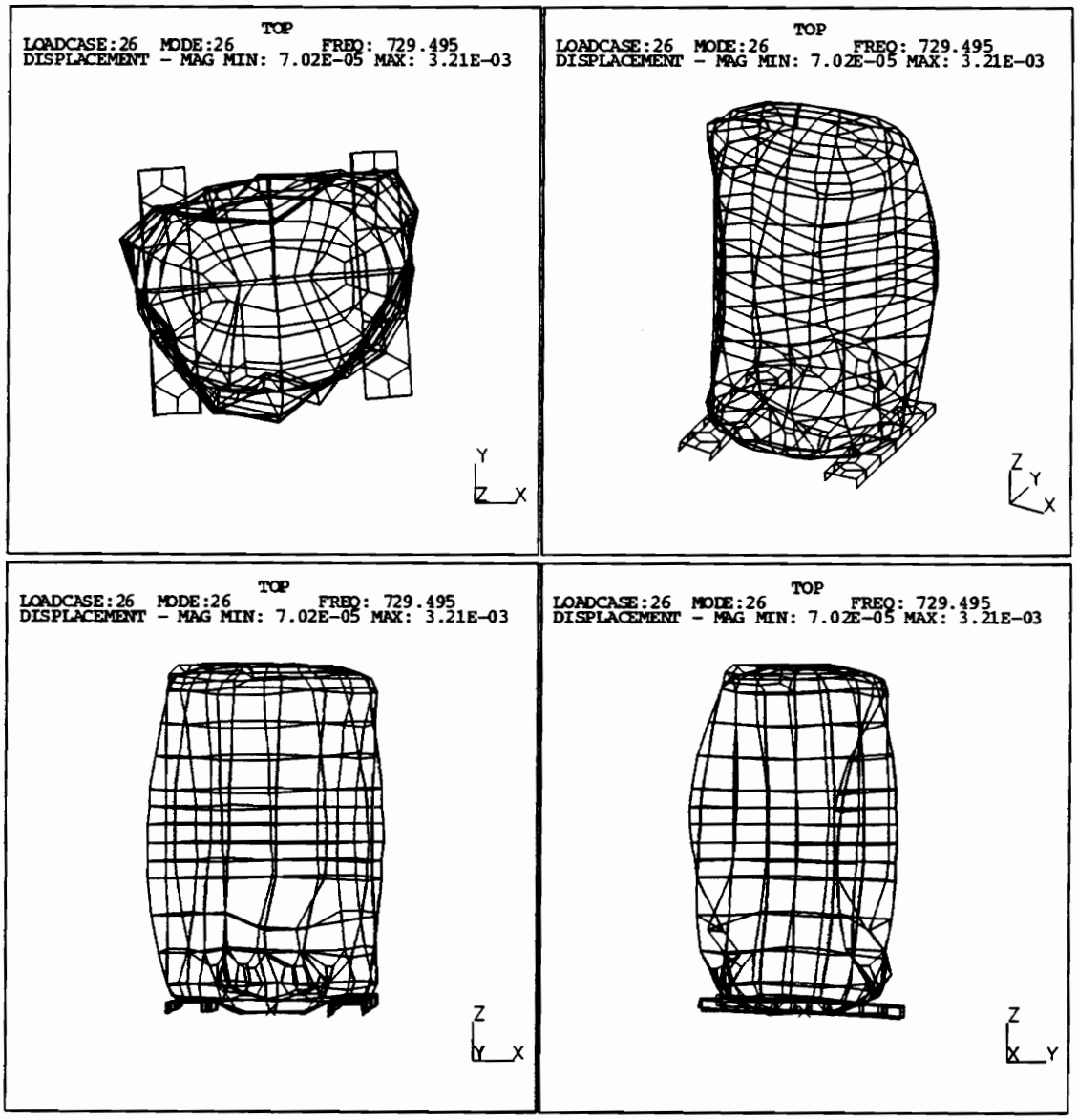

Figure 29. Compressor Assembly Mode Example (full model):

Exaggerated housing deflection due to side spring surge mode at 729 Hz. Resulting housing shape is unique to the loaded assembly.

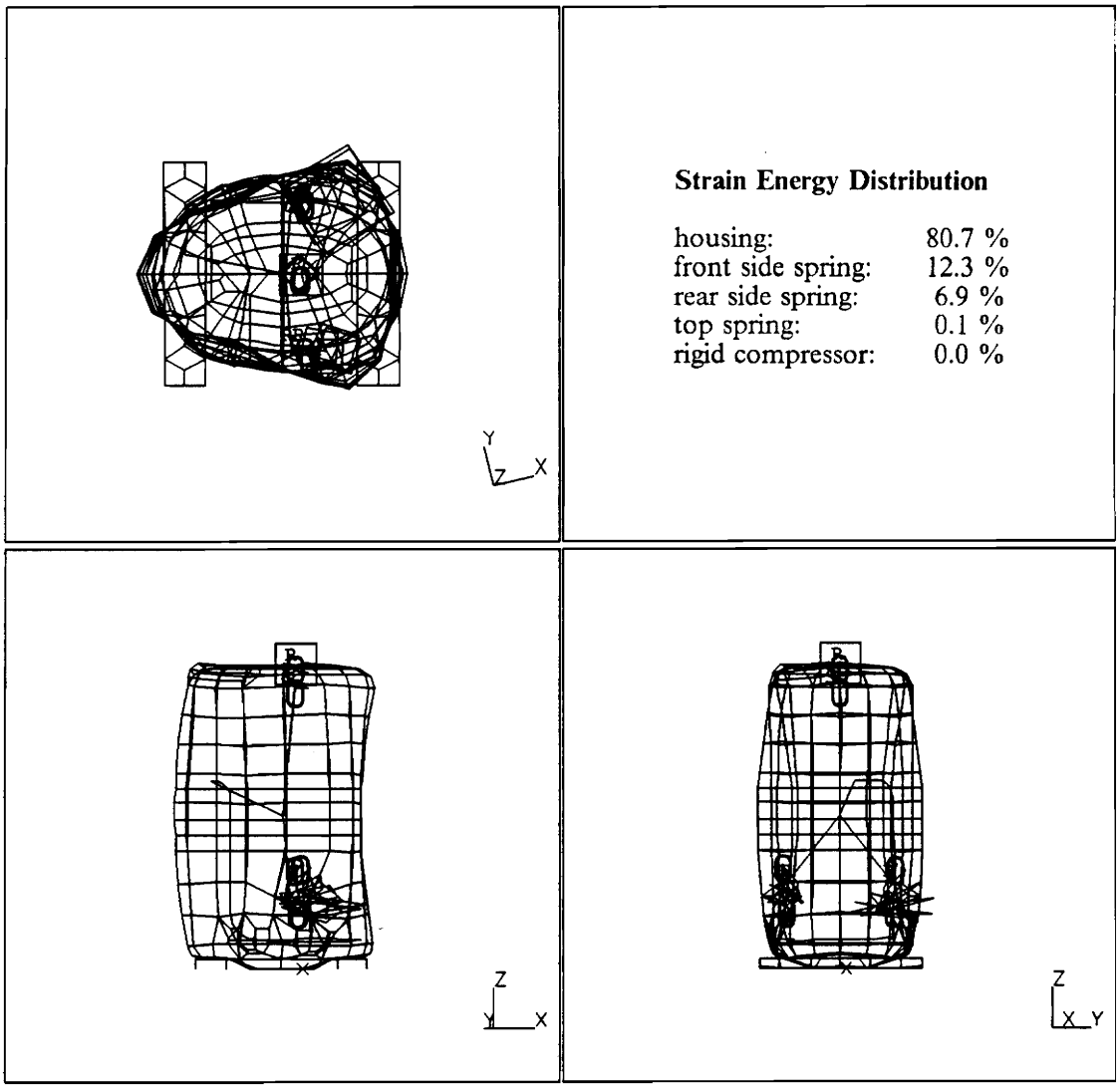

Figure 30. Compressor Assembly Mode Example (CMS model):
Modified housing mode M9(3,1) at 706 Hz

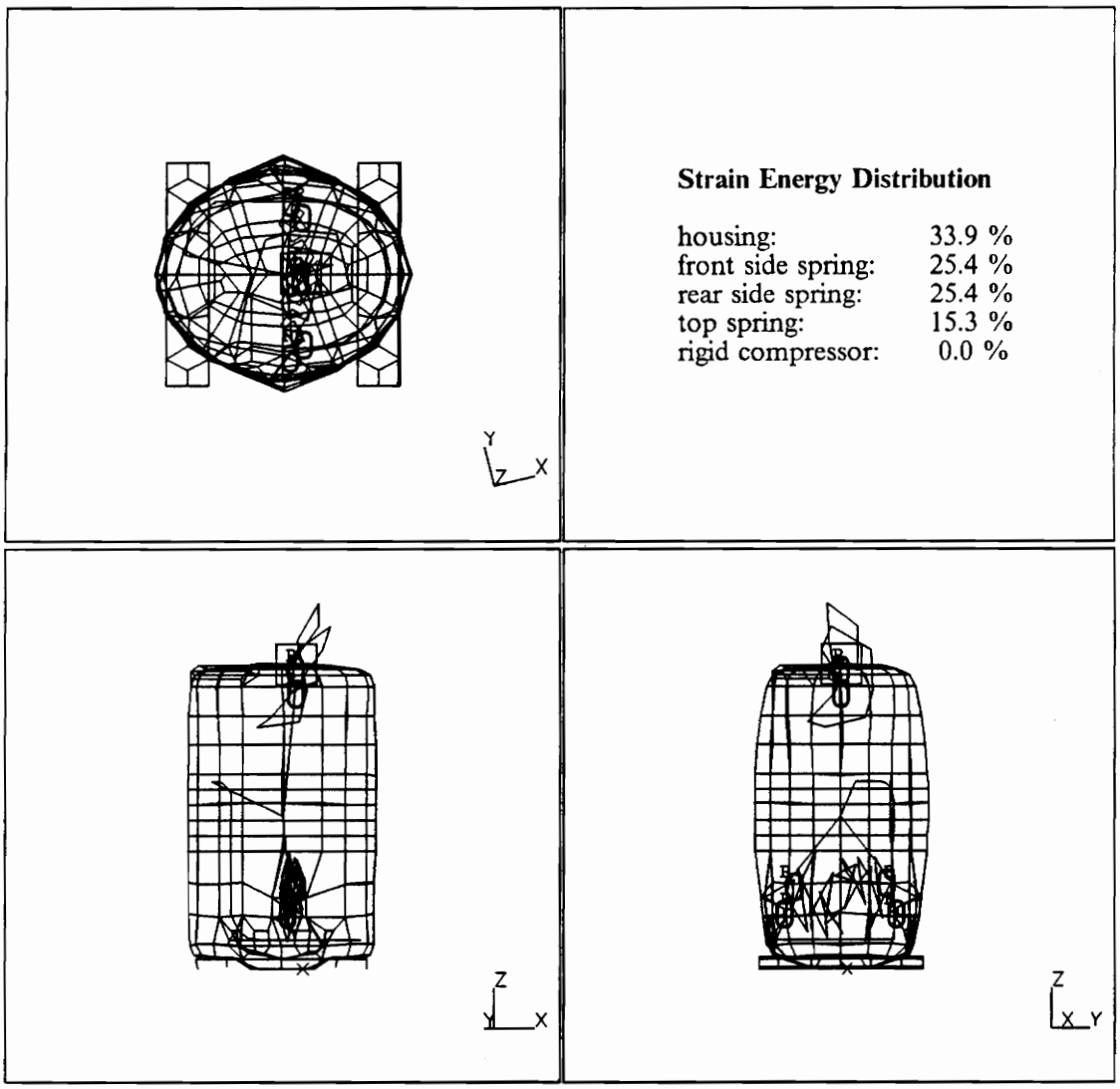

Figure 31. Compressor Assembly Mode Example (CMS model):

Top and side spring surge modes significantly coupled to housing flexure at 809 Hz

A complete summary of all sixty compressor assembly modes are listed in Table 13, for both the full model and the CMS model. Differences are attributed to approximations inherent to the CMS reduction method and to differences between the models. The full model was developed at an earlier stage of the investigation and is not node-for-node equivalent to the CMS model. The CMS model has additional refinements in the housing and shockloop components. Overall, the agreement existing between the two solutions is reassuring.

Table 13. Assembly Model Normal Modes

Mode	CMS Model Freq., Hz	Full Model Freq., Hz	Mode Description
1-6	0	0	Rigid Body
7	18.4	18.4	
8	20.1	20.2	
9	22.1	21.7	compressor suspension modes
10	31.8	32.3	
11	33.5	33.9	
12	35.6	36.8	
13	99.4		shockloop [1]
14	163		shockloop
15	208		shockloop
16	347		top spring
17	369	(103 - 512 unclassified)	top spring
18	493		shockloop
19	497		top spring
20	504		top spring
21	536		shockloop
22	627	639 [2]	top spring (coupling differs)
23	646	649	side spring, housing mode 8
24	652	650	side spring
25	**661**	**656** [2]	**modified housing mode 8**
26	685	688	top spring
27	689	690	top spring
28	**706**	**709** [2]	**modified housing mode 9**
29	719	760	top spring
30	730	729 [2]	side springs, housing modes 9 and 10
31	733	729	side springs
32	**746**	**735** [2]	**modified housing mode 10**
33	760	741 [2]	side springs
34	777	764 [2]	side springs, housing mode 9
35	790	774	side springs
36	808	807	top spring
37	809	800	all springs, housing mode 10
38	854		shockloop
39	**872**	**877** [2]	**modified housing mode 11**
40	909	925	top spring
41	937	956	top spring, housing modes 12,13
42	**966**	**969** [2]	**modified housing mode 13**
43	968	965	top spring, housing modes 13,12
44	**977**	**1026** [3]	**modified housing mode 12, top spring**
45	985	990	top spring, modes 12,13
46	1020		shockloop
47	**1098**	**1123** [3]	**modified housing mode 14**
48	1266		shockloop
49	**1282**		**modified housing mode 15**
50	1286		top spring, housing mode 15
51	**1304**		**modified housing mode 16**
52	1344		side springs
53	1349		side springs
54	1395		side spring, housing mode 18
55	1486		side spring, housing mode 17
56	**1445**		**modified housing mode 17**
57	**1502**		**modified housing mode 19**
58	1516		top spring, housing mode 19
59	1539		side spring, housing mode 18
60	1589		side spring, housing mode 20

1 Shockloop deactivated in full model
2 Identified housing deflection experimentally
3 Full model has less top refinement in housing

5.3 *Compressor Assembly Normal Modes Correlation*

Comparison of the compressor eigenvalue models with test data shows several areas of agreement. First, loading the model more than tripled the modal density in the 650 to 1150 Hz. frequency range, when all internal surge effects were included. For comparison, the test data showed a doubling in the number of natural frequencies found in the same frequency range. One may suspect that all internal resonances found analytically are not externally visible. Also upon loading, the natural frequencies corresponding to modified housing modes typically decrease. The average analytical decrease for both the full model and the CMS model is on the order of 1%. Experimentally, the average decrease is found to be 9%, excluding one mode which increased drastically.

Next, efforts were made to correlate the mode shapes calculated by the compressor assembly model with the test data. The complex interactions and the large number of modes in the loaded compressor presented difficulties to visual comparison. However, the analytical mode shapes thought to agree best are indicated in Table 13 with a superscript. These modes are also shown in Table 14 with comparison to the corresponding experimental natural frequencies. Modified housing modes or cases when an internal resonance is coupled to a housing mode tend to agree best. Results are very encouraging since most shapes agree and several frequencies are within 5 % of the experimental values.

Conversely, two experimental shapes were not found by the compressor assembly model eigensolution. The 989 Hz test shape is a modified version of the "shapes differ" housing mode which was also missed by the housing eigenvalue models. Recall that this shape was not correlated in the housing model until the effects of modal combination were included. The 1054 Hz test shape involves translation of the internal compressor mechanism along the major axis of the housing, as shown in Figure 7 on page 31. As the plot shows, the housing appears to respond primarily in the mode M9(3,1) shape, combined with opposite-phase motion of the internal compressor. The

internal motion is identified by a local reaction at the side-spring mounting brackets. No analytical mode shapes were found by the compressor-assembly model with a similar interaction by the internal mass. It is, however, probable that refinement of the shell element size around the side mounting brackets will be necessary to predict this effect. Currently, the coarse mesh around the connection point does not have the local flexibility needed to find this mode in the frequency range considered. As with the housing model, these shapes will be further investigated by forced response analysis in the following section.

Table 14. Compressor Assembly Model Correlation

Mode Shape	Analytical Frequency [Hz]	Experimental Frequency [Hz]	Difference
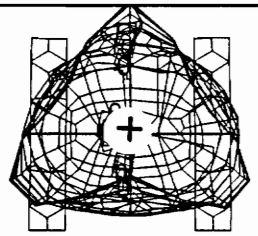 Modified M8(3,1)	639 656	640	-0.2 % + 2.5 %
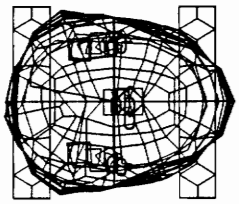 Modified M9(3,1)	709	652	+ 8.7 %
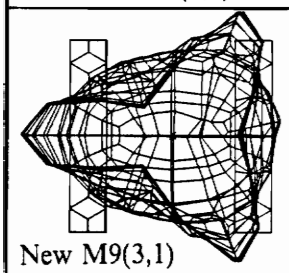 New M9(3,1)	709 764	691	+ 2.6 % + 10 %
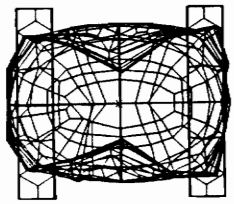 Modified M10(2,1)	729 735	702	+ 3.8 % + 4.7 %
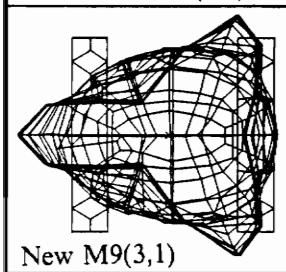 New M9(3,1)	764	807	-5.3 %

Legend: + indicates displacement out of page; - indicates displacement into page

Compressor Assembly Model Correlation (continued)

Mode Shape	Analytical Frequency [Hz]	Experimental Frequency [Hz]	Difference
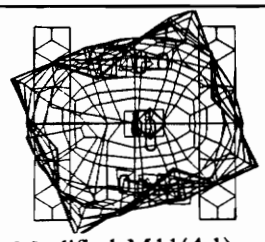 Modified M11(4,1)	741 877	894	-17 % -1.9 %
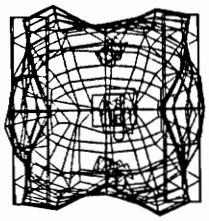 Modified M13(4,1)	969	951	+ 1.9 %
Shapes Differ	-----	989	-----
Internal Translation	-----	1054	-----
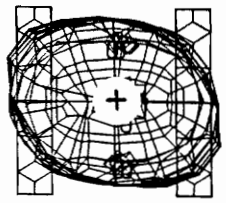 Modified M14(2,1,T1)	1123	1092	+ 2.8 % Rough Match

Legend: + indicates displacement out of page; - indicates displacement into page

5.4 *Compressor Assembly Model Forced Response*

This section describes analytical simulation of the experimental dynamics analysis test setup with the compressor assembly model. As with the housing models, frequency response functions and forced response deflection shapes were calculated for further evaluation of the model. Mode superposition calculations were performed with the 60 modes of the CMS model previously discussed. The same procedures are followed as with the housing model, including the excitation forces and the stinger assembly. Modal damping ratios of $\zeta_r = 0.005$ are defined for each of the 60 system modes. Results are presented directly.

Frequency Response Functions

A frequency response function calculated with the compressor-assembly model is shown in Figure 32. The FRF indicates a mobility transfer function from a point on the girth to a point on the top of the compressor assembly. It is informative to compare the analytical FRF peaks to the mode summary of Table 13. The peaks are found to correspond with modified housing modes and to significantly coupled internal resonances.

The equivalent experimental FRF is shown in Figure 5 on page 28. It would be over-ambitious at this point to overlay the graphs for comparison, but similarities can be found. For example, the modal density change is in better agreement because inconsequential internal resonances are not visible in the FRFs, or appear only as "glitches" on the sides of major housing dominated resonances. As with the housing FRF comparison, response amplitude varies between analytical response and the test data. The modal damping value of 0.005 appears to be too high and a value approximately 1/5 of the present value should be used. Damping is more difficult to estimate in the compressor assembly due to an increase in damping complexity. Two additional damping mechanisms which affect the experimental FRF are oil which fills the bottom of the compressor

and interface friction between components [25]. Further scrutiny or point-to-point evaluation of the curves with the current level of agreement is difficult. More information is available by comparing response over the full housing at each peak.

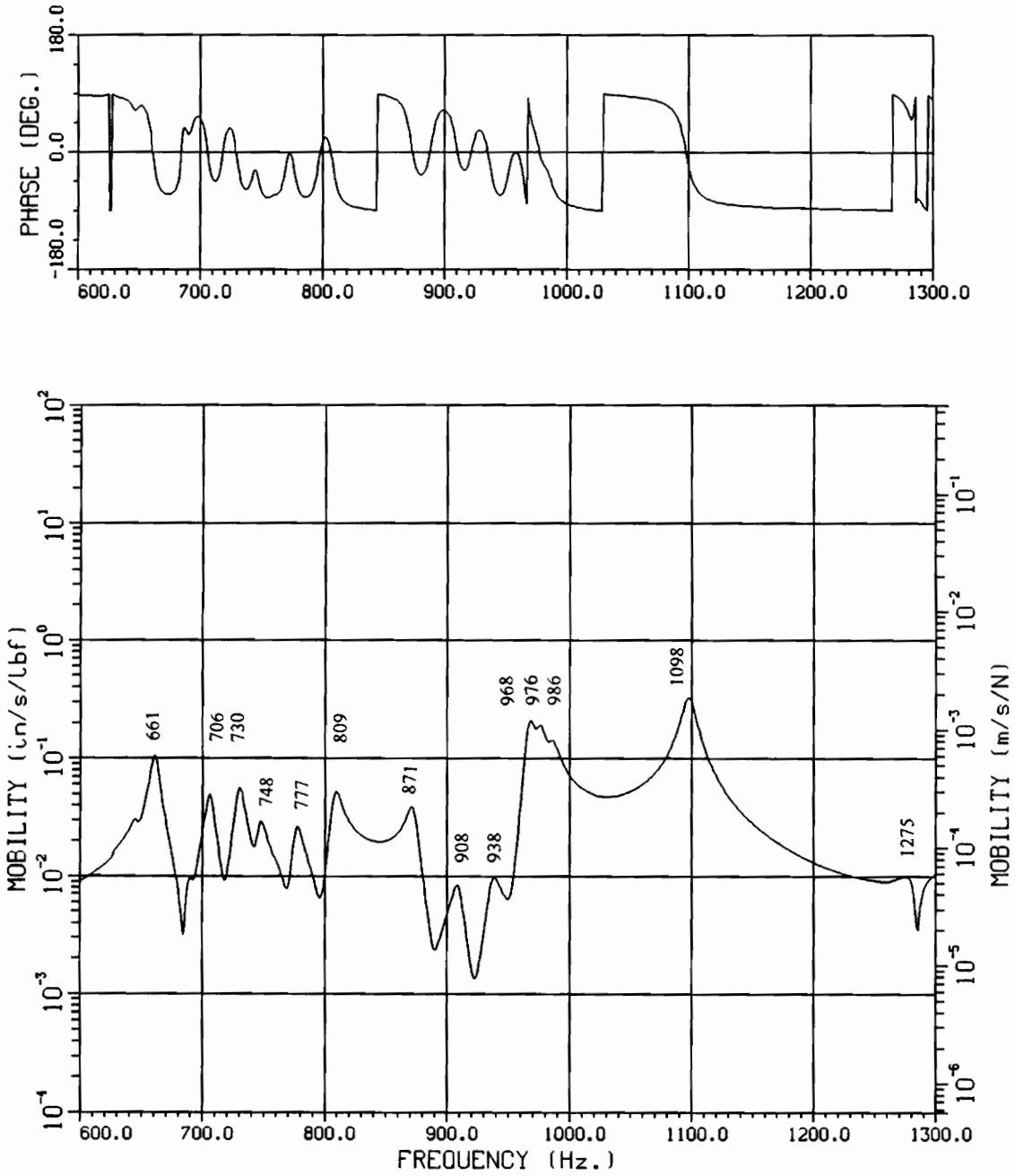

Figure 32. Analytical Compressor Assembly Response:

Force at girth; response at top

Forced Response Deflection Shapes

The labeled peaks of the FRFs indicate frequencies that were selected to determine corresponding resonance deflection shapes. Analytically, in most regions of the FRF, the peaks correspond to the calculated natural frequencies of the CMS model which are listed in Table 13. This is analogous to the experimental procedure in which the peaks indicate a proximity to resonance. However, the test procedure requires a comparison of the phase angle between the excitation force and the velocity response to determine the true natural frequency.

A top view summary of the analytical deflection shapes is shown in Figure 33. The first shape shows the forced deflection response to an excitation at 342 Hz which is below the fundamental housing mode. In five cases, the response shape is dominated by the mode shape corresponding to the forcing frequency. This can be observed in the 661, 706, 872, 976, and 1100 Hz. shapes. For comparison, the reader is encouraged to review the CMS compressor assembly mode descriptions of Table 13, and to the housing modes of Figure 19 on page 62.

In the remaining cases, the shapes appear to include influence by adjacent modes or interactions with the internal components. For example, the analytical shapes found at 938, 966, and 976 Hz show combinations of the top and side motion that is associated with the mode shapes of this frequency region. The same applies to the 730 and 746 Hz shapes, which show attributes of both the M9(3,1) and M10(2,1) mode shapes. Finally, the similar shapes found at 777 and 809 Hz appear to agree with the unique compressor assembly mode shape shown in Figure 29 on page 93. This shape is attributed primarily to surge of the internal side springs. As described in section 5.2, unique mode shapes can result from the combination of housing modes at the surge frequencies. This shape emphasizes the importance of considering the internal spring surge effects.

Many of the analytical resonance deflection shapes were verified experimentally, as indicated in the summary figure. The forced response shape at 1100 Hz agreed with the test better than the corre-

sponding analytical mode shape. The corresponding mode shape was previously classified as a "rough match" as in Table 14.

In contrast to the correlation improvements found in the housing models, forced response of the compressor assembly did not find the two uncorrelated experimental shapes. The 989 Hz "shape differs" experimental mode may occur at an intermediate frequency in the compressor assembly model as in the housing model. This avenue was not explored. In addition, the 1054 Hz. "internal translation" shape was not matched specifically by the model. Other analytical shapes were found which involve local broadside deformations due to interaction with the internal components, however, none were found coupled to the M9(3,1) housing mode with the same phase relation as the experimentally documented shape. Most analytical interactions with the internal mechanism are found to be in phase with the housing motion. For example, the deflection shape at 777 Hz shows increased motion at the housing bracket in the same direction as the housing.

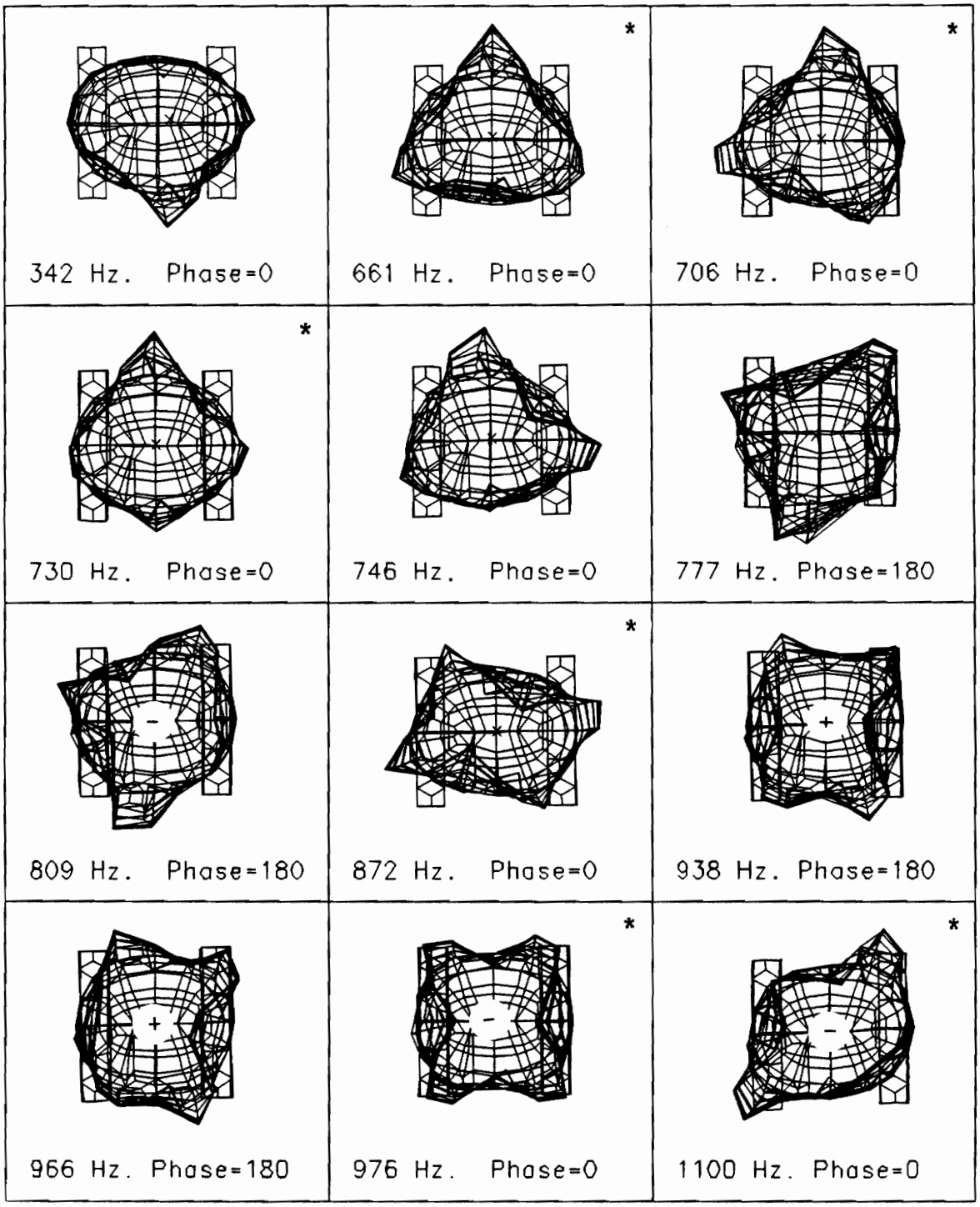

Figure 33. Compressor Assembly Analytical Deflection Shapes:

+ indicates displacement out of the page;

- indicates displacement into the page;

* indicates experimentally documented shapes

5.5 *Comments on the Compressor Assembly Model*

Absolute correlation between the analytical results and experimental test data was not obtained in this study. However, the compressor assembly model predicted many of the characteristics documented in the experimental database. Numerous additional modes were calculated for the compressor assembly, many due to surge of internal components. The increase in modal density found upon loading agreed well with the experimental increase, particularly when only the modes involving significant (and, therefore, experimentally visible) housing motion were considered. Many of the analytical mode shapes were verified by visual comparison to experimental resonance deflection shapes. The corresponding natural frequencies were found to agree also. Simulation of the test procedure by forced response analysis enhanced comparison efforts by providing frequency response function and resonance deflection calculations. Agreement of one analytical shape improved when the mode superposition effects of forced response analysis were included.

No further updates to the compressor assembly model will be considered to improve the current level of correlation during this study. Once the compressor model is assembled, the complex interactions can become intractable and reduce the chance of identifying any specific cause for differences between test data and analytical predictions. Therefore, further updates must be directed towards the unresolved errors at the component level or the additional assumptions made upon assembly. For example, it was necessary to revise the spring components to include surge effects. As shown in Chapter 4, additional revisions to the housing component are needed also. Finally, the most significant modeling assumption is thought to be the absence of internal pressure in the analytical model. Engineering judgements can anticipate the effect of adding pressure loads, but the actual response was not evaluated.

6.0 Evaluation of Models

In spite of efforts made to insure accurate results such as assuring convergence, updating physical simplifications and varying the theoretical formulations, the model results differ somewhat from the test data. This chapter will try to answer questions such as "is the current level of agreement acceptable?" and "how well will the model serve its intended purpose?". The models will first be evaluated subjectively. Then the model's potential for use in the short-range goal, evaluating design changes in the H23A compressor for noise reduction, will be discussed. Finally the model will be discussed in terms of how well it is suited to achieve the long-range goal, designing quieter compressors by including noise prediction capabilities in the design process.

6.1 Subjective Evaluation

The general agreement necessary, before considering a specific application for the model, requires engineering judgement. Initially, it was desired to predict mode shapes and natural frequencies which agree with the shapes documented experimentally. However, as the work progressed, evidence of modal combination in some of the experimental resonance deflection shapes was found. For cases when correlation of the analytical modes with experimental shapes is inappropriate, the initial agreement criteria is extended to include forced response calculations which include the possibility for modal combinations.

In general, the model's quality is now shown by the extent to which predicted modes and displacement shapes agree with the test data. Many of the experimentally documented dynamic

characteristics were predicted by the models. For example, the compressor housing model found all seven of the test housing shapes. Housing natural frequency differences ranged from -1.7 to -12% (20 to 120 Hz). The compressor-assembly model found eight of the ten test shapes. Assembly model frequency differences ranged from -17 to + 10% (-150 to + 70 Hz). The two uncorrelated shapes were discussed, and are not felt to be critical differences.

6.2 *Potential for Redesign Applications*

In the short-range goal, modifications considered to reduce noise in the H23A compressor are based on modal properties. Thus, one application for the models is to predict the effect of design changes on natural frequencies and mode shapes, prior to prototype construction and testing. This capability is especially important if significant housing changes are made, since a single prototype housing is difficult to develop. Drawing a housing prototype requires cutting a new die for the drawing process, the same as required for multiple housing production. In addition, the relatively fast implementation of the model changes allows the evaluation of more design changes.

One redesign option is to re-position the modes of compressor components in the frequency spectrum to avoid coincidence with excitation force frequencies. This procedure is known as spectral mismatching and is discussed by Laurson [7]. In redesigns for spectral mismatching, the FEM model would predict the resonance frequencies which result from changing design parameters. Examples of design modifications to the housing include local shape changes such as ribs or domes and material thickness changes.

The present level of natural frequency differences limits the model's ability to accurately isolate modes from excitation forces. Specific difficulties include the modes which are closely-spaced in the frequency spectrum and compressor pumping forces which occur at 57 Hz intervals. The model

will, however, be effective to show the direction of frequency shifts and estimate the relative magnitude of frequency changes which occur upon changing design parameters. This can be valuable if natural frequencies of several components are found concentrated near a specific, and probably troublesome, frequency.

Another approach to reduce noise is to avoid exciting certain modes. The specific modes targeted in redesign efforts are dominant modes which contribute significantly to response, modes which are efficient acoustic radiators or modes which coincide with high levels of the compressor's measured sound spectrum. Dominant modes are indicated by the larger peaks in the test frequency response functions. Note that these modes must be selected from the full ensemble of FRFs, not just the top responses shown in this document. The dominant modes also show high response in the mobility maps which have calibrated scales. For example, the shapes with mobility levels of 600 m-in/s/lbf (3.43 mm/s/N) would be considered of greater importance than shapes having 300 m-in/s/lbf (1.71 mm/s/N) levels. Radiation efficiency of modes is determined by intuition or acoustic modeling. Acoustic modeling can predict the acoustic intensity resulting from each mode shape. Since the mode shapes are normalized displacements, the amplitudes may be scaled by an experimental weighting factor for calibration to the appropriate response level. The displacements components are also scaled by a $j\omega$ operation for conversion to velocity. The sound intensity associated with each mode could be compared for ranking with regard to acoustic radiation efficiency.

In this approach, the FEM model would provide mode shape data to assist selection of the dominant modes or to rank by acoustic efficiency. Then redesigns, such as a new internal suspension systems which avoid excitation at the antinodal points of the selected housing modes, would be evaluated using the FEM model. Confident mode selection and evaluation by this means is limited to the correlated modes.

The possibilities for redesign which employ the FEM model are numerous and only two approaches were listed here. Although the existing level of correlation restricts the range of potential

applications which can be made with confidence, the model should contribute significantly to the short-range redesign efforts on the H23A compressor.

6.3 *Potential for Noise Prediction Applications*

Model development led to several advances which contribute to the long-range goal of implementing noise prediction into the design process. Component and system modal properties were calculated, which is part of the FEM model's role in the noise prediction scheme. However, to fully satisfy the noise prediction requirements, the model must calculate the forced vibration response to mechanical and acoustic forcing functions. Response calculations are limited by the accuracy of modal properties (predicted mode shapes, natural frequencies and damping estimates) and the number of modes calculated.

Inaccurate prediction of response will limit the acoustic model's ability to calculate intensity. The current level of correlation shows that forced response deflection shapes agree with test data well. However, the noise prediction scheme will require accurate velocity response amplitudes over the full housing surface as well. In this study, the amplitude of response was considered in the frequency response function of a single point, and found to differ from the test data. Currently, the sensitivity of intensity calculation to response amplitude errors are unknown. Improving the velocity response predictions may be as simple as adjusting the modal damping estimates for each mode, or may require further model updates to improve modal properties. Alternatively, amplitude may be adjusted with an experimentally determined scale factor.

Initial acoustic prediction work has been performed in which predicted intensities were compared to measured intensities at a single frequency. That is, the sound intensity radiated while shaking the compressor at the single analytical natural frequency, Ω_a, was calculated from one of the ana-

lytical deflection shapes. The compressor was also driven by a shaker at the single test natural frequency, Ω_t, and intensities were measured. Since the predicted natural frequencies will always differ from the test data to some degree, ($\Omega_a \neq \Omega_t$), there is a question of which frequency to compare intensities at. Note that a small frequency shift to either side of resonance peak will result in very large velocity amplitude changes and consequently, large intensity changes. Therefore, sound intensities should be predicted at Ω_a, and compared to experimental intensities measured at Ω_t. Thus, it is important to assure that the analytical and measured intensities correspond to the same analytical and experimental shapes.

Finally, the number of modes available limit the frequency range of forced response calculations. Recall that component modes in the 0 to 1580 Hz. frequency range were calculated by the models. Therefore the frequency range of forcing functions must be kept below a cutoff frequency (Cook suggests 1/3 the highest natural frequency or 530 Hz.) in mode superposition solutions. Neither the acoustic nor the mechanical forcing functions of the operating compressor were considered, but high frequency content is anticipated. Eventually, the models must be developed to find additional modes at higher frequencies accurately. Calculation of higher modes will raise computational requirements and require additional mesh refinements to the model.

To summarize, the model can be generally viewed as having good quality because most of the analytical calculations, including both normal mode shapes and response shapes, agree with the experimental database. However, speicific applications are limited by the the level of correlation achieved. If redesigns are considered to modify the modal properties of the compressor, evaluations by the model should reflect the range of potential frequency prediction errors. Redesign evaluation is also limited to the shapes which are correlated. Noise prediction is limited by response amplitude calculations and the number of modes available for the superposition solutions.

7.0 Conclusions and Recommendations

The dynamic finite element models of this study were developed to calculate modal properties of the Bristol Compressor, Inc. model H23A refrigeration compressor. The models are valuable tools to study the short-range goal of reducing noise emission by the H23A. The models also contribute to a longer-range task of developing an FEM compressor model for use in noise prediction. Specifically this work (1) addressed the interactions between test and analysis for model updating and verification, (2) determined several causes for discrepancies between test and analysis, and (3) identified modeling issues that warrant further study. This final section summarizes the significant conclusions determined in this study. In addition, recommendations for future modeling efforts will be discussed.

The analysis and test interactions of this study involved natural frequency correlation and visual comparison of mode shapes. The visual comparison localized regions having discrepancies to guide model updating. Approaches to model updating vary, but this study emphasized the need to follow physical insights during revisions. This approach preserves the physical understanding of model changes, as opposed to arbitrarily changing stiffness matrix coefficients or material property values to adjust model performance. Therefore, the changes made during model development are generally applicable to other compressor structures and future modeling efforts.

Another issue concerning analysis and test interactions was found to be compatibility of the analytical and the experimental databases. Analytical results showed a potential for modal combination in the resonance dwell procedure used to experimentally document modes. Modal superposition is believed to cause the coupling between housing top modes and side modes found by the experimental tests. It is recommended that future efforts adopt measures to insure pure

mode extraction during experimental tests or supplement the modeling effort with forced response analysis as done in this study. If automated model adjusting procedures are considered, modal combinations should be eliminated prior to forcing the model to agree with the test data. Regardless of the model correlation and adjustment scheme followed, the experimental data must be compatible with the analytical data.

As the models were developed, several discrepancies between analytical predictions and test data were resolved by model updating. Numerous revisions which targeted both physical and theoretical modeling limitations were made. The history of model updates provided insight into the potential causes of modeling errors and established procedures which may guide future efforts to model the housing and internal compressor components.

Most updates concentrated on the compressor housing model. Results showed that natural frequency calculations in the housing model are most sensitive to the following physical parameters: (1) geometry representation, (2) representation of the girth joint, and (3) Local mass loading by accessories. Difficulties representing the girth joint were not investigated by the appropriate means necessary for a solid understanding. Since the girth is thought to play a significant role in the structural characteristics of the housing, future modeling efforts should pursue a more effective modeling approach to represent the girth joint. Theoretical parameters, such as element formulation and solution algorithms, were found to affect natural frequency calculations nearly as much as physical parameters. These may be beyond the analyst's control. Another theoretical parameter which can be of greater importance than shown in this study is assuring convergence through adequate mesh refinement. Several parameters were identified which do not significantly affect the calculation of modal properties. Results showed little relative significance of thickness variations and no influence by residual stresses within the compressor housing. This information should be equally valuable to future modeling efforts.

Procedures were established for modeling internal components. Accurate components are vital to the compressor assembly model because once assembled, numerous interactions between compo-

nents make errors difficult to isolate. Surge or resonance of internal components was found to be a significant factor in the compressor assembly dynamics. Details were provided to represent the helical coil mounting springs and the shockloop with linear beam elements. This representation is necessary to include surge effects. Internal resonances partially account for the increase in modal density upon loading the housing. In many cases the internal resonances were inconsequential with respect to housing flexure, but some resulted in new modes which significantly affected the housing. Modeling the springs with simple spring elements or as discussed, a single massless beam element which approximates the full 12 x 12 spring stiffness matrix, will not include surge effects. Eigensolutions which did not consider surge effects performed at higher frequencies as if the compressor was empty. Several aspects of the compressor model were not investigated in this study. Further analysis might consider the effects of pressurizing the housing or resonance of the compressor mechanism itself.

The finite element method can only approximate the dynamic behavior of compressor structures. Therefore, the analytical predictions will always differ from the test data to some degree. A quantitative agreement criteria is needed which clearly states the required accuracy in regard to the intended application. For the noise prediction scheme, ultimately the sound intensities will be desired to some degree of accuracy. The FEM velocity response accuracy needed to meet the sound intensity requirements should be established. Subsequently, the accuracy of modal properties needed to insure the velocity response requirements could be established.

References

1. Hurst, C.J., Knight, C.E., Mitchell, L.D., et. al., Investigation of the Potential for Noise Reduction of a Reciprocating Compressor, Final report to Bristol Compressors, Inc., Virginia Polytechnic Institute and State University, Dept. of Mechanical Engineering, Blacksburg, VA, 1990.

2. Ingles, D. J., "Understanding Noise Radiation from a Hermetic Compressor", Proceedings of International Compressor Engineering Conference - at Purdue, West Lafayette, IN., pp. 69-73, 1972.

3. Soedel, W., "Simple Mathematical Models of Mode Splitting of Hermetic Compressor Shells that Deviate from Axisymmetry." Proceedings of International Compressor Engineering Conference - at Purdue, West Lafayette, IN., pp. 259-262, 1980.

4. Maeda, S., Okubo, N.,Saito, F., Uetsuji, T., "Noise Reduction of Hermetic Compressor by Improvement of its Shell Shape", Proceedings of International Compressor Engineering Conference - at Purdue, West Lafayette, IN., pp. 228-234, 1980.

5. Kawai, H., Sasano, H., Kita, I., Ohta, T., "The Compressor Noise-Shell and Steel Materials", Proceedings of International Compressor Engineering Conference - at Purdue, West Lafayette, IN., pp. 307-314, 1988.

6. Singh, R., and Tavakoli, M. S., "Alternate Models of the Dynamics of a Refrigeration Compressor Shell", Proceedings of International Compressor Engineering Conference - at Purdue, West Lafayette, IN., pp. 300-306, 1988.

7. Laursen, M. B., "Mismatching Noise Source and Resonance Spectra of Reciprocating Compressor Shells", Proceedings of International Compressor Engineering Conference - at Purdue, West Lafayette, IN., pp. 808-817, 1990.

8. Johnson, O. et. al., "The Application of Advanced Analysis Methods to the Reduction of Noise from Air Compressors", Proceedings of International Compressor Engineering Conference - at Purdue, West Lafayette, IN., pp. 800-807, 1990.

9. Hasselman, T. K., "A Perspective on Dynamic Model Verification", ASME Bound Volume, Modal Testing and Model Refinement, Applied Mechanics Division, Vol.59, presented at the Winter Annual Meeting of the ASME, Boston, MA, November 13-18, pp. 101-117, 1983.

10. Ewins, D. J., Modal Testing: Theory and Practice, John Wiley & Sons, New York, NY, 1984.

11. Chen, J. C., Garba, J. A., "Structural Analysis Model Validation Using Modal Test Data", Combined Experimental/Analytical Modeling of Dynamic Structural Systems, Applied Mechanics Division, Vol. 67, presented at the Joint ASCE/ASME Mechanics Conference, Albuquerque, NM, June 24-26, pp. 109-137, 1985.

12. Wada, B. K., "Required Developments in Structural Dynamics", The Shock and Vibration Bulletin, Bulletin 52, Part 1, May 1982.

13. Wada, B. K., Garba, J. A., Chen, J. C., "Modal Test and Analysis Correlation", Modal Testing and Model Refinement, Applied Mechanics Division, Vol.59, presented at the Winter Annual Meeting of the ASME, Boston, MA, November 13-18,, pp. 85-99, 1983.

14. Ewins, D. J. and Sidhu, J., "Correlation of Finite Element and Modal Test Studies of a Practical Structure", Proceedings of IMAC-II, International Modal Analysis Conference, Orlando, Florida, February 6-9, 1984, published by Union College, Schenectady, NY, pp. 756-762.

15. Dascotte, E., "Applications of Finite Element Model Tuning using Experimental Modal Data", Sound and Vibration, Vol. 25 No. 6, June 1991, pp. 22-26.

16. Blakely, K. D. and Dobbs, M. W., "Integrated System Identification: The Union of Testing and Analysis", Proceedings of IMAC-I, International Modal Analysis Conference, Orlando, Florida, 1982, published by Union College, Schenectady, NY, pp. 259-264.

17. Chen, J. C., "Analytical Model Accuracy Requirements for Structural Dynamic Systems", Journal of Spacecraft and Rockets, Vol. 21, No. 4, July-August 1984.

18. Anonymous, I-DEAS ™ Model Solution and Optimization Engineering Analysis User's Guide, Structural Dynamics Research Corporation, Milford, Ohio, 1988.

19. Anonymous, I-DEAS ™ Systan ™ Engineering Analysis System Dynamics User's Guide, Structural Dynamics Research Corporation, Milford, Ohio 1988.

20. Cook, R. D., Malkus, D. S., Plesha, M. E., Concepts and Applications of Finite Element Analysis, John Wiley & Sons, New York 1989.

21. Craig, Roy R., Structural Dynamics, An Introduction to Computer Methods, John Wiley and Sons, 1981.

22. Craig, Roy R. and Chang, Ching-Jone, "A Review of Substructure Coupling Methods for Dynamic Analysis", NASA CP-2001, Vol. 2, pp. 391-408. National Aeronautics and Space Administration, Washington, D.C. 1976.

23. Knight, Charles E., The Finite Element Method in Mechanical Design, Virginia Polytechnic Institute and State University, Mechanical Engineering Dept., 1989.

24. Thomson, William T., Theory of Vibration with Applications, 3rd Ed., Prentice Hall, 1988.

25. Agee, B. L., Kelly, A. D., Mitchell, L. D., "Finite Element Model Updating Using Laser-Based Experimental Dynamics for Noise Prediction Purposes", Proceedings of Noise-Con 91, Tarrytown, NY, July, 1991, pp. 657-666.

26. Bathe, K. J., Finite Element Procedures in Engineering Analysis, Prentice-Hall, Inc., Englewood Cliffs, N.J., 1982.

27. Mitchell, L.D. and Shigley, J. E., Mechanical Engineering Design. McGraw-Hill, New York, NY, pp. 447-463, 1983.

28. Joseph, Jerrard A, ed. MSC/NASTRAN VERSION 65C Vax Edition Application Manual, The Macneal-Schwendler Corporation, Los Angeles, CA 1988, (pp. 4.4.51 - 4.4.70).

29. Muskivitch, John C. BASIC MSC/NASTRAN ANALYSIS. Linear Static and Normal Modes Analysis (Version 65), The MacNeal-Schwendler Corporation, Rockville, Maryland 1988.

30. Lazan, B. J., Damping of Materials and Members in Structural Mechanics, Pergammon Press, Oxford, London, 1968.

31. Mitchell, Larry. D., Personal Communication, Virginia Polytechnic Institute and State University, Dept. of Mechanical Engineering, 15 April 1991.

32. Rao, Dantum K., "Electrodynamic Interaction between a Resonating Structure and an Exciter", Proceedings of IMAC-V, International Modal Analysis Conference, Imperial College of Science and Technology, London, England, April 6-9, 1987, pp. 1142-1150.

33. Mitchell, L. D. and Elliot, K. B., "How to Design Stingers for Vibration Testing of Structures", Sound and Vibration, Vol. 18, No. 4, April 1984, pp.14-18.

34. Bernhard, R.J. and Seidel, M.R., "Finite Element Modeling of Compressor Discharge Tubes", Proceedings of the 1986 International Compressor Engineering Conference - At Purdue., West Lafayette, IN.,1986, pp. 931-942.

35. Hamilton, James F., Measurement and Control of Compressor Noise, Ray W. Herrick Laboratories, School of Mechanical Engineering, Purdue University. West Lafayette, IN, 1988, pp. 148-150.

Appendix A. Mode Designator Scheme

The four-view layouts shown in the mode shape plots such as Figure 9 on page 37 were frequently used for visual mode shape comparisons. As mode complexity increases, color contour plots become necessary to fully describe the housing mode shapes. For convenient documentation, a mode shape descriptor scheme has been adopted from Ingles [2] to describe the compressor housing eigenvectors. Mode shape descriptors are defined as follows:

$$\#(N,M,L)$$

where

# = the number corresponding to the mode shape as found consecutively by the solver.
N = one-half the number of circumferential antinodes
M = one-half the number of axial antinodes
L = the number of top or bottom antinodes

Antinodes are the lines along which maximum housing motion occurs. Figure 34 shows circumferential, axial, top and bottom deflection patterns which exemplify the mode descriptors. Note that modes are not uniquely identified by this scheme. Repetition of the circumferential designation occurs due to the "mode splitting" phenomenom described by Soedel [3]. Housing modes often split into two modes at separate frequencies due to housing features (additional mass, additional stiffness or ovalness) which disrupt axisymmetry. Although the circumferential node pattern is the same, the split modes are identified by a rotation.

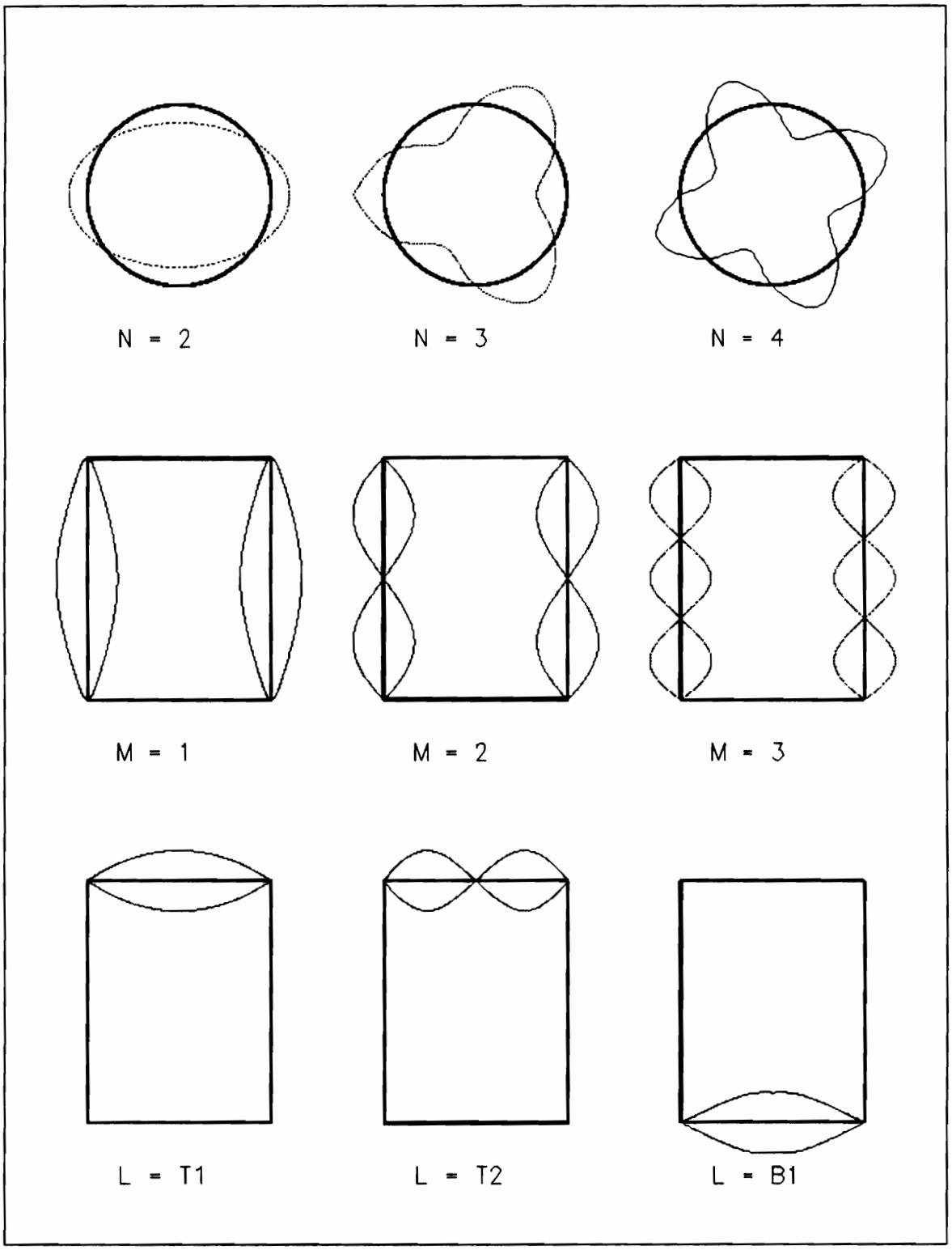

Figure 34. Sample Mode Descriptors

Appendix B. Closed-Form Solution to Spring Surge

For a helical coil spring between two flat and parallel plates [27]:

Spring Weight:

$$W_s = \frac{\pi^2 d^2 D N \rho}{4} \qquad \text{lbf (N)}$$

Axial Stiffness:

$$K = \frac{d^4 G}{8 D^3 N} \qquad \frac{\text{lbf}}{\text{in}} \left(\frac{\text{N}}{\text{m}} \right)$$

Torsional Stiffness:

$$K_t = \frac{E d^4}{64 N D} \qquad \frac{\text{lbf•in}}{\text{rad}} \left(\frac{\text{N•m}}{\text{rad}} \right)$$

Axial Surge Frequency:

$$f_i = \frac{i}{2} \sqrt{\frac{Kg}{W_s}} \qquad \text{Hz}$$

where

i	= mode number, i = 1,2,3...n	
d	= wire diameter	in (m)
D	= mean coil diameter	in (m)
N	= number of active coils	
ρ	= specific weight	lbf/in^3 (N/m^3)
G	= modulus of rigidity	lbf/in^2 (N/m^2)
E	= modulus of elasticity	lbf/in^2 (N/m^2)
g	= 386 in/s^2 (9.8 m/s^2)	

Vita

The author was born April 12, 1968 in Man, West Virginia to Larry Douglas Kelly and Rose Marie Perovich. He was raised in Princeton, West Virginia where he recieved his secondary education from the public schools of Mercer County. In 1986 he earned an Associate of Science degree in Pre-Engineering from Bluefield State College, and in 1990, a Bachelor of Science degree in Mechanical Engineering from Virginia Polytechnic Institute and State University. Upon completion of the Master of Science degree, he will begin a career in Mechanical Engineering.

Allan Douglas Kelly